The Dissertation Committee for Brooklyn Ames Robertson certifies that this is the approved version of the following dissertation:

Evolution and Divergence in the Tautomerase Superfamily: A Pre-steady State Kinetic Analysis of *cis*-3-Chloroacrylic Acid Dehalogenase and an Inhibition Study of Its Homologue, Cg10062, in *Corynebacterium glutamicum*

Committee:

Christian P. Whitman, Supervisor

Walter L. Fast

Hung-wen Liu

Dean R. Appling

Kenneth A. Johnson

Evolution and Divergence in the Tautomerase Superfamily: A Pre-steady State Kinetic Analysis of *cis*-3-Chloroacrylic Acid Dehalogenase and an Inhibition Study of Its Homologue, Cg10062, in *Corynebacterium glutamicum*

by

Brooklyn Ames Robertson, B.S.

Dissertation

Presented to the Faculty of the Graduate School of

The University of Texas at Austin

in Partial Fulfillment

of the Requirements

for the Degree of

Doctor of Philosophy

The University of Texas at Austin

August 2007

Dedication

I would like to dedicate this dissertation to my mother and father. They have given me incredible strength throughout my graduate career and have guided me down this long journey of finding myself. The support they have given me throughout the years can only be matched by that of God. Thank you so much for everything and I could not have done any of this without you.

Acknowledgements

This dissertation is the compilation of work performed over the last few years due to the help of a number of people and organizations. I am grateful for the financial support received from the National Institutes of Health (GM-65324), the Robert A.Welch Foundation (F-1334), and The University of Texas at Austin. Without this assistance the research would not have been possible. I am sincerely grateful to my advisor, Dr. Christian P. Whitman. His guidance throughout my graduate career has always been plentiful. His patience and encouragement have been the driving force behind my work, and I cannot express enough gratitude. Over the past few years, he has not only been my academic mentor, but also my friend. I would also like to thank Dr. Kenneth Johnson and the members of his research lab for the many valuable discussions that led to my increased understanding of pre-steady state kinetics. Finally, I would like to thank all the people who have helped me in some way during my studies at The University of Texas at Austin. You have made these last few years interesting and fun!

Evolution and Divergence in the Tautomerase Superfamily: A Pre-steady State Kinetic Analysis of *cis*-3-Chloroacrylic Acid Dehalogenase and an Inhibition Study of Its Homologue, Cg10062, in *Corynebacterium glutamicum*

Publication No. _____

Brooklyn Ames Robertson, Ph.D.

The University of Texas at Austin, 2007

Supervisor: Christian P. Whitman

The tautomerase superfamily is a group of structurally homologous proteins characterized by a β-α-β building block and a catalytic amino-terminal proline (Pro-1). The isomer specific hydrolytic dehalogenases, *cis*- and *trans*-3-chloroacrylic acid dehalogenase, (*cis*-CaaD and CaaD, respectively) are two superfamily members found in bacterial pathways for the catabolism of the nematocide 1,3-dichloropropene. The enzyme-catalyzed addition of water produces two products, malonate semialdehyde and a halide ion. Although the enzymes share a common catalytic tetrad, there are two notable differences: two additional residues have been implicated in the *cis*-CaaD mechanism and mutagenesis analysis of the core catalytic residues suggests varying degrees of importance. As part of an effort to understand the origin of these differences, a pre-

steady state kinetic analysis of *cis*-CaaD was carried out. For the analysis, an ion-exchange method was developed for bromide quantification. The analysis produced a five-step kinetic model in which substrate binding is followed by a conformational change. Halide ion is released first in the rate limiting step followed by the release of malonate semialdehyde. The stage is now set for a similar analysis of CaaD and the *cis*-CaaD and CaaD mutants. In the second part of the dissertation, (*R*)- and (*S*)-oxirane-2-carboxylate were determined to be active-site-directed irreversible inhibitors of the *cis*-CaaD homologue designated Cg10062 and found in *Corynebacterium glutamicum*. Kinetic analysis indicates that the (*R*)-enantiomer binds more tightly and is the more potent inhibitor. Pro-1 is the sole site of modification by the (*R*)- and the (*S*)-enantiomer. The results are similar to those found for the irreversible inactivation of *cis*-CaaD by (*R*)-oxirane-2-carboxylate with an important distinction: the alkylation of *cis*-CaaD is stereospecific. Cg10062 exhibits a relaxed substrate specificity processing both the *cis*- and *trans*-3-chloroacrylic acid. Delineation of the factors responsible for the stereoselective inactivation would provide a more complete picture of the substrate specificity determinants for *cis*-CaaD and CaaD.

Table of Contents

List of Tables

List of Figures

List of Schemes

Supplement Figure List

Supplement List of Tables

Chapter 1: Introduction

1.1 An Overview of the Tautomerase Superfamily

The tautomerase superfamily is a group of structurally homologous proteins that are characterized by a β–α–β building block and a catalytic amino-terminal proline (Pro-1) (1-3). The signature β–α–β fold begins with Pro-1 at the start of a β-strand (β1), followed by an α-helix (α1) and a 3_{10} helix, which precedes a second parallel β-strand (β2). The fold ends with a β-hairpin near the C-terminus, which is important for oligomerization (Figure 1) (2). The superfamily consists of five families represented by 4-oxalocrotonate tautomerase (4-OT) (1), 5-(carboxymethyl)-2-hydroxymuconate isomerase (CHMI) (4), macrophage migration inhibitory factor (MIF) (5), *cis*-3-chloroacrylic acid dehalogenase (*cis*-CaaD) (6), and malonate semialdehyde decarboxylase (MSAD) (7). The 4-OT family includes *trans*-3-chloroacrylic acid dehalogenase (CaaD) (8). 4-OT from *Pseudomonas putida* mt-2 and CHMI from *Escherichia coli C* function as tautomerases in degradation pathways for aromatic hydrocarbons and aromatic amino acids, respectively (4,9). MIF is a pro-inflammatory cytokine, but also functions as a phenylpyruvate tautomerase (PPT) (5). CaaD and *cis*-CaaD precede MSAD in a degradation pathway for an isomeric mixture of 1,3-dichloropropene, which is used as a nematocide (3). CaaD, *cis*-CaaD, and MSAD are found in various gram-positive and gram-negative bacteria including *P. pavonaceae* 170 and the coryneform bacterial strain FG41 (10). The characterized members in the superfamily show rich mechanistic and structural diversity.

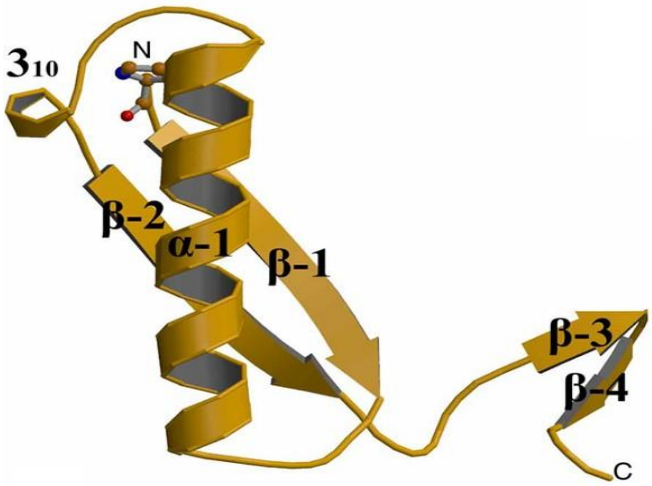

Figure 1.1. The characteristic β-α-β building block of the tautomerase superfamily**.** The key structural elements are labeled and discussed in the text.

In the tautomerase superfamily, Pro-1 can function as a general acid catalyst or a general base catalyst, depending on its protonation state (3). 4-Oxalocrotonate tautomerase (4-OT) and phenylpyruvate tautomerase (PPT) are two examples where Pro-1 functions as a general base catalyst. It functions as a general base because it has a pK_a of 6.4 (4-OT) or 6.0 (PPT) so that Pro-1 exists largely in the unprotonated state at cellular pH (2,5).

4-OT is found in a bacterial pathway that degrades aromatic hydrocarbons (9). It exists as a hexamer where each monomer consists of 62 amino acids (11-13). It is proposed that 4-OT carries out a 1,3-allylic rearrangement where Pro-1 functions as a general base and abstracts a proton from C-3 of 2-oxo-4-hexenedioate (**1**, Scheme 1) to

form the dienol intermediate, 2-hydroxymuconate (**2**, Scheme 1) (14-19). This dienol intermediate then ketonizes to form the product, 2-keto-3-hexenedioate (**3**, Scheme 1).

Scheme 1

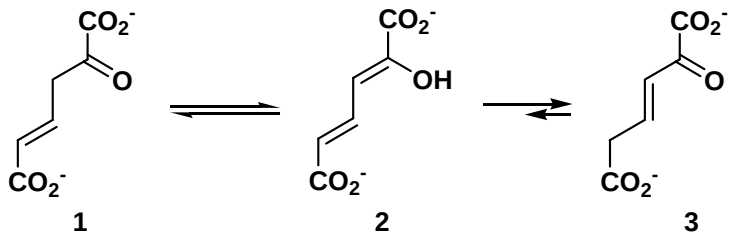

Pro-1 also functions as a general base catalyst in the PPT-catalyzed reaction. PPT converts phenylenolpyruvate (**4**, Scheme 2) to phenylpyruvate (**5,** Scheme 2) (5). The physiological significance of this reaction is not known. PPT is a trimer where each monomer has 114 amino acids (5). The monomers are roughly twice as large as those of 4-OT.

Scheme 2

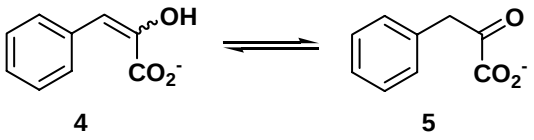

The discovery of the 1,3-dichloropropene catabolic pathway (Scheme 3) and the subsequent mechanistic and structural characterization of three enzymes in this pathway showed the versatility of Pro-1 (3). In *trans*-3-chloroacrylic acid dehalogenase (CaaD), *cis*-3-chloroacrylic acid dehalogenase (*cis*-CaaD), and malonate semialdehyde

decarboxylase (MSAD), Pro-1 functions as a general acid catalyst (3). In these three enzymes, Pro-1 is cationic and charged at cellular pH because it has a pK_a of 9.2 (3).

Scheme 3

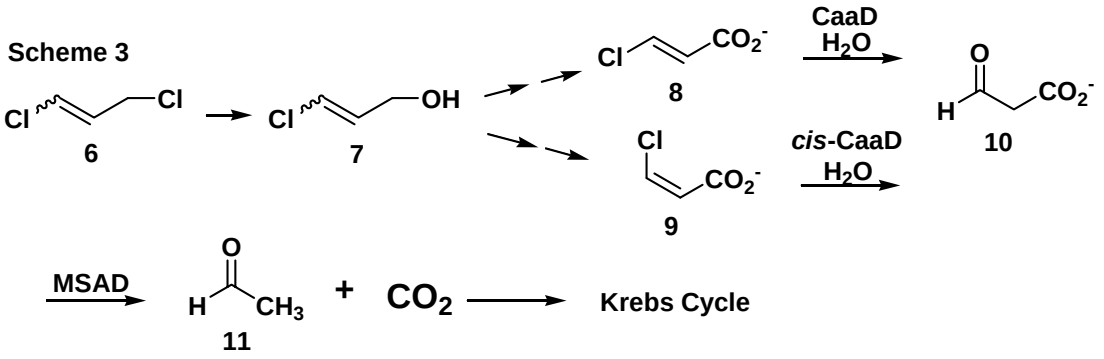

Janssen and co-workers first cloned and expressed CaaD and proposed that the enzyme adds water to *trans*-3-chloroacrylic acid (**8**, Scheme 4) to form an unstable halohydrin intermediate (**13**) (20). This halohydrin then collapses to release HCl and produce malonate semialdehyde (**10**, Scheme 4)**.** CaaD is a heterohexamer with 3 α-subunits (75 amino acids each) and 3 β-subunits (70 amino acids each). CaaD carries out this reaction without any cofactors.

Scheme 4

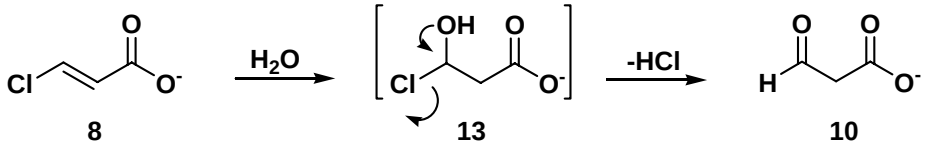

cis-CaaD was been cloned and expressed by Whitman et al. and is highly specific for the *cis*-isomer of 3-chloroacrylic acid (**9**, Scheme 5) (6). It was also proposed that

cis-CaaD adds water to **9** to form an unstable halohydrin intermediate (**13**). Like the proposed mechanism for CaaD, the halohydrin collapses to form HCl and malonate semialdehyde (**10**, Scheme 5). Unlike CaaD, *cis*-CaaD is a trimer where each monomer consists of 149 amino acids. *cis*-CaaD also carries out its reaction without any cofactors.

Scheme 5

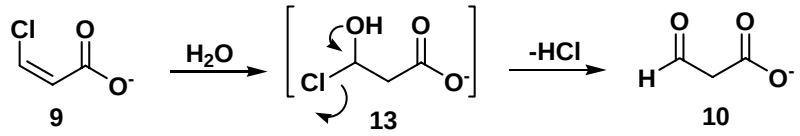

MSAD has also been cloned and expressed by Whitman and co-workers (7). It was determined to be a metal-ion independent decarboxylase. MSAD catalyzes the decarboxylation of malonate semialdehyde (**10**, Scheme 6) where the cationic Pro-1 may polarize the 3-keto group of **10**, and facilitate decarboxylation. Subsequent ketonization of the resulting enol yields **11**. MSAD is a trimer where each monomer consists of 129 amino acids.

Scheme 6

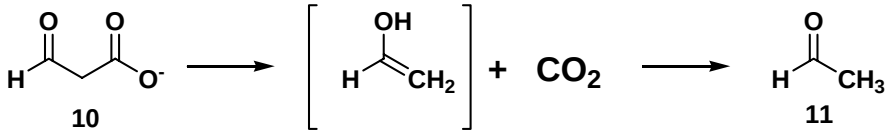

All three enzymes are found in a bacterial pathway that degrades 1,3-dichloropropene (**6**, Scheme 3) (3). The mixture of *cis*- and *trans*-1,3-dichloropropene is

the active ingredient in various nematocides marketed as Telone II and Shell D-D (10). These compounds are mixed into the soil to kill nematodes. This compound is rapidly degraded in soil in part to this pathway. In three enzyme-catalyzed steps, 1,3-dichloropropene (**6**) is converted to the *cis*- and *trans*- isomers of 3-chloroacrylic acid (2,10). CaaD and *cis*-CaaD then process the appropriate isomers of 3-chloroacrylic acid (**8** and **9**, respectively) to malonate semialdehyde (**10**). MSAD processes malonate semialdehyde to acetaldehyde (**11**), which is likely channeled into the Krebs Cycle.

The mechanistic and structural diversity in the tautomerase superfamily raise question about how these enzymes evolved. How enzymes evolve and how new enzymatic activities arise are two questions that have evoked much interest, discussion, and debate (21-24). There is a considerable body of evidence suggesting that many enzymes evolve from a common ancestor by divergent evolution. The growing number of superfamilies, with shared structural and functional features, provides strong support for divergent evolution (25-27). The common explanation for divergent evolution involves gene duplication of the parent enzyme followed by limited random mutagenesis to produce a new enzymatic function. The evolution of the new activity is driven by a selective advantage for the organism (e.g., frequently growth on alternative substrates). After the acquisition of a new activity, sequences likely diverge rapidly and markedly because there is little sequence identity among superfamily members (26a).

In the tautomerase superfamily, Nature has apparently fashioned new activities and structures by "stitching together" various combinations of the same simple structural unit, the β–α–β fold (1-3). Thus far, there are superfamily members made of short

monomers (4-OT, CaaD) and those made of longer monomers (PPT, *cis*-CaaD, and MSAD) (1-3). The lessons learned from studies of these enzymes and how Nature stitched the scaffold together have enormous implications and tremendous potential. If the principles used by Nature to create this diversity can be determined, it may be possible to mimic Nature's strategy and create new proline-based biocatalysts with designed activities using the β-α-β scaffold (2,3).

In addition to the fact that the β–α–β motif has been used in different ways to generate diverse reaction types and structures, tautomerase superfamily members have three unique advantages that make them particularly attractive experimental vehicles for study. The small monomer size, the absence of metal ions or coenzymes, and stability make them easily manipulated and amenable to study by a host of diverse techniques. These same features also make tautomerase superfamily members ideal candidates for the evolution of activities and the resulting insight into divergent evolution. The new constructs are readily purified, their activities determined, and the mechanism and structures delineated by many different techniques. These studies provide insight into the progenitors of these enzymes, suggest scenarios for the diversification of enzymatic function and mechanism within the tautomerase superfamily, and have implications for the evolution of metabolic pathways and enzymatic activities in general.

1.2 *trans*-3-Chloroacrylic Acid Dehalogenase (CaaD)

The genes (for the α- and β-subunits) for CaaD were initially cloned from *P. pavonaceae* strain 170, expressed, and the enzyme purified and characterized by Janssen et al (20). CaaD is a heterohexamer, consisting of 3 α-subunits, (75 amino acid residues),

and 3 β-subunits, (70 amino acid residues). Sequence analysis revealed similarities between the CaaD α-subunit and various 4-OT sequences (pairwise identities range from 23-35%) and the CaaD β-subunit and the same 4-OT sequences (pairwise identities range from 16-25%). This analysis implicated βPro-1 and αArg-11 as key catalytic residues, which was confirmed by site-directed mutagenesis (20). Based on the 4-OT mechanism, it was initially proposed that Pro-1 functioned as a base to activate water and Arg-11 interacted with the C-1 carboxylate group to facilitate the addition of water (20).

With this information in hand, studies on CaaD were continued by Whitman et al. An efficient expression system for CaaD and a direct UV assay for monitoring activity (instead of the cumbersome colorimetric assay) were developed (28). Product formation (i.e., **10** and the hydrate, Scheme 7) was verified by ^{1}H NMR spectroscopy and CaaD's behavior with three acetylene compounds (**15**, Scheme 8 and **19, 20**, Scheme 9) was examined. Compound **15**, 2-oxo-3-pentynoate, is a potent active-site-directed irreversible inhibitor of 4-OT (17), and it was anticipated that if βPro-1 functioned as a base, it would be covalently modified by **15**. Instead, it was found that CaaD processed **15** to acetopyruvate (**18)** quite efficiently (k_{cat} = 0.7 s^{-1}, K_m = 110 mM, k_{cat}/K_m = 6.4 $\times 10^3$ $M^{-1}s^{-1}$) (28). [CaaD processes **8** to **10** with a k_{cat} = 3.8 s^{-1}, a K_m = 31 mM, and a k_{cat}/K_m = 1.2 $\times 10^5$ $M^{-1}s^{-1}$] (28). This was the first indication that there were differences between CaaD and 4-OT. It was proposed that CaaD initiates the Michael addition of water to C-4 of **15** to form **16** (Scheme 8) (28). Protonation at C-3 of **16** leads to **17**, which can, in turn, ketonize to afford acetopyruvate (**18**).

Scheme 7

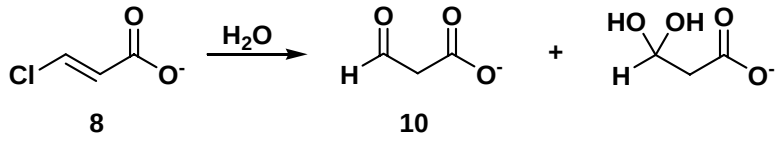

8 10

Scheme 8

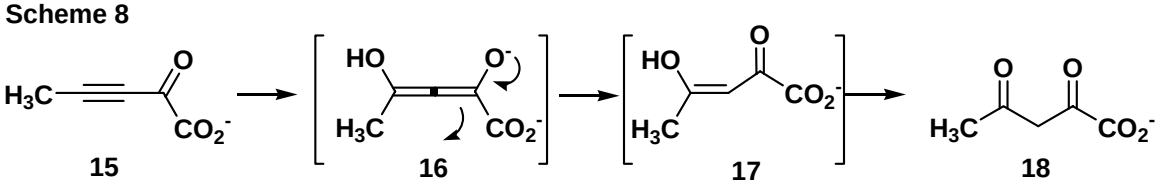

15 16 17 18

The conversion of **15** to **18** suggested that CaaD might also add water to the 3-halopropiolic acids (**19** and **20**, Scheme 9), transforming them into mechanism-based inhibitors. Indeed, it was found that **19** and **20** are potent irreversible inhibitors of CaaD (28). In one mechanism, hydration of these compounds results in the formation of an unstable enol, which ketonizes to an acyl halide (**21**, Scheme 9). Alternatively, the enol can directly expel halide to form a ketene. Subsequent reaction with an active site nucleophile inactivates the enzyme. Mass spectral analysis showed that the site of inactivation is βPro-1. It should be noted that the initial hydration of **19** or **20** by CaaD will presumably remove a proton from βPro-1, making it nucleophilic.

Scheme 9

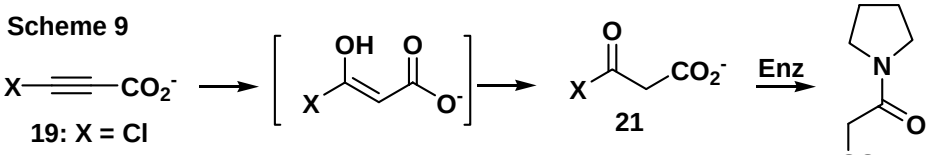

19: X = Cl
20: X = Br

21 22

A crystal structure of CaaD inactivated by **20** was obtained (29). The geometry of the complex identified a new catalytic residue, αGlu-52, and suggested that it activates water for nucleophilic attack while βPro-1 functions as a general acid catalyst (Scheme 10). The 3-carbonyl oxygen in **22** (Scheme 9) is likely derived from water so that the observed hydrogen bond distance between this oxygen and the oxygen of αGlu-52 indicates that αGlu-52 is no longer ionized due to the abstraction of a proton from a water molecule (29). The complex also identified αArg-8 as a second residue, which, along with αArg-11, binds to the carboxylate group of **8** (thus facilitating catalysis). Site-directed mutagenesis confirmed the importance of both αGlu-52 and αArg-8 to the mechanism (29). There was no detectable CaaD activity for the αE52Q mutant even after an extended (24 h) incubation period. The activity observed after extended incubation times reflects slow catalysis, but should not be confused with a "resuscitation" of the enzyme. The αR8A mutant has a small amount of activity over a 24-h incubation period. The βP1A mutant has no detectable activity within a 24-h incubation period but the αR11A mutant retains a small amount of activity. Finally, an NMR titration of the ^{15}N-labeled CaaD showed that βPro-1 has a pK_a of 9.2 (30). Hence, CaaD became the first tautomerase superfamily member where Pro-1 functioned as an acid catalyst and not a base catalyst. These studies led to the current working hypothesis for CaaD (Scheme 10). The mechanism can be extrapolated to provide a mechanism for the hydration of **15** (Scheme 11).

Scheme 10

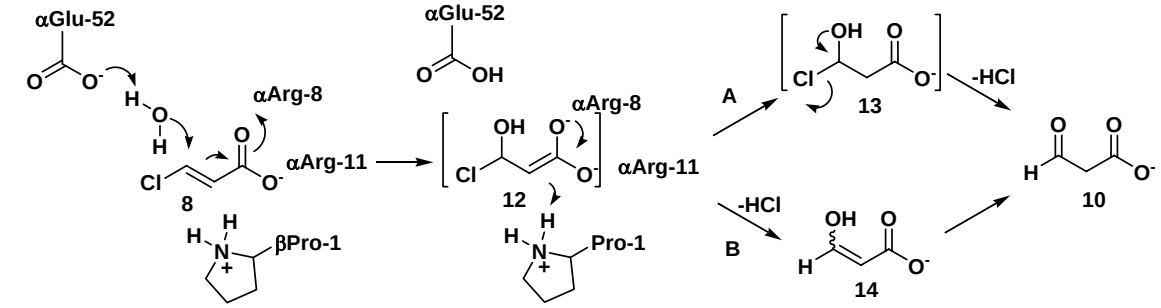

Scheme 11

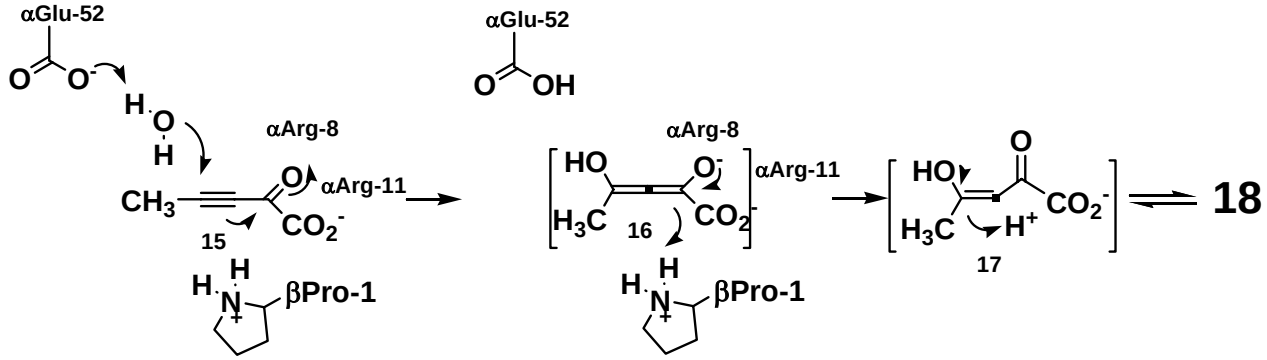

1.3 *cis*-3-Chloroacrylic Acid Dehalogenase (*cis*-CaaD)

The observation that both isomers of 1,3-dichloropropene (**6**, Scheme 3) were processed by various bacteria suggested that a *cis*-CaaD might be present in these bacteria. Indeed a *cis*-CaaD was isolated from coryneform bacterium strain FG41 in 1992 (10). The enzyme was purified and a large fragment sequenced. It was reportedly a dimer or trimer consisting of 16.2 kDa subunits (10b). A comparison of its N-terminal amino acid sequence (48 amino acids) with the α- and β- subunits of CaaD revealed little sequence identity, but the amino-terminal proline was conserved.

With this information in hand, the gene for *cis*-CaaD from coryneform bacterium strain FG41 was cloned, expressed, and subsequently the protein product was purified and characterized (6). The enzyme is a trimer where each monomer consists of 149 amino acids. Like CaaD, it is highly isomer specific. Sequence alignment and structural analysis implicated Pro-1, Arg-70, Arg-73, and Glu-114 as active-site residues (6). Site-directed mutagenesis experiments confirmed their importance. Once again, the acetylene compounds, (**15**, Scheme 8 and **19** and **20**, Scheme 9) were processed by *cis*-CaaD to products consistent with an enzyme-catalyzed hydration reaction previously established for CaaD (6). Hydration of **15** afforded **18** (although not as efficiently as CaaD) while the 3-halopropiolates (e.g., **19** and **20**) are irreversible inhibitors that covalently modify Pro-1. In addition, pH profiles suggested that an acid catalyst (pK_a of 9.3) is required for activity (6). Although the pK_a of Pro-1 has not yet been determined by direct NMR titration, the pK_a is likely that of Pro-1. These results suggested an initial mechanism for *cis*-CaaD that parallels that of CaaD (Scheme 10, replacing αGlu-52 with Glu-114, αArg-8 with Arg-70, αArg-11 with Arg-73, and βPro-1 with Pro-1) (6).

Mutagenesis results and inhibition studies uncovered differences between the CaaD and *cis*-CaaD mechanisms (with potential evolutionary implications). The first difference emerged from a comparison of mutagenesis results (6). The αE52Q mutant of CaaD is *more inactive* than the E114Q mutant of *cis*-CaaD. The E114Q-*cis*-CaaD has diminished activity (~10-fold decrease in k_{cat}/K_m), but clearly shows activity without resorting to a 24-h incubation period. This observation suggested that water activation is more complex (i.e., more residues involved) in *cis*-CaaD than it is in CaaD. The second

difference came from inhibition studies using (*R*)- and (*S*)-oxriane-2-carboxylate (**23**, Scheme 12) (31). Only *cis*-CaaD is inactivated (irreversibly) and only by the *R*-enantiomer. It was also found that Pro-1, Arg-70, and Arg-73 are required for covalent modification (i.e., the P1A, R70A, and R73A mutants are not modified), but Glu-114 is not required (i.e., the E114Q mutant is covalently modified). Mass spectral analysis showed (once again) that Pro-1 is the site of covalent modification.

The crystal structures of native *cis*-CaaD and *cis*-CaaD inactivated by (*R*)-**23** (32) were solved. The observations gleaned from these two structures have four major implications. First, the native structure identified Tyr-103 and His-28 as additional catalytic residues. The structures suggest that Tyr-103 assists Glu-114 in the activation of water and His-28 assists Arg-70/Arg-73 in the activation of substrate through an interaction with the carboxylate group. These observations and mutant analysis suggest that water activation is more important to catalysis in CaaD whereas substrate activation is more important in *cis*-CaaD. Second, the inactivated structure confirmed the nature of the covalent adduct (e.g., **24**, Scheme 12), established that C3 of **23** is the site of nucleophilic attack by Pro-1 (as the neutral form, which, under the pH conditions of the inactivation experiments, is present in ~1%), and implicated His-28 as a major determinant in positioning (*R*)-**23** for alkylation of Pro-1 and subsequent inactivation. Third, His-28 and Tyr-103 appear to be two determinants of the *cis*-CaaD substrate specificity. Finally, the results are consistent with the proposal that *cis*-CaaD and CaaD form two separate lineages that followed the independent duplication of a 4-OT-like sequence (32).

Scheme 12

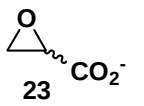

23

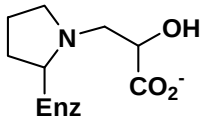

24

The crystal structure of the inactivated *cis*-CaaD [by (*R*)-**23**] and mutant analysis suggest a mechanism for inactivation, a structural basis for the stereospecificity of the reaction [i.e., only the (*R*)-enantiomer inactivates *cis*-CaaD], and a rationale for the observation that CaaD is not inactivated by either enantiomer of **23** (32). The interactions in the crystal structure suggest that Arg-73 and His-28 are involved in binding the carboxylate of (*R*)-**23** (Scheme 13A) and that Arg-70 may facilitate ring opening by direct interaction with the epoxide oxygen or by placing a water molecule in position to interact with the epoxide oxygen (32). If (*S*)-**23** binds with similar interactions between the carboxylate group and Arg-73 and His-28 (Scheme 13B), the C3 carbon is directed away from Pro-1 and towards Arg-70. This binding mode precludes alkylation. The absence of His-28 in CaaD suggests that the carboxylate group of **23** might now interact with both arginines (in CaaD, αArg-8 and αArg-11). This interaction would prevent one of the arginines from functioning as the required proton donor (32).

Scheme 13

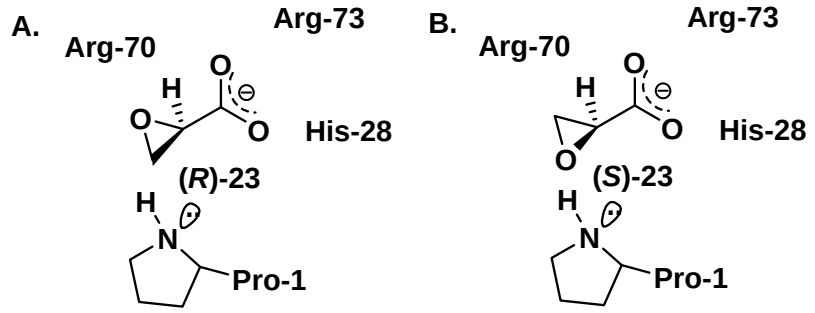

With regard to substrate specificity, a comparison of the *cis*-CaaD and CaaD structures offers an explanation (29,32). In *cis*-CaaD, the carboxylate group of **9** is bound by the His-28/Arg-70/Arg-73 cluster, such that the substrate is directed towards the enzyme's surface (32). In CaaD, the carboxylate group of the substrate is bound by the αArg-8/αArg-11 pair, with the remainder of the substrate projecting deeper into the active site (29). The substrate-binding pockets fit the shape of their respective substrates, that is, the pocket of *cis*-CaaD is more U-shaped, whereas the pocket of CaaD is more elongated. One of the residues responsible for this shape difference is Tyr-103 (αVal-41 in CaaD). In CaaD, αVal-41 creates a hydrophobic region allowing the 3-chloro moiety of **8** to bind between αPhe-39 and αPhe-50. The presence of the larger Tyr-103 residue in *cis*-CaaD effectively blocks the binding of the 3-chloro group of **8**. Instead, a hydrophobic pocket formed by the side chains of Thr-34, Leu-38 and Leu-119 could favor the binding of the 3-chloro moiety of **9**. Thus, His-28 and Tyr-103 might be two determinants of *cis*-CaaD's specificity (32).

1.4 Malonate Semialdehyde Decarboxylase (MSAD)

Janssen et al. reported that the genes for the CaaD α- and β-subunits are found in a cluster (in *P. pavonaceae* 170) that includes two additional open reading frames located immediately downstream (20). One, *orf130*, was hypothesized to function as a malonate semialdehyde decarboxylase (MSAD) (20). The other open reading frame likely encodes a dehydrogenase, based on sequence analysis. Hence, the *orf130* gene was cloned and expressed, and the protein product was purified and characterized (7). MSAD is a trimer where each subunit consists of 129 amino acids. The enzyme was shown to carry out a metal-ion independent decarboxylation reaction (using **10** in Scheme 6, and generating **11** and the hydrate). Sequence analysis uncovered a relationship with the tautomerase superfamily (but representing yet another new family) and implicated Pro-1 and Arg-75 as potential active site residues. Site-directed mutagenesis confirmed the importance of these residues for activity.

It was proposed that MSAD could proceed through a Schiff base mechanism or one in which a cationic Pro-1 polarized the 3-carbonyl group of **10** (33). A distinguishing feature between mechanisms is the ionization state of Pro-1. Accordingly, the behavior of MSAD with **15** (Scheme 8) was determined and the pK_a of Pro-1was measured by direct ^{15}N NMR titration (using uniformly ^{15}N-labeled enzyme) (33).

MSAD converts **15** to **18** (Scheme 8), a process which also required Pro-1 and Arg-75. Hence, MSAD is a decarboxylase with a promiscuous hydratase activity. In addition, the pK_a of Pro-1 was determined to be ~9.2 by NMR titration (33). These observations argued against a Schiff base mechanism and in favor of the mechanism

where Pro-1 polarizes the carbonyl oxygen of substrate by hydrogen bonding and/or an electrostatic interaction (Scheme 14). Arg-75 is postulated to position the carboxylate group in a favorable orientation for decarboxylation. In view of the promiscuous hydratase activity (uncovered by the conversion of **15** to **18**), MSAD was incubated with the potential mechanism-based inhibitors, **19** and **20** (Scheme 9) (34). Analysis showed that both compounds inactivated MSAD and, once again, Pro-1 was the site of modification (34). It is presumed that the initial hydration of **19** or **20** by MSAD removes a proton from Pro-1 making it nucleophilic.

Scheme 14

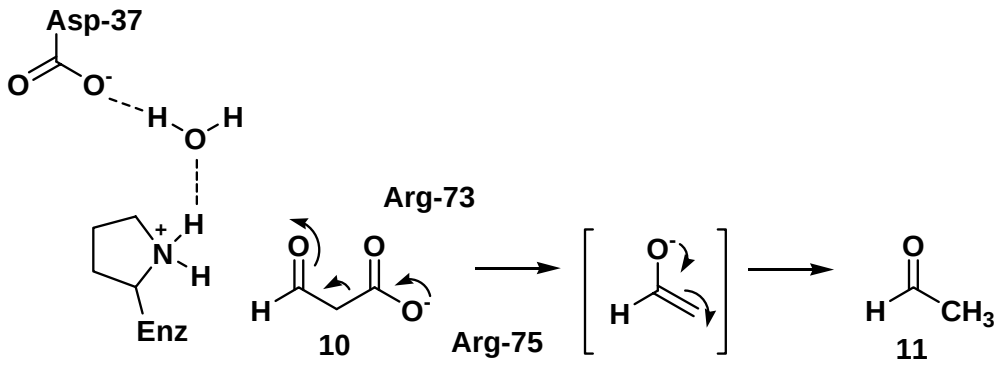

Subsequently, crystal structures of native MSAD, the P1A mutant, and MSAD inactivated by **19** were determined (35). The structures confirm that MSAD is metal-ion independent (i.e., there is no metal ion in the active despite the high concentrations in crystallization buffers). The P1A mutant structure is nearly identical to that of the native structure (except for the mutation) suggesting that the loss of activity associated with this mutant does not result from a structural defect. In the structure of MSAD inactivated by

19, the positioning of the 3-oxopropanoate adduct (**22**, Scheme 9) implicated Asp-37 and Arg-73 as two additional catalytic residues in the decarboxylation and hydration mechanisms. The importance of these residues to both mechanisms was confirmed by site-directed mutagenesis. These observations and all of the preceding mechanistic work led to the current working hypotheses for the hydration and decarboxylation mechanisms (Schemes 11 and 14).

The decarboxylation mechanism is summarized in Scheme 14. Asp-37 may play an indirect role in the decarboxylase activity as it may be partially responsible for the observed pK_a of Pro-1 (~9.2) (35). This putative role for Asp-37 is based on its observed participation in the hydrogen bond network. The proposed mechanism for the hydration of **15** parallels that of CaaD (Scheme 11) where Asp-37 replaces αGlu-52, Arg-73/Arg-75 replace αArg-8/αArg-11, and Pro-1 replaces βPro-1. Asp-37 could activate a water molecule for nucleophilic attack at C-4 of **15** to initiate the Michael addition of water. Arg-73 and Arg-75 could polarize the carbonyl oxygen and assist in binding of the carboxylate group. Pro-1 is an obvious candidate to provide a proton at C-3 to complete the Michael addition of water. Ketonization of **17** to **18** could be enzyme-catalyzed or a non-enzymatic process.

1.5 Evolution of *trans*-3-Chloroacrylic Acid Dehalogenase, *cis*-3-Chloroacrylic Acid Dehalogenase, and Malonate Semialdehyde Decarboxylase

Various scenarios have been proposed for the evolution of CaaD, *cis*-CaaD, and MSAD. For CaaD and *cis*-CaaD, the conservation of the β–α–β fold and the key functional groups [Pro-1, αArg8/αArg11, Arg-70/Arg-73, and αGlu-52/Glu-114]

indicate that the two enzymes are related by divergent evolution from a common ancestor (32). The different oligomer structures (heterohexamer vs trimer) and low sequence identity (<20%) indicate that CaaD and *cis*-CaaD diverged some time ago. The presence of His-28 and Tyr-103 in the *cis*-CaaD active site (*and* the low sequence identity) invoke a scenario in which *cis*-CaaD evolved from an independent gene duplication event of a small β–α–β gene (e.g., a 4-OT-like gene) followed by gene fusion (32). CaaD also might have evolved from gene duplication of a small β–α–β gene, but the two genes co-evolved to form the two subunits of CaaD.

The similarities between CaaD/*cis*-CaaD and MSAD and the fact that they catalyze successive reactions in the 1,3-dichloropropene catabolic pathway suggest that they may have also evolved by "retrograde evolution" in that they diverged from an ancestral enzyme that catalyzed both reactions (21,35). For CaaD and MSAD, the two enzymes are structurally homologous and key catalytic residues (Pro-1 and the two arginines) are positionally conserved (35). These observations are significant in view of the functional similarities between the enzymes. Both function as hydratases, converting **15** to **18**, and both use Pro-1 (with a pK_a of ~9.2) and conserved arginines to catalyze this reaction as well as their physiological reactions (35). Finally, as a result of the hydration reaction, the 3-halopropiolates are converted to reactive species that alkylate and inactivate both enzymes.

In one scenario, the ancestral enzyme may have functioned primarily as a hydratase because the hydration of **8**, an α,β-unsaturated acid, is the chemically more difficult reaction. A random encounter of **10** with the cationic Pro-1 could result in

decarboxylation and make this ancestral hydratase an accidental decarboxylase. In this scenario, gene duplication (and gene fusion) gave rise to separate enzymes that retained the components for the hydration reaction along with the rudimentary decarboxylase activity. Enhancement of the accidental decarboxylase activity could result from a limited number of mutations that increased the probability of encounter and optimized the position of **11** with respect to the cationic Pro-1 and introduced additional catalytic elements to facilitate decarboxylation. The hydratase activity of MSAD is then a remnant.

1.6 Cg10062, a *cis*-Chloroacrylc Acid Dehalogenase Homologue, from *Corynebacterium glutamicum*

In the characterization of the *cis*-CaaD family, a 149-amino acid *cis*-CaaD homologue from *C. glutamicum*, designated Cg10062 was identified (6). The physiological function of Cg10062, (which will be called CgX hereafter), is unknown and the gene has no apparent genomic context. The protein shares 34% sequence identity (and 53% similarity) with *cis*-CaaD and the residues implicated as critical ones for *cis*-CaaD activity are present (Pro-1, His-28, Arg-70, Arg-73, Tyr-103, Glu-114) (6,32). The gene has been cloned, the protein overexpressed, purified, and subjected to kinetic and mechanistic characterization. There is ^{1}H NMR spectroscopic evidence showing that CgX has *cis*-CaaD and CaaD activity. The *cis*-CaaD activity is greater than that of CaaD. Like CaaD, *cis*-CaaD, and MSAD, the protein is inactivated by **19** and **20**, and converts **15** to **18**.

The mechanism of CgX is intriguing for three major reasons. First, it could serve as a future template for the evolution of *cis*-CaaD and CaaD, and recapitulate the

emergence of isomer specificity. Second, CgX has the six core catalytic residues found in *cis*-CaaD but is a very poor *cis*-CaaD. It would be interesting to determine the factors that account for the decreased activity. Third, an analysis of the structural factors responsible for CgX's relaxed specificity could provide a more complete understanding of the substrate specificity of CaaD and *cis*-CaaD. For these reasons, studies of CgX were pursued in this dissertation.

1.7 Summary

The preceding mechanistic, mutagenesis, and structural studies of CaaD, *cis*-CaaD, and MSAD established minimal mechanisms for each enzyme (Schemes 10 and 14). These studies have also uncovered intriguing similarities, fascinating differences, and tantalizing evolutionary histories for the three enzymes. However, many mechanistic and evolutionary questions remain unanswered. For example, in CaaD, the actual interactions of the arginine pair (αArg-8/αArg-11 in Scheme 10) with substrate are not known. Moreover, it seems unusual that two arginines are necessary for substrate activation (i.e., polarization of the carboxylate group of **8**). The structural basis for the pK_a of Pro-1 is unknown as well as the observation that Pro-1 is so critical for activity. These same questions apply to *cis*-CaaD with some differences. It is interesting that the *cis*-CaaD reaction requires additional groups for water activation (i.e., Tyr-103 and Glu-114) and substrate activation (an arginine pair, Arg-70/Arg-73, and His-28). It is also intriguing that water activation appears to be more important in CaaD and substrate activation may be more important for *cis*-CaaD. The structural basis for the isomer specificity is also not known.

For both enzymes, it is not known if there is a halohydrin (e.g., **13**, Scheme 10) or an enol (e.g., **14**) intermediate, and whether either of these putative intermediates undergoes chemical or enzymatic decay (and what groups are involved) to yield product, **10**. It is also not known if CaaD and *cis*-CaaD are physiological dehalogenases or "accidental" dehalogenases. As a physiological dehalogenases, one anticipates that the steps after water addition are enzyme-catalyzed and that there may be a halide-binding pocket. As a physiological hydratase (of an unknown substrate), CaaD may just catalyze the addition of water to various α,β-unsaturated acids (including **8** and **9**). Addition of water to **8** or **9** results in **13**, which could undergo rapid chemical decay.

This dissertation focused on the feasibility and execution of kinetic studies of *cis*-CaaD and CaaD, and inactivation studies of CgX. First, methodology was developed to carry out a pre-steady-state kinetic analysis of CaaD, *cis*-CaaD, and various mutants. Second, the methodology was used in stopped flow and rapid chemical quench experiments on *cis*-CaaD. These experiments resulted in a kinetic mechanism for *cis*-CaaD. Stopped flow experiments were also carried out on the αF39W-CaaD mutant (introducing a fluorophore) and selected mutants of *cis*-CaaD. The completion and comparison of the results may show whether the observed macroscopic properties (substrate activation vs water activation, for example) occur due to differences in kinetic mechanisms, microscopic rate constants, or a combination. The results may also be more informative about how a mutation affects a particular step in the mechanism and the extent to which that mutation impacts the particular step. Finally, the behavior of CgX with the enantiomeric epoxides [e.g., (*R*)- and (*S*)-**23**, Scheme 12] was examined.

Although the (*R*)-enantiomer is more potent, both enantiomers inactivate CgX with Pro-1 being the site of modification. The results set the stage for crystallographic analysis, which may provide insight into structural basis for the relaxed specificity of CgX.

1.8 References

1. Murzin, A.G. (1996) Structural classification of proteins: new superfamilies, *Curr. Opin. Struct. Biol*. *6*, 386-394.

2. Whitman, C.P. (2002) The 4-oxalocrotonate tautomerase family of enzymes: how nature makes new enzymes using a β-α-β structural motif, *Arch. Biochem. Biophys. 402*, 1-13.

3. Poelarends, G.J., Whitman, C.P. (2004) Evolution of enzymatic activity in the tautomerase superfamily: mechanistic and structural studies of the 1,3-dichloropropene catabolic enzymes, *Bioorg. Chem. 32*, 376-92.

4. (a) Sparnins, V.L., Chapman, P.J., Dagley, S. (1974) Bacterial degradation of 4-hydroxyphenylacetic acid and homoprotocatechuic acid, *J. Bacteriol. 120*, 159-167. (b) Jenkins, J.R., Cooper, R.A. (1988) Molecular cloning, expression, and analysis of the genes of the homoprotocatechuate catabolic pathway of *Escherichia coli C*, *J. Bacteriol. 170*, 5317-5324.

5. (a) Suzuki, M., Sugimoto, H., Nakagawa, A., Tanaka, I., Nishihira, J., Sakai, M.(1996) Crystal structure of the macrophage migration inhibitory factor from rat liver, *Nat. Struct. Biol. 3*, 259-266. (b) Sun, H.-W., Bernhagen, J., Bucala, R., Lolis, E. (1996) Crystal structure at 2.6 Å resolution of human macrophage migration inhibitory factor, *Proc. Natl. Acad. Sci. 93*, 5191-5196. (c) Rosengren, E., Aman, P., Thelin, S., Hansson, C., Ahlfors, S., Bjork, P., Jacobsson, L., Rorsman, H. (1997) The macrophage migration inhibitory factor MIF is a phenylpyruvate tautomerase, *FEBS Lett. 417*, 85-88. (d) Lubetsky, J.B., Swope, M., Dealwis, C., Blake, P. Lolis, E. (1999) Pro-1 of macrophage migration inhibitory factor functions as a catalytic base in the phenylpyruvate tautomerase activity, *Biochemistry 38*, 7346-7354.

6. Poelarends, G. J., Serrano, H., Person, M. D., Johnson, W. H., Jr., Murzin, A. G., Whitman, C.P. (2004) Cloning, expression, and characterization of a *cis*-3-chloroacrylic acid dehalogenase: insights into the mechanistic, structural, and evolutionary relationship between isomer-specific 3-chloroacrylic acid dehalogenases, *Biochemistry 43*, 759-772.

7. Poelarends, G.J., Johnson, W.H.,Jr., Murzin, A.G., Whitman, C.P. (2003) Mechanistic characterization of a bacterial malonate semialdehyde decarboxylase: identification of a new activity in the tautomerase superfamily, *J. Biol. Chem. 278*, 48674-48683.

8. Almrud, J.J., Kern, A.D., Wang, S.C., Czerwinski, R.M., Johnson, W.H., Jr., Murzin, A.G., Hackert, M.L., Whitman, C.P. (2002) The crystal structure of YdcE, a

4-oxalocrotonate tautomerase homologue from *Escherichia coli*, confirms the structural basis for oligomer diversity, *Biochemistry 41*, 12010-12024.

9. (a) Harayama, S., Lehrbach, P.R., Timmis, K.N. (1984) Transposon mutagenesis analysis of *meta*-cleavage operon genes of the TOL plasmid of *Pseudomonas putida mt-2*, *J. Bacteriol. 160*, 251-255. (b) Harayama, S., Rekik, M., Ngai, K.-L., Ornston, L.N. (1989) Physically associated enzymes produce and metabolize 2-hydroxy-2,4-dienoate, a chemically unstable intermediate formed in catechol metabolism via *meta* cleavage in *Pseudomonas putida*, *J. Bacteriol.*, *171*, 6251-6258.

10. (a) Hartmans, S., Jansen, M.W., van der Werf, M.J., de Bont, J.A.M. (1991) Bacterial metabolism of 3-chloroacrylic acid, *J. Gen. Microb. 137*, 2025-2032. (b) Van Hylckama Vlieg, J.E.T., Janssen, D.B. (1992) Bacterial degradation of 3-chloroacrylic acid and the characterization of *cis*- and *trans*-specific dehalogenases, *Biodegradation 2*, 139-150. (c) Poelarends, G.J., Wilkens, M., Larkin, M.J., van Elsas, J.D., Janssen, D.B. (1998) Degradation of 1,3-dichloropropene by *Pseudomonas cichorii* 170, *Appl. Environ. Microbiol. 64*, 2931-2936.

11. Whitman, C.P., Aird, B.A., Gillespie, W.R., Stolowich, N.J. (1991) Chemical and enzymatic ketonization of 2-hydroxymuconate, a conjugated enol, *J. Am. Chem. Soc. 113*, 3154-3162.

12. Whitman, C.P., Hajipour, G., Watson, R.J., Johnson, Jr., W.H., Bembenek, M.E., Stolowich, N.J., (1992) Stereospecific ketonization of 2-hydroxymuconate by 4-oxalocrotonate tautomerase and 5-(carboxymethyl)-2-hydroxymuconate isomerase, *J. Am. Chem. Soc. 114*, 10104-10110.

13. Chen, L.H., Kenyon, G.L., Curtin, F., Harayama, S. Bembenek, M.E., Hajipour, G., Whitman, C.P. (1992) 4-Oxalocrotonate tautomerase, an enzyme composed of 62 amino acid residues per monomer, *J. Biol. Chem. 267*, 17716-17721.

14. Subramanya, H.S., Roper, D.I., Dauter, Z., Dodson, E.J., Davies, G.J., Wilson, K.S., Wigley, D.B. (1996) Enzymatic ketonization of 2-hydroxymuconate: specificity and mechanism investigated by the crystal structures of two isomerases, *Biochemistry 35*, 792-802.

15. Stivers, J.T., Abeygunawardana, C., Mildvan, A.S., Hajipour, G., Whitman, C.P., Chen, L.H. (1996) The catalytic role of the amino-terminal proline in 4-oxalocrotonate tautomerase: affinity labeling and heteronuclear NMR studies, *Biochemistry 35*, 803-813.

16. Stivers, J.T., Abeygunawardana, C., Mildvan, A.S., Hajipour, G., Whitman, C.P. (1996) 4-Oxalocrotonate tautomerase: pH dependence of catalysis and pK_a values of active site residues, *Biochemistry 35*, 814-823.

17. (a) Johnson Jr., W.H., Czerwinski, R. M., Fitzgerald, M.C., Whitman, C.P. (1997) Inactivation of 4-oxalocrotonate tautomerase by 2-oxo-3-pentynoate, *Biochemistry 36*, 15724-15732. (b) Taylor, A.B., Czerwinski, R. M., Johnson Jr., W. H., Whitman, C.P., Hackert, M.L. (1998) Crystal structure of 4-oxalocrotonate tautomerase inactivated by 2-oxo-3-pentynoate at 2.4 Å resolution: analysis and implications for the mechanism of inactivation and catalysis, *Biochemistry 37*, 14692-14700.

18. Harris, T.K., Czerwinski, R. M., Johnson Jr., W.H., Legler, P.M., Abeygunawardana, C., Massiah, M.A., Stivers, J.T., Whitman, C.P., Mildvan, A.S. (1999) Kinetic, stereochemical, and structural effects of mutations of the active site arginine residues in 4-oxalocrotonate tautomerase, *Biochemistry 38*, 12343-12357.

19. Czerwinski, R. M., Harris, T.K., Johnson Jr., W.H., Legler, P.M., Stivers, J.T., Mildvan, A.S., Whitman, C.P. (1999) Effects of mutations of the active site arginine residues in 4-oxalocrotonate tautomerase on the pK_a values of active site residues and on the pH dependence of catalysis, *Biochemistry 38*, 12358-12366.

20. Poelarends, G.J., Saunier, R., Janssen, D.B. (2001) *trans*-3-Chloroacrylic acid dehalogenase from *Pseudomonas pavonaceae* 170 shares structural and mechanistic similarities with 4-oxalocrotonate tautomerase, *J. Bacteriol. 183*, 4269-4277.

21. Horowitz, N.H. (1945) On the evolution of biochemical syntheses, *Proc. Natl. Acad. Sci. USA, 31*, 153-157.

22. Jensen, R.A. (1976) Enzyme recruitment in evolution of new function, *Ann. Rev. Microbiol. 30*, 409-25.

23. (a) Hughes, A.L. (1994) The evolution of functionally novel proteins after gene duplication, *Proc. R. Soc. London Ser. B 256* 119-124. (b) Hughes, A.L. (2005) Gene duplication and the origin of novel proteins, *Proc. Natl. Acad. Sci. USA, 102*, 8791-8792.

24. (a) Perona, J.J., Craik, C.S. (1997) Evolutionary divergence of substrate specificity within the chymotrypsin-like serine protease fold, *J. Biol. Chem. 272*, 29987-29990. (b) Babbitt, P.C., Gerlt, J.A. (1997) Understanding enzyme superfamilies, *J. Biol. Chem. 272*, 30591-30594. (c) Neidhart, D.J., Kenyon, G.L., Gerlt, J.A., Petsko, G.A. (1990) Mandelate racemase and muconate lactonizing enzyme are mechanistically distinct and structurally homologous, *Nature 347*, 692-694.

25. (a) Babbitt, P.C., Gerlt, J.A. (2001) New functions from old scaffolds: how nature reengineers enzymes for new functions, *Adv. in Protein Chem. 55*, 1-28. (b) Holden, H.M., Benning, M.M., Haller, T., Gerlt, J. A. (2001) The crotonase superfamily: divergently related enzymes that catalyze different reactions involving acyl coenzyme A thioesters, *Acc. Chem. Res. 34*, 145-157. (c) Gerlt, J.A., Raushel, F.M.

(2003) Evolution of function in $(\beta/\alpha)_8$-barrel enzymes, *Curr. Opin. Chem. Biol. 7*, 252-264. (d) Gerlt, J.A., Babbitt, P.C., Rayment, I. (2005) Divergent evolution in the enolase superfamily: the interplay of mechanism and specificity, *Arch. Biochem. Biophys.* 433, 59-70.

26. (a) O'Brien, P.J., Herschlag, D. (1999) Catalytic promiscuity and the evolution of new enzymatic activities, *Chem. Biol. 6*, R91-R105. (b) O′Brien, P.J., Herschlag, D. (2001) Functional interrelationships in the alkaline phosphatase superfamily: phosphodiesterase activity of *Escherichia coli* alkaline phosphatase, *Biochemistry 40*, 5691-5699. (c) Copley, S.D. (2003) Enzymes with extra talents: moonlighting functions and catalytic promiscuity, *Curr. Opin. Chem. Biol. 7*, 265-272. (d) Yoshikuni, Y., Ferrin, T.E., Keasling, J.D. (2006) Designed divergent evolution of enzyme function, *Nature 440*, 1078-1082.

27. (a) Roodveldt, C., Tawfik, D.S. (2005) Shared promiscuous activities and evolutionary features in various members of the amidohydrolase superfamily, *Biochemistry 44*, 12728-12736. (b) Aharoni, A., Gaidukov, L., Khersonsky, O., McQ Gould, S., Roodveldt, C., Tawfik, D.S. (2005) The ′evolvability′ of promiscuous protein functions, *Nat. Genet. 37*, 73-76.

28. Wang, S.C., Person, M.D., Johnson, W.H., Jr., Whitman, C.P. (2003) Reactions of *trans*-3-chloroacrylic acid dehalogenase with acetylene substrates: consequences of and evidence for a hydration reaction, *Biochemistry 42*, 8762-8773.

29. de Jong, R.M., Brugman, W., Poelarends, G.J., Whitman, C.P., Dijkstra, B.W. (2004) The X-ray structure of *trans*-3-chloroacrylic acid dehalogenase reveals a novel hydration mechanism in the tautomerase superfamily, *J. Biol. Chem. 279*, 11546-11552.

30. Azurmendi, H.F., Wang, S.C., Massiah, M.A., Poelarends, G.J., Whitman, C.P., Mildvan, A.S. (2004) The roles of active-site residues in the catalytic mechanism of *trans*-3-chloroacrylic acid dehalogenase: a kinetic, NMR, and mutational analysis, *Biochemistry 43*, 4082-4091.

31. Poelarends, G.J., Serrano, H., Johnson, Jr., W.H., Whitman, C.P. (2004) Stereospecific alkylation of *cis*-chloroacrylic acid dehalogenase by (*R*)-oxirane-2-carboxylate: Analysis and Mechanistic Implications, *Biochemistry 43*, 7187-7196.

32. de Jong, R.M., Bazzacco, P., Poelarends, G.J., Johnson, Jr, W.H., Kim, Y.-J., Burks, E.A., Serrano, H., Whitman, C.P., Dijkstra B.W., Crystal Structures of Wild Type and Inactivated *cis*-3-Chloroacrylic Acid Dehalogenase: The Structural Basis for Substrate Specificity and Inactivation by (*R*)-Oxirane-2-carboxylate, *J. Biol. Chem. 282*, 2440-2449 (2007).

33. Poelarends, G.J., Serrano, H., Johnson, Jr., W.H., Hoffman, D.W., Whitman, C.P. (2004) The hydratase activity of malonate semialdehyde decarboxylase: mechanistic and evolutionary implications, *J. Am. Chem. Soc*. *126*, 15658-15659 (2004).

34. Poelarends, G.J., Serrano, H., Johnson, Jr., W.H., Whitman, C.P. (2005) Inactivation of malonate semialdehyde decarboxylase by 3-halopropiolates: evidence for the hydratase activity, *Biochemistry 44*, 9375-9381.

35. Almrud, J.J., Poelarends, G.J., Johnson, Jr., W.H., Serrano, H., Hackert, M.L., Whitman, C.P. (2005) Crystal structures of the wild-type, P1A mutant, and inactivated malonate semialdehyde decarboxylase: a structural basis for the decarboxylase and hydratase activities, *Biochemistry 44*, 14818-14827.

Chapter 2: A Pre-steady State Kinetic Analysis of *cis*-3-Chloroacrylic Acid Dehalogenase

2.1 Introduction

The catabolism of 1,3-dichloropropene (**1**, Scheme 1) in *Pseudomonas pavonaceae* 170 and coryneform bacterium strain FG41 involves the hydrolytic dehalogenation of *cis*- and *trans*-3-chloroacrylic acid (**2** and **3**, respectively) resulting in malonate semialdehyde (**4**) (1,2). Subsequently, the β-keto acid undergoes an enzyme-catalyzed decarboxylation to yield acetaldehyde (**5**), which is presumably funneled into the Krebs cycle (1,2). Each isomer of 3-chloroacrylic acid is converted to **4** by a separate dehalogenase known as *cis*- or *trans*-3-chloroacrylic acid dehalogenase, (*cis*-CaaD and CaaD, respectively) (2). Both enzymes are members of the tautomerase superfamily, although from different families, and share a common β–α–β building block and a catalytic amino-terminal proline (2-4).

Scheme 1

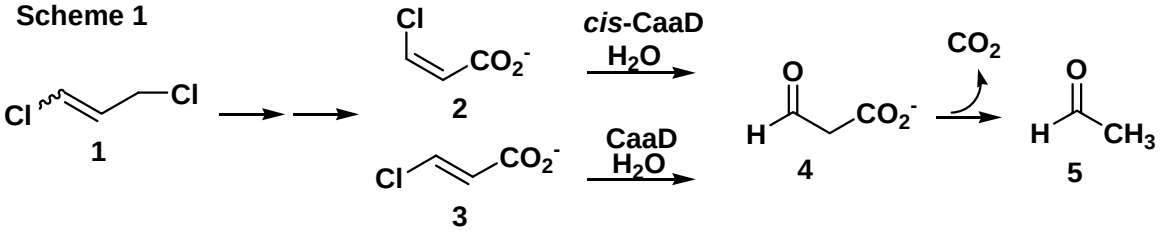

In the current working hypotheses for the CaaD and *cis*-CaaD mechanisms, the same four active site residues are key components (Scheme 2). In CaaD, a

heterohexamer made up of 3 α-subunits and 3 β-subunits, αGlu-52 abstracts hydrogen from water for addition to C-3 of **3** and a pair of arginines (αArg-8 and αArg-11) interacts with the C-1 carboxylate group. This interaction binds and polarizes the substrate to facilitate attack at C-3. The addition of water to the double bond of **3** is completed by the delivery of a proton to C-2 by βPro-1, functioning as a general acid catalyst (5-8). A similar sequence of events is proposed for the trimeric *cis*-CaaD where the corresponding residues are Pro-1, Arg-70, Arg-73, and Glu-114 (9-11).

Scheme 2

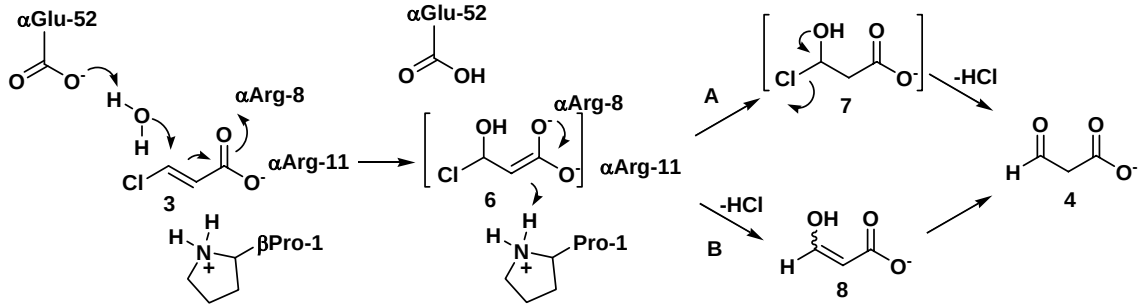

In the proposed catalytic mechanism, the polarization of **3** and addition of water generate an enediolate species (**6**, Scheme 2) (11). Subsequent ketonization by route A results in an unstable chlorohydrin intermediate, which can undergo chemical or enzymatic decay to afford **4** and HCl. Alternatively, the enediolate species can expel the chloride ion (i.e., an α,β-elimination), as shown in route B, to form the enol intermediate, **8**. Ketonization of **8** then produces **4**. Recent experiments showing that the ketonization of phenylenolpyruvate to phenylpyruvate is kinetically competent in the overall CaaD

reaction is consistent with route B, but not conclusive (12). The reaction is also stereoselective when carried out in D_2O (12).

In addition to the different quaternary structures (i.e., heterohexamer vs trimer), there are mechanistic distinctions between the two enzymes (11). Crystallographic studies identified two additional residues, His-28 and Tyr-103, that assist catalysis in *cis*-CaaD (11). The positions of these residues in the structures suggested that Tyr-103 assists Glu-114 in the activation of water and His-28 assists the two arginines in the binding and polarization of substrate. Moreover, mutagenesis analysis suggests that water activation is more critical for the CaaD mechanism whereas substrate activation plays a more significant role in the *cis*-CaaD mechanism (11). For example, replacing αGlu-52 of CaaD with a glutamine renders the enzyme totally inactive, but the analogous mutant in *cis*-CaaD only diminishes activity (7, 9). Likewise, replacing Arg-70 or Arg-73 with an alanine completely eliminates *cis*-CaaD activity (11), but the corresponding mutations in CaaD do not (7). The amino-terminal proline is critical for both activities (5, 6, 9).

Although mutant analysis has provided some measure of the relative importance of key residues in these two enzymes, it has not generally been highly informative. Most mutants show very little or no measurable activity and long incubation periods are necessary to gauge the importance of a residue in the mechanism. For these reasons and the fact that many details of catalysis are not well understood, a pre-steady state kinetic analysis of both enzyme-catalyzed reactions and their mutants is being pursued. Similar

studies on other dehalogenases have been enlightening, identifying the rate limiting steps and uncovering details about halide release (13).

It was not clear at the outset how feasible these experiments would be. The reaction is functionally irreversible and one product, malonate semialdehyde (**4**), is in rapid equilibrium with the hydrate, and undergoes a facile chemical decarboxylation to form acetaldehyde, which is also in equilibrium with the hydrate. Nonetheless, for *cis*-CaaD, conditions have now been identified to carry out stopped-flow fluorescence and chemical quench experiments and an assay developed to quantify bromide ion. Thus far, these studies led to a five-step kinetic model for the wild type enzyme. The mechanism involves substrate binding, conformational change, formation of product, and product release in two steps: release of bromide followed by the release of malonate semialdehyde. Global fitting of the data to this model provided kinetic constants for each of these steps. In addition, stopped flow experiments have been carried out on the six mutants of *cis*-CaaD and their ground-state binding constants derived. A rapid chemical quench experiment was also done on the E114Q mutant of *cis*-CaaD. Like wild type, a burst of product formation is observed, suggesting that there is a rate limiting step after a chemical step.

2.2 Materials and Methods

Materials. Chemicals, biochemicals, buffers, and solvents were purchased from Sigma- Aldrich Chemical Co. (St. Louis, MO), Fisher Scientific Inc. (Pittsburgh, PA), Fluka Chemical Corp. (Milwaukee, WI), or EM Science (Cincinnati, OH). Reagents used in the ion chromatography and rapid quench experiments were at least 99.99% pure

or higher. Enzymes and reagents used for molecular biology procedures were obtained from New England Biolabs, Inc. (Ipswich, MA). The PolyVial 0.5 mL vials, filter caps, and 0.5 mL automated sampler cassettes were purchased from Dionex Corporation (Sunnyvale, CA). The Microcon centrifugal filter devices, 3,000 MWCO, the Amicon stirred cells, and the YM3 and YM10 ultrafiltration membranes were purchased from Millipore Corporation (Billerica, MA). Pre-packed PD-10 Sephadex G-25 columns were purchased from Biosciences AB (Uppsala, Sweden).

Bacterial Strains, Plasmids, and Growth Conditions. *E. coli* BL21-Gold(DE3) cells were purchased from Stratagene (La Jolla, CA). The construction of plasmids for the expression of *cis*-CaaD is described elsewhere. The sources for the components of Luria-Bertani (LB) media are reported elsewhere (6, 14).

General Methods. Mass spectral data were obtained on an LCQ electrospray ion-trap mass spectrometer (ThermoFinnigan, San Jose, CA) in the Analytical Instrumentation Facility Core in the College of Pharmacy at the University of Texas at Austin (6). Steady-state kinetic parameters were obtained at 24 °C on an Agilent 8453 diode-array spectrophotometer. Nonlinear regression data analysis was performed using the program Grafit (Erithacus Software Ltd., Staines, U.K.) obtained from Sigma-Aldrich. The pre-steady state kinetic data were fit and simulated using KinTek Global Kinetic Explorer (Austin, TX). Protein concentrations were determined by the method of Waddell (15). Proteins were analyzed by SDS-PAGE under denaturing conditions on gels containing 15% polyacrylamide (16).

Ion Chromatography. The dehalogenation of *cis*-3-bromoacrylate in chemical quench experiments was quantified by measuring the bromide ion concentration by ion chromatography (IC). The Dionex ion chromatograph (Dionex Corp) (equivalent to the 3500 model), consisted of a LC25 chromatography oven, an EG50 eluent generator, a GS50 gradient pump, an ED50 electrochemical detector, and an AS40 autosampler. The instrument was equipped with an AG12A pre-column (4 × 40 mm), an IonPac AS12A column (4 × 200 mm) and an anion self-regenerating suppressor (ASRS) ULTRA II, 4 mm suppressor. Anion detection was performed by electrical conductivity. A solution of 2.7 mM Na_2CO_3/0.3 mM $NaHCO_3$ (pH 9.6) was used as the eluent at a flow rate of 1.5 mL/min.

Composition of SOB and SOC Media. The SOB medium was made by mixing tryptone (4 g) and yeast extract (1 g) in 100 mL of deionized water (14). The mixture was then autoclaved for 45 min and stored in a sealed glass bottle at 22 °C until ready to use. The SOC medium (10 mL) was made by mixing 4.7 mL of deionized water with SOB medium (5 mL). To this mixture, $MgSO_4$ (0.1 mL of a 1 mg/mL stock solution), NaCl/KCl (0.1 mL of a 1 mg/mL stock solution), and glucose (0.1 mL of a 1 mg/mL stock solution) were added. The solution was mixed at 22 °C and used immediately after being made.

2.2.1 Transformation, Expression and Purification of *cis*-CaaD

Transformation of Expression Cells for cis-CaaD. E. coli BL21-Gold(DE3) competent cells were thawed and stored on ice. Competent cells (~100 μL) were pipetted into a pre-chilled 15-mL Falcon 2059 tube along with pCC5 [also known as pET(*cis*-

CaaD#5)] (~50 ng). The construction of pCC5 is described elsewhere and encodes the gene sequence for *cis*-CaaD (9). The reaction mixture was gently incubated on ice for 30 min. During this time, 900 μL of SOC medium was preheated in a water bath to 42 °C. The reaction mixture was heat-pulsed for 20 s in a water bath at 42 °C and then incubated on ice. After 2 min, the 900-μL aliquot of SOC medium was added to the reaction mixture. The cells were incubated at 37 °C for 1 h in an environmental shaker at 225 rpm. The cells were then concentrated by centrifugation (500 rpm for 5 min), and a 600-μL portion of the supernatant was removed. The cells were resuspended in the remaining supernatant. A portion of the resulting transformation reaction mixture (200 μL) was plated, using a sterile spreader, onto a single LB/Ap (50 μg/mL) plate. The plate was then incubated overnight (~ 16 h) at 37 °C.

Expression and Purification of cis-CaaD. Wild-type *cis*-CaaD was produced in *E. coli* BL21-Gold(DE3) cells using the T7 expression system (9). The freshly transformed cells, with the plasmid containing the *cis*-CaaD gene, were collected from a plate and used to inoculate two 2-liter flasks containing 1L of LB/Ap (100 mg/L). After overnight growth at 30 °C in an environmental shaker at 225 rpm, cells were harvested by centrifugation (15 min at 7,000 rpm) and stored at -20 °C until further use. Typically, 1 L of culture yields 5 g of cells.

Cells (10 g) were thawed and suspended in 10 mL of 10 mM Tris-SO_4 buffer, pH 8.0, and placed on ice (9). Cells were disrupted, while stirring on ice, by sonication at 60 W output (using a W385 sonicator of Heat Systems-Ultrasonics, Inc.) for ten 2-min intervals using 5-s pulses with a cycle time of 50%. After each 2-min interval, the cells

were allowed to sit for 5 min. DNase (10 μL of a 10 Units/μL solution) and RNase (10 μL of a 500 μg/mL solution) were added to the solution and allowed to stir on ice for 1 h. The lysed cells were then centrifuged at 17,000 rpm for 45 min. The supernatant was retained and centrifuged at 60,000 rpm for 1 h.

Subsequently, the supernatant was filtered through a 0.2 μm-pore diameter filter and applied to a TSKgel DEAE-5PW anion-exchange column (150 × 21.5 mm) which had been previously equilibrated with 10 mM Tris-SO_4 buffer, pH 8.0 (9). The protein was eluted with a linear gradient (0-0.5 M Na_2SO_4) at a flow rate of 5 mL/min over a 90 min period. Fractions were collected at 1.75 min intervals (8.75 mL). Fractions (#5-13) with the highest purity (as determined by SDS-PAGE) were pooled and concentrated to ~20 mL using an Amicon stirred cell equipped with a YM10 (10,000 MW cutoff) ultrafiltration membrane.

Solid $(NH_4)_2SO_4$ was added to the concentrate to make a final concentration of 1.0 M and the resulting solution was stirred for 1 h at 4 °C (9). The solution was then centrifuged at 11,000 rpm for 15 min and the supernatant was filtered through a 0.2 μm-pore diameter filter and applied to a TSKgel Phenyl-5PW column (150 × 21.5 mm), which had been previously equilibrated with 10 mM Tris-SO_4 buffer, pH 8.0, containing 1.0 M $(NH_4)_2SO_4$. The protein was eluted using a decreasing linear gradient [1.0-0 M $(NH_4)_2SO_4$] at a flow rate of 5 mL/min. Fractions were collected at 1.75 min intervals (8.75 mL) during the 90 min program. Fractions (#10-12) with the highest purity (as determined by SDS-PAGE) were pooled and concentrated to ~6 mL using an Amicon stirred cell equipped with a YM10 (10,000 MW cutoff) ultrafiltration membrane and

stored at 4 °C. This purification resulted in ~100 mg of 95% pure protein as assessed by ESI mass spectroscopy and SDS-PAGE. The observed monomer mass for *cis*-CaaD was 16,622 Da.

2.2.2 Steady-State Kinetic Parameters for *cis*-CaaD

Steady-State Kinetic Parameters for cis-CaaD.. The steady-state parameters for *cis*-CaaD was measured using *cis*-3-chloro- or *cis*-3-bromoacrylic acid. The assays were carried out at 22 °C in 20 mM Na_2HPO_4 buffer, pH 9.0, or in 20 mM $NaHCO_3$-NaOH buffer, pH 9.0, as indicated. A 25 mL solution of enzyme (2 μM based on monomer mass) was made up in each buffer and allowed to equilibrate at 22 °C for 1 h. The assay was initiated by the addition of *cis*-3-chloro or *cis*-3-bromoacrylic acid (10-700 μM), which were obtained from a 10 mM or 50 mM stock solutions (in 100 mM Na_2HPO_4 buffer, pH 9.0). The addition of *cis*-3-chloro- or *cis*-3-bromoacrylic acid to the 100 mM sodium phosphate buffer adjusted the pH of the stock solution from 9.0 to 7.3. The 10 mM stock solution was made by diluting an aliquot of the 50 mM stock solution into 100 mM NaH_2PO_4 buffer, pH 7.3. For wild type enzyme, the decrease in absorbance at 224 nm, corresponding to the hydration of *cis*-3-chloroacrylate ($\varepsilon = 2900\ M^{-1}\ cm^{-1}$) (9) or *cis*-3-bromoacrylate ($\varepsilon = 3600\ M^{-1}\ cm^{-1}$) (9), was monitored over a 40s time period, recording readings every 1.5 s. The two mutants were monitored over a 60s time period. The rates of substrate depletion over the first 20 s were then plotted versus the corresponding concentrations. The hyperbolic curve was fit to the Michaelis-Menten equation by nonlinear regression analysis, provided in the Grafit program (Erithacus Software Ltd., Horley U.K.), to determine the values of k_{cat} and K_m.

2.2.3 Inhibition of *cis*-CaaD by Halide Ion

Inhibition of cis-CaaD by Halide Ion. The inhibition of *cis*-CaaD by halide ion was carried out using *cis*-CaaD (2 μM based on monomer mass) in 50 mL of 20 mM $NaHCO_3$-NaOH buffer, pH 9.0. The enzyme solution was made up and allowed to sit at room temperature for 1 h before two 15-mL aliquots were removed and placed in separate 50-mL Falcon tubes. Two portions of KBr (17.85 mg and 4.46 mg) were added to the individual tubes to give final concentrations of 2.5 mM and 10 mM bromide, respectively. Steady-state kinetic parameters were then measured in the presence of *cis*-3-bromoacrylic acid (10–800 μM). The reactions were initiated by the addition of substrate. The decrease in absorbance was monitored at 224 nm over 40 s taking readings every 1.5 s. The rate was then calculated over the initial 20s period and plotted versus increasing substrate concentration. These data were then fit to the Michaelis-Menten equation, provided in the Grafit program (Erithacus Software Ltd.), to determine the values of k_{cat} and K_m for the enzyme in the presence of bromide.

For NaCl, the enzyme solution (75 mL of a 2 μM solution in 20 mM-$NaHCO_3$-NaOH buffer, pH 9.0, that had equilibrated for 1 h at 22 °C) was divided into 3 25-mL aliquots. Two portions of NaCl (2.215 mg and 8.863 mg) were added to two of the enzyme solutions to make a final chloride concentration of 2.5 mM and 10 mM, respectively. The steady-state kinetic parameters were measured and the data analyzed as described above.

2.2.4 Stopped Flow Experiments Using *cis*-CaaD

Stopped Flow Experiments Using cis-CaaD. All stopped flow experiments and measurements were carried out using a SF 2004 series stopped flow apparatus from Kintek Corp. (http://www.kintek-corp.com). *cis*-CaaD (20 μM based on monomer molecular mass) was made up in 20 mM Na_2HPO_4 buffer, pH 9.0, or 20 mM $NaHCO_3$-NaOH buffer, pH 9.0 (as indicated), and allowed to equilibrate at 22 °C for 1 h. Various concentrations of *cis*-3-chloro- or *cis*-3-bromoacrylic acid (100-9,000 μM before mixing) were made up in 100 mM Na_2HPO_4 buffer, pH 9.0, or in 50 mM $NaHCO_3$-NaOH buffer, pH 10.0. The addition of *cis*-3-chloro- or *cis*-3-bromoacrylic acid to the buffer adjusted the pH to ~7.8. The enzyme (10 μM after mixing) and substrate (50-4,500 μM after mixing) solutions were then mixed in the stopped flow apparatus at 22 °C. The pH after mixing was 7.8. The samples were excited at 280 nm and fluorescence emission was monitored using a photomultiplier tube equipped with a 340 nm long pass Corion filter. In order to reduce photobleaching, the slit width on the xenon light source and the light filter were set at 3.16 mm. The high voltage output was set at 643 volts. Three time intervals (0.2 s, 2 s, and 12-180 s) were recorded for each substrate concentration. The length of the variable time interval (12-180 s) depended on the time needed for the fluorescence signal to return to its initial fluorescence value. Each experiment was repeated 5 times.

2.2.5 Control Experiments for Stopped Flow Analysis

Fluorescence Quenching by Buffer. *cis*-CaaD (20 μM based on monomer molecular mass) was made up in 20 mM Na_2HPO_4 buffer, pH 9.0, and allowed to

equilibrate at 22 °C for 1 h. The enzyme (10 μM after mixing) and 20 mM NaH_2PO_4 buffer (10 μM after mixing), pH 9.0, were mixed in the stopped flow apparatus at 22 °C. The samples were excited at 280 nm and fluorescence emission was monitored using a photomultiplier tube equipped with a 340 nm long pass Corion filter. Various combinations of the slit width on the light source and light filter, along with the HV settings, were used in order to detect a fluorescence signal. There was no detectable quenching by the buffer.

Fluorescence Quenching by Malonate Semialdehyde and Bromide Ion. cis-CaaD and CaaD (20 μM based on monomer molecular mass) were each made up in 2 mL of 20 mM Na_2HPO_4 buffer, pH 9.0, and allowed to equilibrate at 22 °C for 1 h. An 80-μL aliquot of CaaD (in 20 mM Na_2HPO_4 buffer, pH 9.0) was diluted into 720 μL of 20 mM Na_2HPO_4 buffer, pH 9.0, to give a final volume of 800 μL. A 200-μL aliquot of *trans*-3-chloroacrylic acid (from a 10 mM stock solution in 100 mM NaH_2PO_4 buffer, pH 9.0) was added to the enzyme solution and allowed to sit at 22 °C for 5 min. Equal volumes of the reaction mixture were rapidly mixed with equal volumes of 20 μM cis-CaaD in Na_2HPO_4 buffer, pH 9.0, in the stopped flow apparatus at 22 °C. The samples were excited at 280 nm and fluorescence emission was monitored using a photomultiplier tube equipped with a 340 nm long pass Corion filter. Various combinations of the slit width on the light source and light filter, along with the HV settings, were used in order to detect a fluorescence signal. There was not detectable quenching by malonate semialdehyde or bromide.

2.2.6 Buffer Exchange

Buffer Exchange for Rapid Quench Experiments. *cis*-CaaD is stored in 10 mM Tris-SO_4 buffer, pH 9.0, at 4 °C. The enzyme is exchanged into 20 mM $NaHCO_3$-NaOH buffer, pH 9.0, by diluting ~1.2 mL (of a 12.75 mg/mL stock solution of *cis*-CaaD in 10 mM Tris-SO_4 buffer, pH 8.0) into 10 mL of 20 mM $NaHCO_3$-NaOH buffer, pH 9.0, to give a final volume of ~11.2 mL. The solution was then placed in an Amicon stirred cell equipped with a YM10 (10,000 MW cutoff) ultrafiltration membrane and concentrated to ~1.2 mL. The enzyme was then diluted with a 10 mL portion of 20 mM $NaHCO_3$-NaOH buffer, pH 9.0, and concentrated to 1.2 mL. This procedure was repeated 4 times to ensure complete exchange of buffer.

2.2.7 Rapid Chemical-Quench Flow Experiments Using *cis*-CaaD

Rapid Chemical-Quench Flow Measurements Using cis-CaaD and cis-3-Bromoacrylic Acid. The time course needed to measure the reaction between *cis*-CaaD and *cis*-3-bromoacrylic acid is too fast to measure by manually mixing and quenching. Hence, rapid quench experiments were carried using a quench-flow apparatus (RQF-3 Rapid Quench Flow) from Kintek Corp (http://www.kintek-corp.com). These reactions were carried out at 22 °C. Typcially, one syringe was loaded with *cis*-CaaD (250, 500 or 1000 μM made up in 20 mM $NaCO_3$-NaOH buffer, pH 9.0). Another syringe was loaded with freshly prepared 10,000 μM *cis*-3-bromoacrylic acid (made up in 50 mM $NaHCO_3$-NaOH buffer, pH 10.0). Each reaction was initiated by the rapid mixing of aliquots (15 μL) of the reactants from both syringes. The reaction mixture was quenched at various intervals ranging from 3-750 ms with 80 μL of 0.6 M H_2SO_4. The amount of bromide

formed was then quantified using ion chromatography. Kinetic parameters were derived by fitting the data to the appropriate equation by non-linear regression analysis.

Preparation of Quenched Reaction Samples for Bromide Ion Analysis. The individually quenched reaction mixtures were centrifuged at 1000 rpm for 5 s. The supernatant from each sample was then transferred to a 1.5 mL ependorf tube equipped with 3,000 MW cutoff Microcon centrifugal filter devices. The samples were centrifuged at 9,000 rpm for 50 min to remove the enzyme from the reaction mixture. A 20-μL aliquot was diluted into 780 μL of 20 mM $NaCO_3$-NaOH buffer, pH 9.0, to give a final volume of 800 μL. The concentration of bromide was quantified using ion chromatography.

Identification of Quench Conditions for the cis-CaaD-catalyzed Reaction. Various acids (CF_3CO_2H, HNO_3, H_2SO_4, HPO_4) were examined to determine which one terminated the reaction between *cis*-CaaD and *cis*-3-bromoacrylic acid. The protocol to quantify bromide ion content, described below, was used for all four acids but is only described in detail for H_2SO_4. A 50 mL stock solution of 1.5 M acid H_2SO_4 was made by mixing 4.14 mL of 18 M ultra pure H_2SO_4 with 45.83 mL of deionized water. A 20 mM stock solution of *cis*-CaaD was then made up in 20 mM Na_2HPO_4 buffer, pH 9.0, and allowed to equilibrate for 1 h at 22 °C. A 8000 μM stock solution of *cis*-3-bromoacrylic acid in 100 mM Na_2HPO_4 buffer, pH 9.0, was also made up as described previously. In a 1.5 mL ependorf tube, 300 μL of 20 mM *cis*-CaaD solution was mixed with 300 μL of 8000 μM *cis*-3-bromoacrylic acid and allowed to incubate at 22 °C. After 10 s, sufficient H_2SO_4 (92.3 μL) was added to the reaction mixture to bring the final concentration of

acid to 0.2 M. The reaction mixture was then divided into equal proportions and analyzed using ion chromatography. One portion was analyzed immediately and the other portion was analyzed 24 h later. The same procedure was repeated, only changing the initial concentration of H_2SO_4 such that the final concentration acid was 0.3 M, 0.4 M, 0.5 M, and 0.6 M.

2.2.8 Quantification of Bromide Ion Concentration Using Ion Chromatography

Quantification of Bromide Ion Concentration Using Ion Chromatography. A 400-μL portion of each quenched mixture was loaded into 500 μL sample vials (Dionex) and placed in an AS40 autosampler. Only 10 μL of sample from each vial was loaded onto the AS12A column by the autosampler. The column had been previously equilibrated with 2.7 mM Na_2CO_3/0.3 mM $NaHCO_3$ buffer, pH 9.6. The contents of the mixture were eluted isocratically (1.5 mL/min) over 15 min. The bromide ion was detected by supressed conductivity using an electrochemical detector with an applied current of 100 mA. The quench samples were alternated with deionized water samples (400 μL) in order to elute any remaining anions from the column before loading the next sample.

Calibration Curve for Ion Chromatography. The calibration curve used in bromide analysis was constructed using 8 known concentrations of bromide (0-10 ppm) made from a stock solution of KBr (12.51 mM, 1000 ppm Bromide ion) in 2.7 mM Na_2CO_3/0.3 mM $NaHCO_3$ buffer, pH 9.6. The stock solution of KBr was made by dissolving KBr (148.93 mg) in 100 mL of 2.7 mM Na_2CO_3/0.3 mM $NaHCO_3$ buffer, pH 9.6, giving a final bromide concentration of 1000 mg/L. A 10 ppm solution of bromide

(10 mL) was made from the stock solution by diluting 100 μL into 9900 μL of Na_2CO_3/0.3 mM $NaHCO_3$ buffer, pH 9.6. This solution was then used to make 7 solutions (2 mL) with the following concentrations of bromide: 5 ppm, 2.5 ppm, 1.25 ppm, 0.625 ppm, 0.3125 ppm, 0.0156 ppm, and 0 ppm (2 mL of Na_2CO_3/0.3 mM $NaHCO_3$, pH 9.6).

2.3 Results and Discussion

2.3.1 Purification and Characterization of *cis*-CaaD

Purification and Characterization of cis-CaaD. The gene encoding *cis*-CaaD was expressed under the control of the T7 promoter and the enzyme was purified to homogeneity by a variation of published protocols (9). This protocol yielded ~ 100 mg of purified enzyme from 2 L of cell culture. ESI-MS analysis of the purified protein showed a mass of 16,622 Da, indicating that the initiating N-formyl methionine had been post-translationally removed from the protein. Hence, Pro-1 is available for catalysis.

2.3.2 Steady-State Kinetic Parameters for *cis*-CaaD

Determination of the Steady-State Kinetic Parameters for cis-CaaD. The steady state kinetic parameters for *cis*-CaaD using *cis*-3-chloro and *cis*-3-bromoacrylate were measured in three buffer systems, 20 mM Na_2HPO_4 buffer (9), 20 mM Tris-H_2SO_4 buffer, and 20 mM $NaHCO_3$-NaOH buffer. The pH of all three buffers was adjusted to pH 9.0. The results of these experiments provided the necessary framework for the pre-steady state analysis. The values of K_m and k_{cat} (Table 1) for both *cis*-3-chloro- and *cis*-3-bromoacrylic acid were similar in the Na_2HPO_4 and Tris buffers (data not shown), but decreased in the $NaHCO_3$ buffer. For *cis*-3-bromoacrylate, the values of K_m and k_{cat}

showed 1.5- and 2.3-fold decreases, respectively. This resulted in a 3.3-fold decrease in the value of k_{cat}/K_m. The K_m and k_{cat} values for *cis*-3-chloroacrylic acid were not determined in $NaHCO_3$ buffer.

Table 1. Steady-State Kinetic Parameters for *cis*-CaaD

substrate	k_{cat} (s^{-1})	K_m (μM)	k_{cat}/K_m (M^{-1} s^{-1})
cis-3-Chloroacrylic Acid[a]	5.9 ± .1	200 ± 15	2.9×10^4
cis-3-Bromoacrylic Acid[a]	5.4 ± .2	200 ± 17	2.7×10^4
cis-3-Bromoacrylic Acid[b]	2.4 ± 0.1	300 ± 32	8.1×10^3

[a]The steady-state kinetic parameters were determined in 20 mM sodium phosphate buffer (pH 9.0) at 22 °C. Errors are standard deviations.

[b]The steady-state kinetic parameters were determined in 20 mM sodium bicarbonate buffer (pH 9.0) at 22 °C. Errors are standard deviations.

2.3.3 Inhibition of *cis*-CaaD by Halide Ion.

Inhibition of cis-CaaD by Halide Ion. In the presence of 2.5 and 10 mM bromide ion, k_{cat} dropped 1.6-fold and 2.1-fold, respectively. In the presence of 2.5 and 10 mM chloride ion, there was no significant decrease in the k_{cat} (within experimental error). The values of K_m were not affected. These observations suggest that bromide ion exhibits a

non-competitive type of inhibition on *cis*-CaaD (Figure 2.1). The purpose of this experiment was to determine whether halide ion binds at the active site, perhaps indicative of a halide binding pocket. The results suggest that it does not.

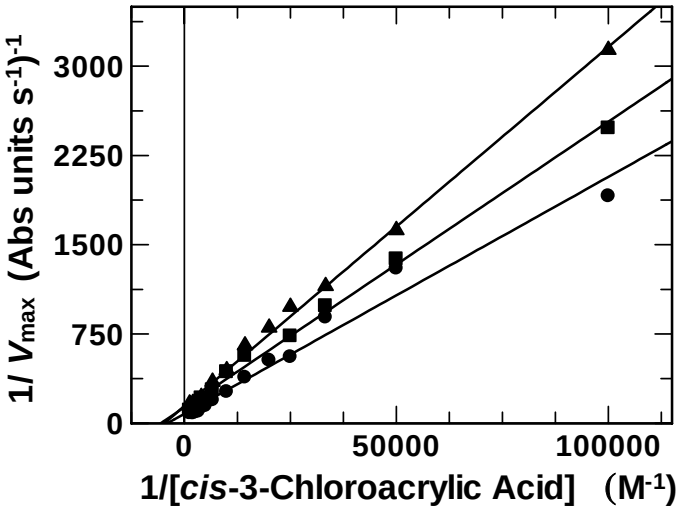

Figure 2.1. Noncompetitive inhibition of *cis*-CaaD by bromide (0 mM, filled circles; 2.5 μM, filled squares; and 10 μM, filled triangles) using *cis*-chloroacrylic acid (10-800 μM) as substrate in $NaHCO_3$-NaOH buffer, pH 9.0, at 22 °C.

2.3.4 Quantification of Bromide Ion Concentration Using Ion Chromatography

Quantification of Bromide Ion Concentration Using Ion Chromatography. The bromide ion concentration in the burst experiments was quantified by ion chromatography. A series of control experiments was carried out (Figures 2.2-2.7) to validate the methodology. The individual components of a burst experiment (buffer, *cis*-

3-bromoacrylate, bromide ion, and sulfate ion) were individually eluted from the column and their elution times identified (Figures 2.2-2.5). Subsequently, the mixed components were eluted at two different concentrations of bromide ion (10 and 2 ppm). The chromatograph (Figure 2.6) for the mixture containing 10 ppm bromide ion shows clear separation of these components using 2.7 mM Na_2CO_3/0.3 mM $NaHCO_3$, pH 9.6, as the eluent at a flow rate of 1.5 mL/min. The chromatograph (Figure 2.7) for the mixture using 2 ppm bromide ion also shows clear separation under the same conditions. Finally, a chromatograph (Figure 2.8) from a typical quenched reaction mixture is shown. Again, there is clear separation of bromide ion from the components of the reaction mixture. Separation could only be achieved using the $NaHCO_3$ buffer because the signal generated by the phosphate ion from the sodium phosphate buffer overlapped with the signal from the bromide ion (data not shown). The detection limits ranged from a low of 7.5 ppb (92 nM) to a high of 25 ppm (313 μM) (data not shown).

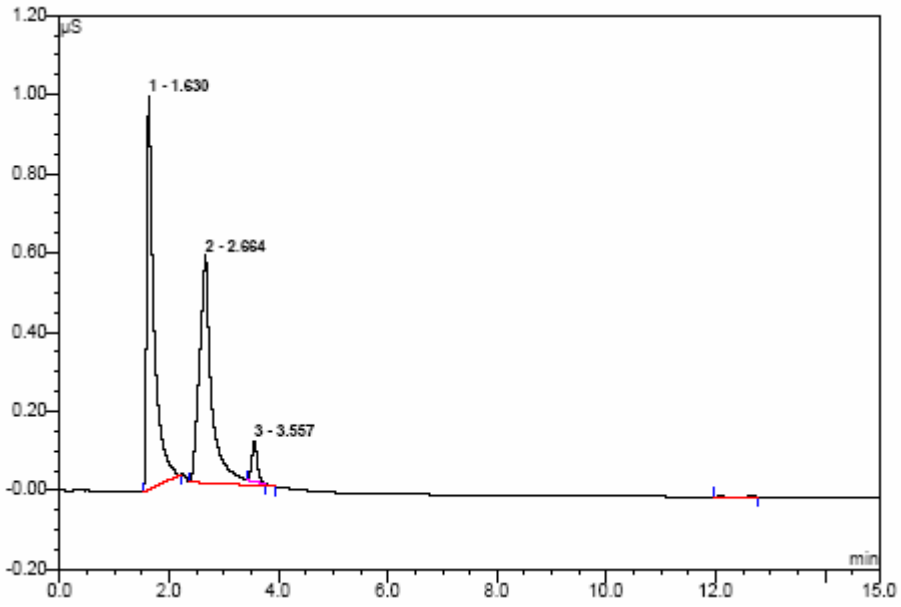

Figure 2.2. Ion chromatograph of 20 mM $NaHCO_3$-NaOH buffer, pH 9.0, as analyzed over a 15-min period at 22 °C. The three signals could not be identified.

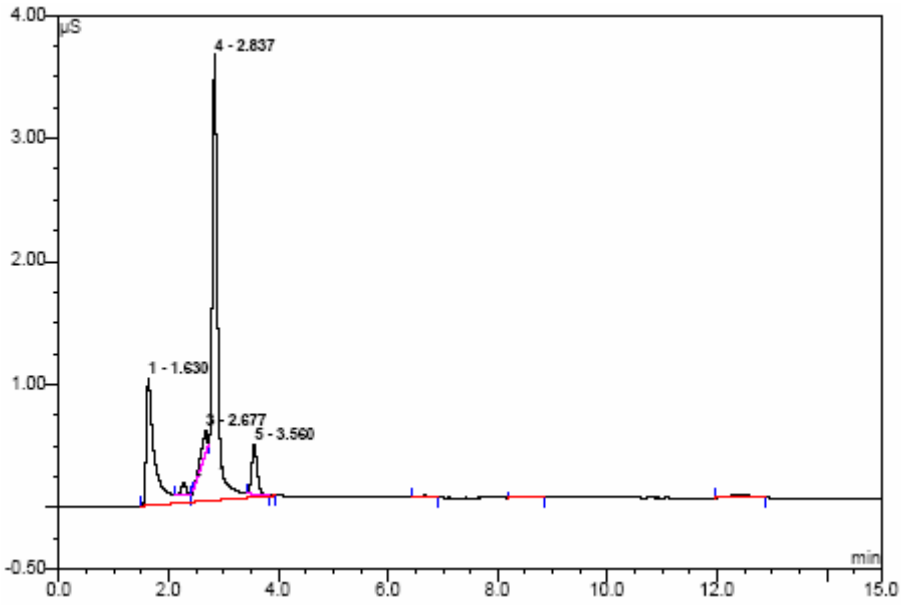

Figure 2.3. Ion chromatograph of 25 ppm of *cis*-3-bromoacrylic acid in 20 mM $NaHCO_3$-NaOH buffer, pH 9.0, eluted over a 15-min period at 22 °C. The prominent signal at 2.837 min corresponds to *cis*-3-bromoacrylic acid.

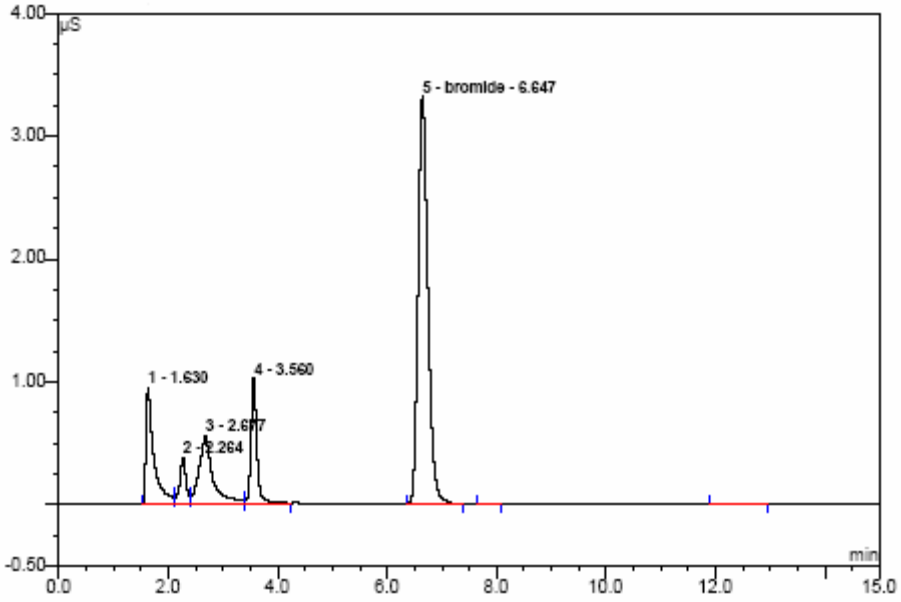

Figure 2.4**.** Ion chromatograph of 25 ppm of bromide in 20 mM $NaHCO_3$-NaOH buffer, pH 9.0, eluted over a 15-min period at 22 °C. The prominent signal at 6.647 min corresponds to bromide.

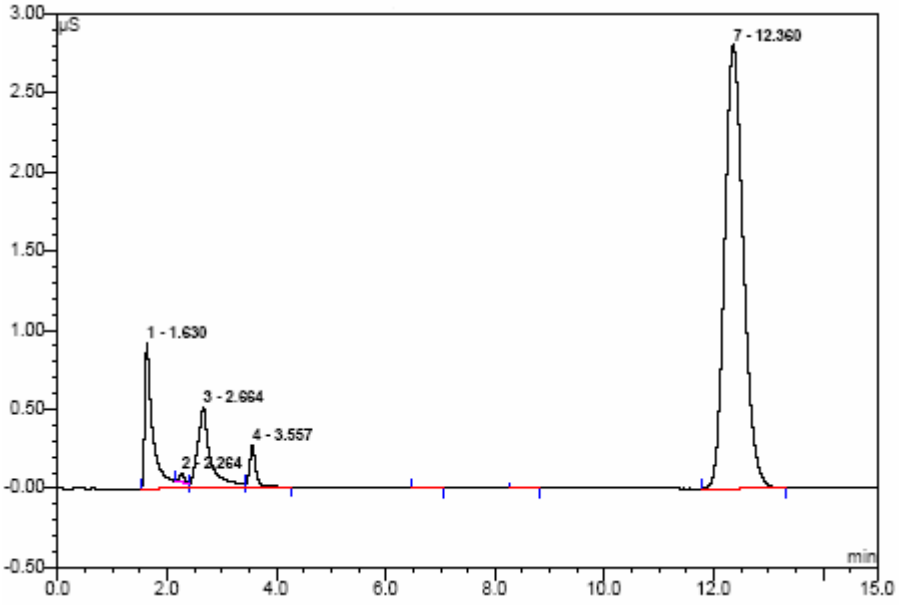

Figure 2.5. Ion chromatograph of 25 ppm of sulfate from Na_2SO_4 in 20 mM $NaHCO_3$-NaOH buffer, pH 9.0, eluted over a 15-min period at 22 °C. The prominent signal at 12.360 min corresponds to sulfate.

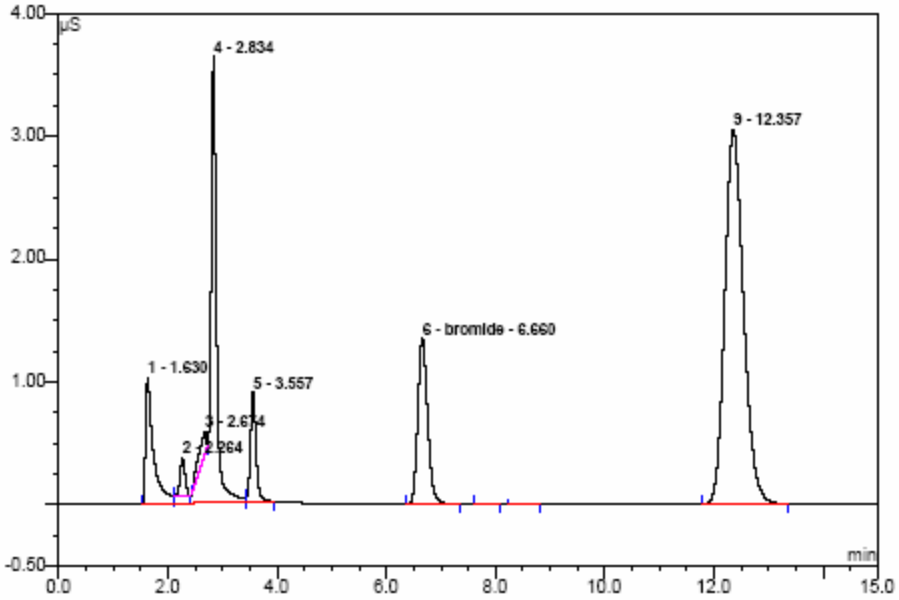

Figure 2.6. Ion chromatograph of *cis*-3-bromoacrylic acid (25 ppm), bromide (10 ppm), and sulfate (25 ppm) in 20 mM $NaHCO_3$-NaOH buffer, pH 9.0, eluted over a 15-min period at 22 °C. The signals at 2.834 min, 6.660 min, and 12.357 min correspond to *cis*-3-bromoacrylic acid, bromide, and sulfate, respectively.

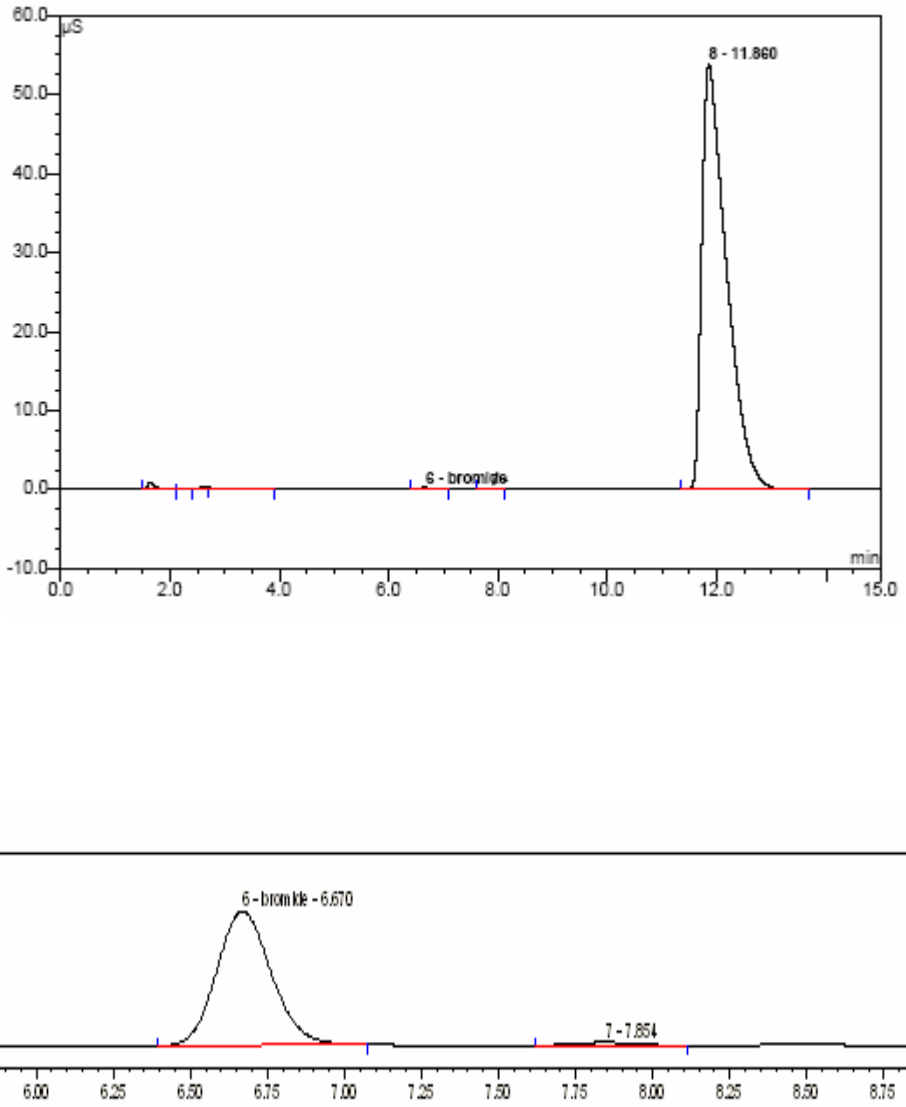

Figure 2.7. Ion chromatograph of *cis*-3-bromoacrylic acid (25 ppm), bromide (2 ppm), and sulfate (500 ppm) in 20 mM $NaHCO_3$-NaOH buffer, pH 9.0, eluted over a 15-min period at 22 °C (top panel). The signal at 6.670 min corresponds to bromide and the signal at 11.860 min corresponds to sulfate. A blow-up of the chromatograph showing the bromide signal is shown in the bottom panel.

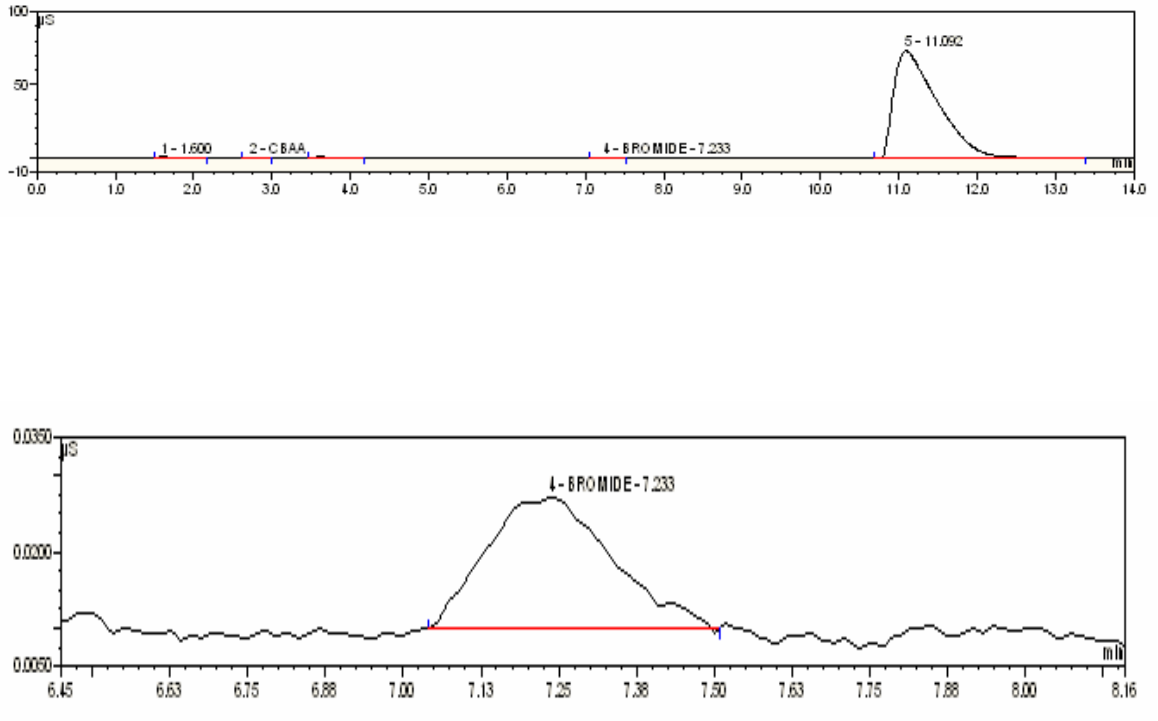

Figure 2.8. Ion chromatograph of a quenched reaction mixture from a rapid quench experiment with *cis*-CaaD (500 µM) and *cis*-3-bromoacrylic acid (5000 µM) in 20 mM $NaHCO_3$-NaOH buffer, pH 9.0, at 22 °C. The reaction was quenched after 0.075 sec with 0.6 M H_2SO_4 and analyzed. The signal at 2.834 min corresponds to *cis*-3-bromoacrylic acid, the signal at 7.233 min corresponds to bromide (0.099 ppm), and the signal at 11.092 min corresponds to sulfate. A blow-up of the chromatograph showing the bromide signal is shown in the bottom panel.

2.3.5 Rapid Chemical-Quench Flow Experiments

Rapid Chemical-Quench Flow Experiments Using cis-CaaD. In order to identify the rate-limiting step, pre-steady state burst experiments were conducted on the *cis*-CaaD reaction. Three experiments were initiated by mixing different concentrations of *cis*-CaaD (final concentrations 125 μM, 250 μM, and 500 μM) with an excess of *cis*-3-bromoacrylic acid (final concentration 5 mM). At fixed time intervals (3-750 ms), the reactions were quenched and the amount of bromide ion quantified. A pre-steady state burst of product (i.e., bromide ion) was observed in all three experiments when the concentration of bromide ion was plotted versus time (Figures 2.9-2.12) with a fast initial rate followed by a slower steady-state rate of product formation. The data can be fit to a burst equation (equation 1),

$$Y = Ae^{(-k_1 t)} + k_2 t + C \qquad (1)$$

where Y is the bromide ion concentration, A is the amplitude of the burst, k_1 is the burst rate constant, k_2 is the steady-state rate constant, and C is the offset constant (17). The exponential burst rate constants (i.e., k_1) are 41.4 ± 7.8 s^{-1}, 36.2 ± 4.5 s^{-1}, 24.4 ± 1.8 s^{-1} for the experiments using 125, 250, 500 μM enzyme, respectively. The steady-state rate constants for the same experiments are 3.8 s^{-1}, 3.6 s^{-1} and 5.0 s^{-1}, respectively. The steady-state rate constants were determined by dividing k_2 by the active enzyme concentrations, obtained from the amplitude of the burst. These values are in good agreement with the steady-state k_{cat} values reported (in Table 1) above for *cis*-CaaD and *cis*-3-bromoacrylate (in 20 mM Na_2HPO_4 and $NaHCO_3$ buffers at pH 9.0). The active

enzyme concentration obtained in these experiments corresponded to ~66% of that determined by the Waddell method (15).

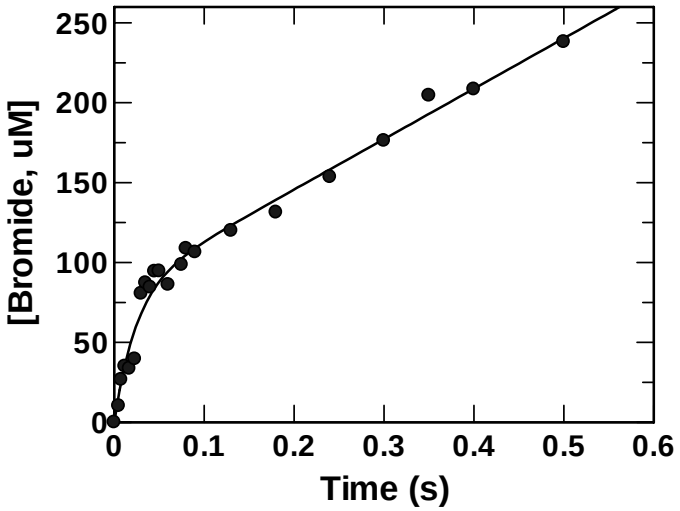

Figure 2.9. Rapid quench experiment using 125 μM *cis*-CaaD with 5000 μM *cis*-3-bromoacrylic acid in 20 mM $NaHCO_3$-NaOH buffer, pH 9.0, at 22 °C. The reported concentrations are those after mixing enzyme and substrate. The reaction shows a burst of bromide formation followed by a steady-state rate.

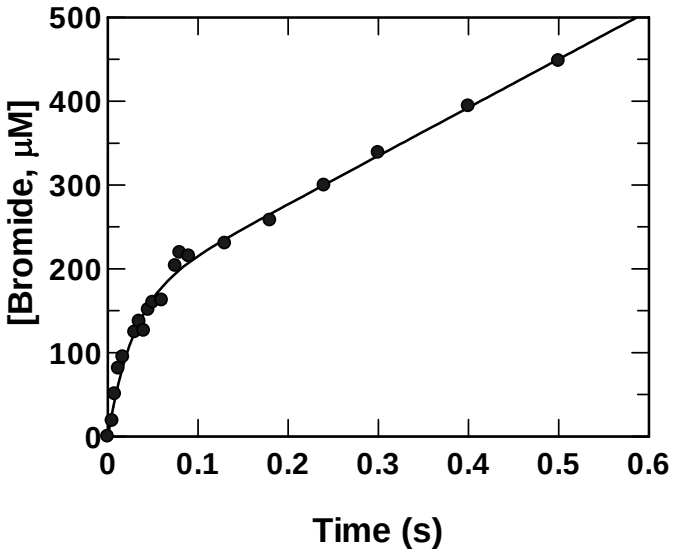

Figure 2.10. Rapid quench experiment using 250 μM *cis*-CaaD with 5000 μM *cis*-3-bromoacrylic acid in 20 mM $NaHCO_3$-NaOH buffer, pH 9.0, at 22 °C. The reported concentrations are those after mixing enzyme and substrate. The reaction shows a burst of bromide formation followed by a steady-state rate.

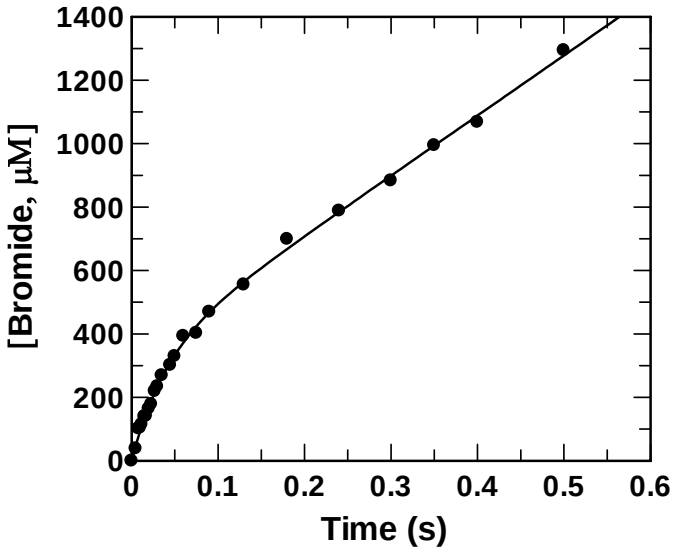

Figure 2.11. Rapid quench experiment using 500 μM *cis*-CaaD with 5000 μM *cis*-3-bromoacrylic acid in 20 mM $NaHCO_3$-NaOH buffer, pH 9.0, at 22 °C. The reported concentrations are those after mixing enzyme and substrate. The reaction shows a burst of bromide formation followed by a steady-state rate.

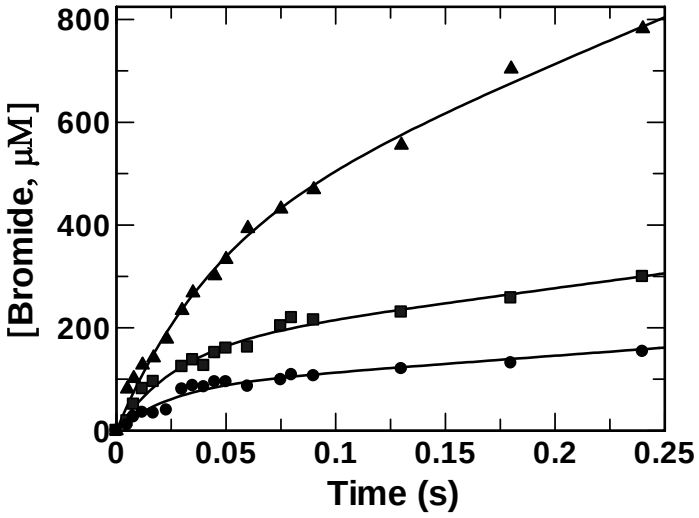

Figure 2.12. Rapid quench experiments using 125 μM (solid circles), 250 μM (solid squares), and 500 μM (solid triangles) *cis*-CaaD with 5,000 μM *cis*-3-bromoacrylic acid in 20 mM $NaHCO_3$-NaOH buffer, pH 9.0, at 22 °C. The reported concentrations are those after mixing enzyme and substrate. The reactions show a burst of bromide formation followed by a steady-state rate.

The presence of a pre-steady state burst indicates that a step after chemistry is rate limiting, presumably product release. Hence, we propose that the product formation at the active site is fast, but is followed by a slow release of bromide ion. The burst rate obtained from fitting the data is a sum of the rates of the chemical reaction and the product release. In the case of the three burst reactions, the burst rate is much faster than the steady state turnover rate, suggesting that the burst rates are dominated by the chemical reaction. The chemical reaction includes all steps up to, and including product

formation. This includes substrate binding, any conformational changes that occur within the enzyme upon substrate binding, and chemistry (e.g., the formation of **7** and **8** in Scheme 2).

2.3.6 Stopped Flow Kinetic Experiments

Stopped Flow Kinetic Experiments. In order to determine whether *cis*-CaaD undergoes a conformational change upon substrate binding, stopped flow experiments were carried out by following the changes in tryptophan fluorescence upon substrate binding. There are two tryptophans in *cis*-CaaD, Trp-101 and Trp-128 (11). According to the crystal structures, Trp-101 is in the active site, and Trp-128 is on the surface. The tryptophan at the active site could report the conformational changes of the enzyme during substrate binding and catalysis (17).

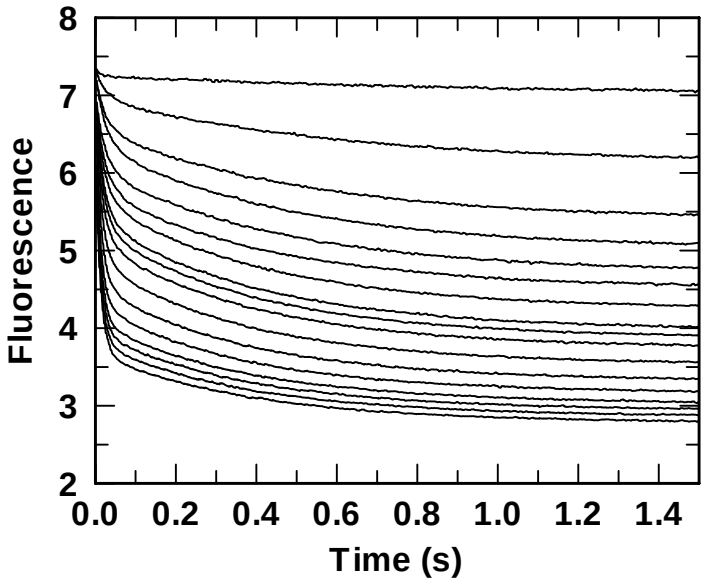

Figure 2.13. Traces from 17 stopped-flow experiments in which *cis*-CaaD (10 μM) in 20 mM Na_2HPO_4 buffer, pH 9.0, was mixed with an equal volume of *cis*-3-bromoacrylic acid (50-4500 μM, top to bottom) at 22 °C. The decrease in fluorescence was fit to a double exponential. The signals returned to the initial fluorescence value at times ranging from 10-200 s. The reported concentrations are those after mixing enzyme and substrate. The individual reactions were monitored for 2 s. Only the first 1.5 s of the reaction is shown.

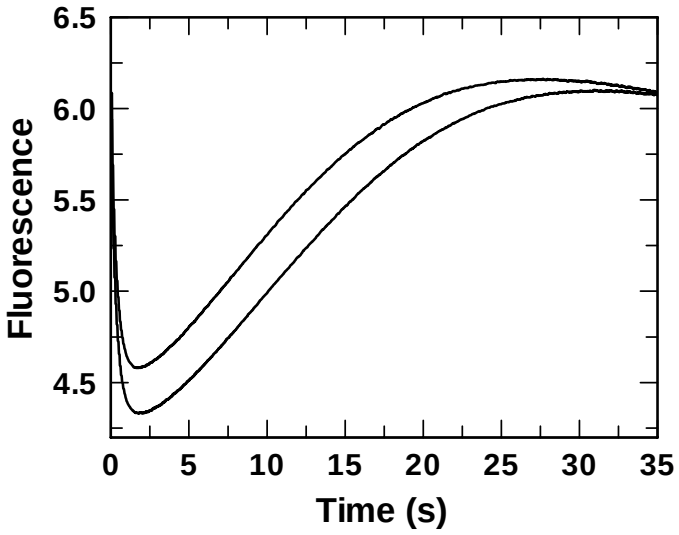

Figure 2.14. Two representative traces from 17 stopped-flow experiments in which *cis*-CaaD (10 μM) in 20 mM Na_2HPO_4 buffer, pH 9.0, was mixed with an equal volume of *cis*-3-bromoacrylic acid (400 μM and 500 μM, top to bottom) at 22 °C. These two traces show the return to the initial fluorescence value after 35 s. The reported concentrations are those after mixing enzyme and substrate

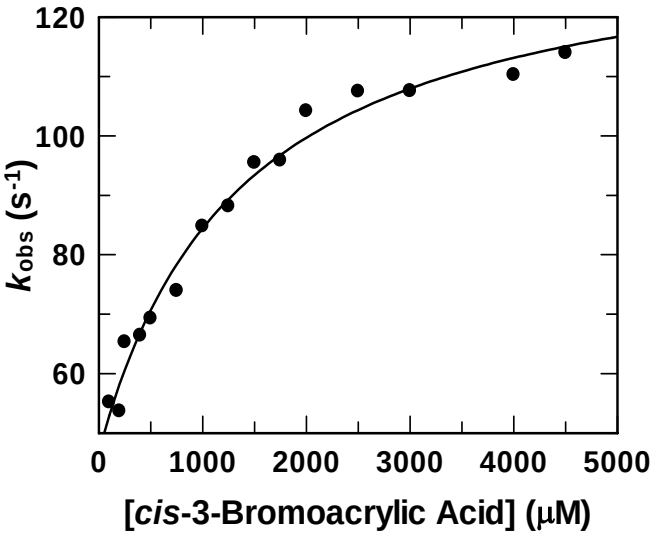

Figure 2.15. Concentration dependence of k_{obs} for binding of *cis*-3-bromoacrylic acid (50–4500 μM) to *cis*-CaaD (10 μM) in 20 mM Na_2HPO_4 buffer, pH 9.0, at 22 °C. The concentration dependence of the fast phase was fit to an equation for a hyperbola. The reported concentrations are those after mixing enzyme and substrate.

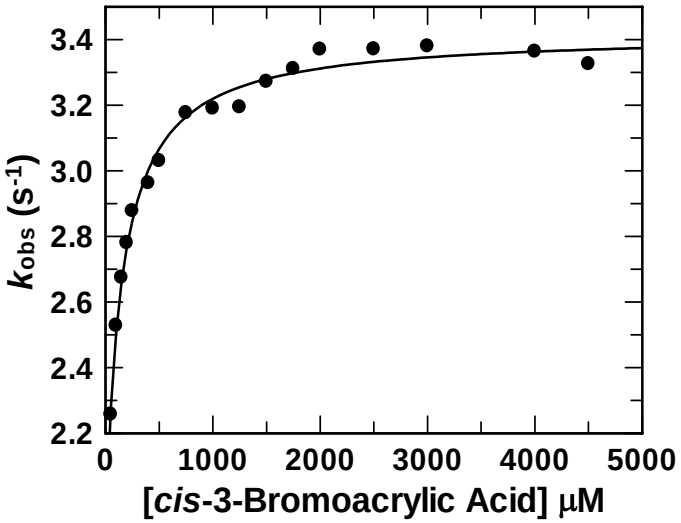

Figure 2.16. Concentration dependence of k_{obs} for binding of *cis*-3-bromoacrylic acid (50–4500 μM) to *cis*-CaaD (10 μM) in 20 mM Na_2HPO_4 buffer, pH 9.0, at 22 °C. The concentration dependence of the slow phase was fit to an equation for a hyperbola. The reported concentrations are those after mixing enzyme and substrate.

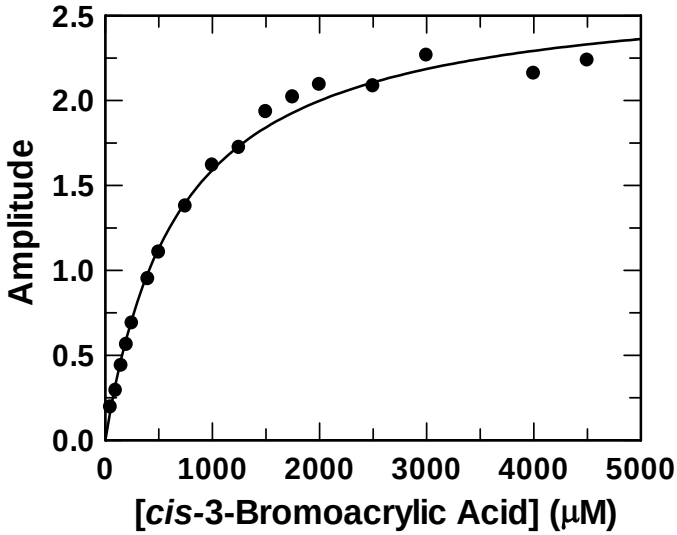

Figure 2.17. Concentration dependence of the amplitude for the fast phase binding of *cis*-3-bromoacrylic acid (50–4500 μM) to *cis*-CaaD (10 μM) in 20 mM Na_2HPO_4 buffer, pH 9.0, at 22 °C. The concentration dependence of the amplitude was fit to an equation for a hyperbola. The reported concentrations are those after mixing enzyme and substrate.

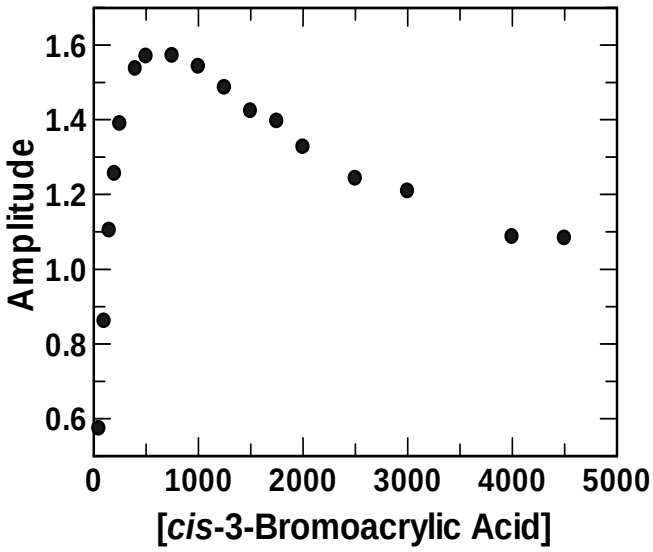

Figure 2.18. Concentration dependence of the amplitude for the slow phase binding of *cis*-3-bromoacrylic acid (50–4500 μM) to *cis*-CaaD (10 μM) in 20 mM Na_2HPO_4 buffer, pH 9.0, at 22 °C. The data could not be fit. The reported concentrations are those after mixing enzyme and substrate.

In these experiments, *cis*-CaaD was mixed with increasing concentrations of *cis*-3-chloro- or *cis*-3-bromoacrylic in 20 mM Na_2HPO_4 or 20 mM $NaHCO_3$ buffer, pH 9.0, as indicated. The results for the stopped flow kinetic experiments using *cis*-3-bromoacrylic acid are shown in Figures 2.13-2.18. (The results for the stopped flow kinetic experiments using *cis*-3-chloroacrylic acid can be found in the supplement to this chapter.) Each trace shows a rapid decrease in fluorescence followed by a slow decrease in fluorescence. The decay in fluorescence can be fit to a double exponential equation to yield rates, (k_{obs}), and amplitudes for the fast and slow phases (17). The values for k_{obs}

for the fast phase were plotted versus the concentrations of substrate. The data can be fit to a an equation for a hyperbola (equation 2),

$$k_{obs} = \frac{k_{for}[S]}{(K_d + [S])} + k_{rev} \quad (2)$$

where k_{obs} is the observed rate, k_{for} is the forward reaction rate of the conformational change, k_{rev} is the reverse reaction rate of the conformational change, [S] is the concentration of substrate, and K_d is the binding constant. This fit yields a K_d of 1366 ± 300 μM and a maximum k_{obs} of 136 s^{-1} (the sum of k_{for} of 89 s^{-1} and k_{rev} of 47 s^{-1}) for *cis*-CaaD with *cis*-3-bromoacrylic acid. The same experiments were conducted in 20 mM $NaHCO_3$-NaOH buffer, pH 9.0, using *cis*-3-bromoacrylic acid. However, at high concentrations of substrate (>3500 μM) the fluorescence signals were not reproducible so that reliable rate constants could not be determined. For *cis*-3-chloracrylic acid in 20 mM phosphate buffer, pH 9.0, this analysis gives a K_d of 1101 ± 137 μM, a maximum k_{obs} of 103 s^{-1} (sum of k_{for} of 95 s^{-1} and k_{rev} of 8 s^{-1}) (data shown in supplement).

The slow rates were also plotted versus the concentrations of substrate. The data can be fit to an equation for a hyperbola (equation 2) and gives a K_d of 151 ± 21 μM, a maximum k_{obs} of 3.4 s^{-1} (sum of k_{for} of 1.5 s^{-1} and k_{rev} of 1.9 s^{-1}) for *cis*-CaaD with *cis*-3-bromoacrylic acid, and a K_d of 130 ± 21 μM, a maximum k_{obs} of 3.2 s^{-1} (sum of k_{for} of 1.5 s^{-1} and k_{rev} of 1.7 s^{-1}) with *cis*-3-chloroacrylic acid in 20 mM phosphate buffer, pH 9.0 (data shown in supplement).

The concentration dependence of the rates and amplitudes of the reaction mirrors changes in the kinetics of substrate binding. The hyperbolic behavior suggests a two-step

mechanism that approaches a maximum rate and is limited by a first order isomerization (i.e., conformational change) of the enzyme-substrate complex (17). This suggests that *cis*-CaaD binds *cis*-3-bromoacrylic acid in the first step (with a K_d of ~1400 μM) and then the complex undergoes a change in conformation.

2.3.7 Proposed Kinetic Mechanism for *cis*-CaaD

Data Analysis and Computer Simulation. The combination of the rapid quench and stopped flow kinetic experiments allows a determination of the rates for a five-step reaction mechanism (Scheme 3) by global fitting and computer simulation. Stopped flow kinetic experiments provide information about the rates of substrate binding, and rapid quench experiments provide information about the rest of the reaction. Accordingly, two data sets were fit globally using the KinTek Global Kinetic Explorer program. The first data set consisted of the two burst experiments carried out with *cis*-CaaD (125 and 250 μM) and *cis*-3-bromoacrylic acid (5000 μM) in 20 mM $NaHCO_3$ buffer, pH 9.0 (Figure 2.19).

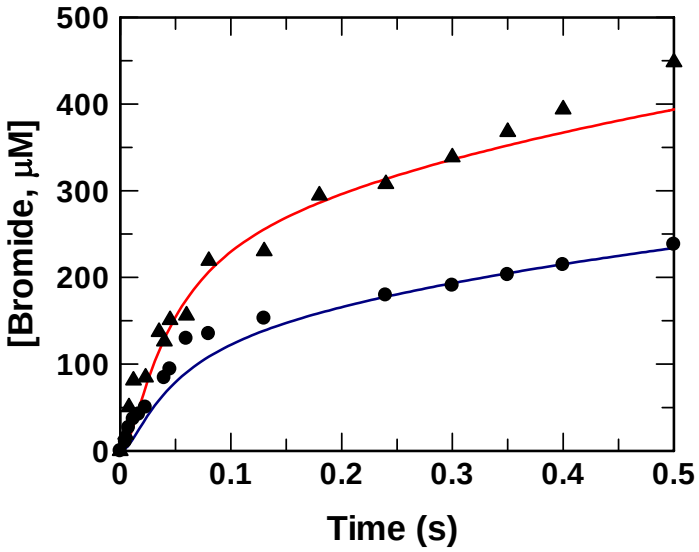

Figure 2.19. Burst kinetics of *cis*-CaaD with *cis*-3-bromoacrylic acid (125 μM filled circles, 250 μM filled triangles) in 20 mM $NaHCO_3$ buffer, pH 9.0. Simulated curves at 125 μM and 250 μM are shown in blue and red, respectively.

The second data set consisted of four stopped flow fluorescence traces carried out with *cis*-CaaD (10 μM) and *cis*-3-bromoacrylic acid (1000 μM, 1250 μM, 1500 μM, and 2000 μM after mixing) in 20 mM $NaHCO_3$ buffer, pH 9.0 (Figure 2.20). The data obtained in the $NaHCO_3$ buffer were used in the simulation experiments because the rapid quench reactions were carried out in this buffer. The fluorescence signals at these four concentrations of substrate are reproducible.

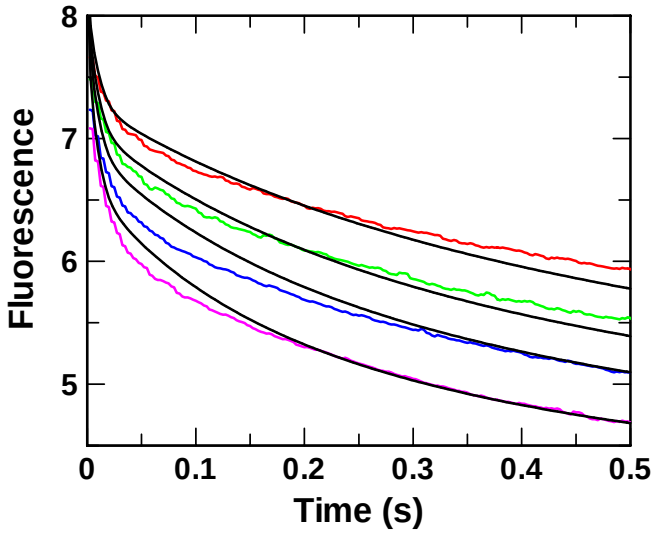

Figure 2.20. Stopped flow fluorescence traces with *cis*-CaaD (10 μM) and *cis*-3-bromoacrylic acid (1000 μM, red; 1250 μM, green; 1500 μM, blue; 2000 μM, purple) in 20 mM $NaHCO_3$ buffer, pH 9.0. The black lines represent the simulated traces.

These two data sets can be fit to a five-step mechanism (Scheme 3) where the enzyme binds the substrate, followed by a conformational change to FS, followed by fast product formation to EPQ, and then a slow release of one product P, followed by fast release of a second product Q .

Scheme 3

$$\mathbf{E + S} \underset{359\ s^{-1}}{\overset{0.057\ \mu M^{-1}\ s^{-1}}{\rightleftharpoons}} \mathbf{ES} \underset{16\ s^{-1}}{\overset{86\ s^{-1}}{\rightleftharpoons}} \mathbf{FS} \xrightarrow{132\ s^{-1}} \mathbf{EPQ} \underset{163\ \mu M^{-1}\ s^{-1}}{\overset{154\ s^{-1}}{\rightleftharpoons}} \mathbf{EQ + P} \xrightarrow{274\ s^{-1}} \mathbf{E + Q + P}$$

The rate constants shown in Scheme 3 were estimated by the computer simlution of the two burst experiments and the four stopped-flow experiments. In the simulation, it was assumed that product formation is irreversible (k_{-3}). It was also assumed that product binding to free enzyme was negligible. The simulation was carried out by a trial and error process. However, the fit was constrained by the experimentally determined k_{for} and k_{rev} from the fast phase of the stopped flow experiment.

A k_{cat} of 29 s^{-1} was calculated from these simulated rate constants (17). This value does not agree with the value measured experimentally for *cis*-3-bromoacrylic acid (~2.7 s^{-1}). However, the value of k_{-4} (the binding of P to EQ) is concentration dependent. When this concentration dependence is factored into the calculation, the k_{cat} value becomes ~5 s^{-1}, which is in reasonable agreement with the experimentally determined value. According to the model, the build up of bromide ion inhibits product release from the EPQ complex, thereby making product release rate limiting.

2.4 Summary: Analysis and Implications

Our results clearly show that *cis*-CaaD is amenable to pre-steady state kinetic analysis, and a minimal kinetic model has been obtained. In addition, the Y103F and E114Q mutants of *cis*-CaaD can be analyzed by both stopped flow and rapid quench methods. These experiments are currently being pursued and will provide insight into the mechanism for the addition of water to substrate. Stopped-flow kinetic analysis of the P1A mutant of *cis*-CaaD shows non-interpretable fluorescence decay. This mutant may "damage" the active site such that events at the active site cannot be reliably monitored by Trp-101. Finally, the R70A-, R73A-, and H28A-*cis*-CaaD show no fluorescence

change upon substrate binding. These observations could suggest that the substrate doesn't bind to these mutants or binds very weakly (> 5 mM), thereby accounting for the observed lack of activity. These residues are currently being investigated using more conservative mutations (e.g., the R70K-, R73K-, and H28Q-*cis*-CaaD).

The observation that bromide release is the rate limiting step in the *cis*-CaaD-catalyzed reaction could argue for or against the presence of a halide binding pocket. A halide binding pocket is identified by crystallographic analysis, competitive inhibition by halide, and fluorescence quenching by halide. The purpose of the pocket is to assist the cleavage of the carbon-halogen bond and stabilization of the negative charge of the halide product. For example, in haloalkane dehalogenase, two tryptophan residues (Trp-125 and Trp-175) form hydrogen bonds with chloride, as shown by crystallographic studies (13a, d). Before another turnover can occur the halide, in this case chloride, must leave the binding pocket. Burst experiments on the haloalkane dehalogenase show halide release is rate limiting and suggested that "escape' of the halide from the pocket limits the overall reaction. In the W175Y mutant, halide release is accelerated and no longer rate limiting. It was suggested that this mutation allowed the halide to "escape" more easily from the pocket (18).

In *cis*-CaaD (and CaaD), a halide-binding pocket may not be necessary. Examination of Scheme 2 shows that addition of water to substrate results in three unstable species, the enediolate species, the halohydrin **5**, and the enol intermediate **6**. These putative intermediates may not need much catalysis for decay. The lifetime of the enediolate in water should be even shorter than the lifetime of ~10^{-9} s for the enolate of

ethyl acetate (19). The lifetimes of **5** and **6** are longer but still require little catalysis for decay. Although a halide binding pocket may not be necessary and may not be present, the escape of halide from the *cis*-CaaD active site could still limit overall catalysis.

2.5 References

1. (a) Hartmans, S., Jansen, M.W., van der Werf, M.J., de Bont, J.A.M. (1991) Bacterial metabolism of 3-chloroacrylic acid, *J. Gen. Microb. 137*, 2025-2032. (b) Van Hylckama Vlieg, J.E.T., Janssen, D.B. (1992) Bacterial degradation of 3-chloroacrylic acid and the characterization of *cis*- and *trans*-specific dehalogenases, *Biodegradation 2*, 139-150. (c) Poelarends, G.J., Wilkens, M., Larkin, M.J., van Elsas, J.D., Janssen, D.B. (1998) Degradation of 1,3-dichloropropene by *Pseudomonas cichorii* 170, *Appl. Environ. Microbiol. 64*, 2931-2936.

2. Poelarends, G.J., Whitman, C.P. (2004) Evolution of enzymatic activity in the tautomerase superfamily: mechanistic and structural studies of the 1,3-dichloropropene catabolic enzymes, *Bioorg. Chem. 32*, 376-92.

3. Murzin, A.G. (1996) Structural classification of proteins: new superfamilies, *Curr. Opin. Struct. Biol*. *6*, 386-394.

4. Whitman, C.P. (2002) The 4-oxalocrotonate tautomerase family of enzymes: how nature makes new enzymes using a β-α-β structural motif, *Arch. Biochem. Biophys. 402*, 1-13.

5. Poelarends, G.J., Saunier, R., Janssen, D.B. (2001) *trans*-3-Chloroacrylic acid dehalogenase from *Pseudomonas pavonaceae* 170 shares structural and mechanistic similarities with 4-oxalocrotonate tautomerase, *J. Bacteriol. 183*, 4269-4277.

6. Wang, S.C., Person, M.D., Johnson, W.H., Jr., Whitman, C.P. (2003) Reactions of *trans*-3-chloroacrylic acid dehalogenase with acetylene substrates: consequences of and evidence for a hydration reaction, *Biochemistry 42*, 8762-8773.

7. de Jong, R.M., Brugman, W., Poelarends, G.J., Whitman, C.P., Dijkstra, B.W. (2004) The X-ray structure of *trans*-3-chloroacrylic acid dehalogenase reveals a novel hydration mechanism in the tautomerase superfamily, *J. Biol. Chem. 279*, 11546-11552.

8. Azurmendi, H.F., Wang, S.C., Massiah, M.A., Poelarends, G.J., Whitman, C.P., Mildvan, A.S. (2004) The roles of active-site residues in the catalytic mechanism of *trans*-3-chloroacrylic acid dehalogenase: a kinetic, NMR, and mutational analysis, *Biochemistry 43*, 4082-4091.

9. Poelarends, G. J., Serrano, H., Person, M. D., Johnson, W. H., Jr., Murzin, A. G., Whitman, C.P. (2004) Cloning, expression, and characterization of a *cis*-3-chloroacrylic acid dehalogenase: insights into the mechanistic, structural, and evolutionary relationship between isomer-specific 3-chloroacrylic acid dehalogenases, *Biochemistry 43*, 759-772.

10. Poelarends, G.J., Serrano, H., Johnson, Jr., W.H., Whitman, C.P. (2004) Stereospecific alkylation of *cis*-chloroacrylic acid dehalogenase by (*R*)-oxirane-2-carboxylate: analysis and mechanistic implications, *Biochemistry 43*, 7187-7196.

11. de Jong, R.M., Bazzacco, P., Poelarends, G.J., Johnson, Jr, W.H., Kim, Y.-J., Burks, E.A., Serrano, H., Whitman, C.P., Dijkstra B.W., Crystal structures of wild type and inactivated *cis*-3-chloroacrylic acid dehalogenase: the structural basis for substrate specificity and inactivation by (*R*)-oxirane-2-carboxylate, *J. Biol. Chem. 282*, 2440-2449 (2007).

12. (b) Poelarends, G.J., Serrano, H., Johnson, Jr., W.H., and Whitman, C.P. (2007) The phenylpyruvate tautomerase activity of *trans*-3-chloroacrylic acid dehalogenase: evidence for an enol intermediate?", *Biochemistry* (in press).

13. (a) Verschueren, K.H.G., Kingma, J., Rozeboom, H.J., Kalk, K.H., Janssen, D.B., Dijkstra, B.W., (1993) Crystallographic and fluorescence studies of the interaction of haloalkane dehalogenase with halide ions. Studies with halide compounds reveal a halide binding site in the active site, *Biochemistry 32,* 9031-9037. (b) Schanstra, J.P., Janssen, D.B., (1996) Kinetics of halide release of haloalkane dehalogenase: evidence for a slow conformational change, *Biochemistry 35,* 5624-5632. (c) Schindler, J.F., Naranjo, P.A., Honaberger, D.A., Chang, C-H., Brainard, J.R., Vanderberg, L.A., Unkefer, C.J., (1999) Haloalkane dehalogenases: steady-state kinetics and halide inhibition, *Biochemistry 38,* 5772-5778. (d) Bosma, T., Pikkemaat, M.G., Kingma, J., Dijk, J., Janssen, D.B., (2003) Steady-state and pre-steady-state kinetic analysis of halopropane conversion by a *Rhodococcus* haloalkane dehalogenase, *Biochemistry 42,* 8047-8053. (e) Tang, L., Pazmiño, D.E.T., Fraaije, M.W., de Jong, R.M., Dijkstra, B.W., Janssen, D.B., (2005) Improved catalytic properties of halohydrin dehalogenase by modification of the halide-binding site, *Biochemistry 42,* 6609-6618.

14. Sambrook, J., Fritsch, E. F., and Maniatis, T. (1989) *Molecular Cloning: A Laboratory Manual*, 2nd ed, Cold Spring Harbor Laboratory, Cold Spring Harbor, NY.

15. Waddell, W. J. (1956) A simple ultraviolet spectrophotometric method for the determination of protein, *J. Lab. Clin. Med. 48*, 311-314.

16. Laemmli, U.K. (1970) Cleavage of structural proteins during the assembly of the head of bacteriophage T4, *Nature 227*, 680-685.

17. Johnson, K.A. (1992) Transient state kinetic analysis of enzyme reaction pathways, *The Enzymes,* XX, 1-61.

18. Krooshof, G.H., Ridder, I.S., Tepper, A.W., Vos, G.J., Rozeboom, H.J,, Kalk, K.H,, Dijkstra, B.W., Janssen, D.B. (1998) Kinetic analysis and X-ray structure of haloalkane dehalogenase with a modified halide-binding site, *Biochemistry 37*, 15013-23.

19. Amyes, T.L., and Richard, J.P. (1996) Determination of the pK_a of ethyl acetate: bronsted correlation for deprotonation of a simple oxygen ester in aqueous solution, *J. Am. Chem. Soc. 118* , 3129 -3141.

Supplement to Chapter 2: Purification, Characterization, and Pre-Steady State Kinetic Studies of *cis*-CaaD Mutants

S.2.1 Introduction

The supplement contains the purification protocols for the P1A-, H28A-, R70A-, R73A-, Y103F-, and E114Q-mutants of *cis*-CaaD, and steady-state kinetic parameters for the Y103F- and E114Q-mutants. In addition, it reports the stopped-flow kinetic experiments for the six *cis*-CaaD mutants using *cis*-3-chloro- and *cis*-3-bromoacrylic acid, as indicated. Some additional data obtained for the wild type enzyme is included. Where possible, the decays in fluorescence have been fit to double or single exponentials. The k_{obs} and amplitudes have also been determined and plotted versus substrate concentration where possible. The apparent K_d values and rate constants are reported. Finally, the rapid chemical quench experiment for the E114Q mutant of *cis*-CaaD, analysis of the burst, and derived rate constants are reported.

S.2.2 Materials and Methods

The materials and methods used in the supplement are described in the parent chapter.

S.2.2.1 Transformation, Expression and Purification of *cis*-CaaD Mutants

Expression and Purification of P1A-cis-CaaD. The pCC5 plasmid containing the P1A-*cis*-CaaD gene (9) was transformed as described in the parent chapter for the wild type *cis*-CaaD gene into *E. coli* BL21-Gold(DE3) cells for protein expression. The gene product was expressed using the T7 expression system as described for wild type.

Typically 1 L of culture yields 5 g of cells which were frozen until ready for use. The cells (~10g) were thawed and processed following the protocol described for lysis of wild type cells and subsequent protein purification. Fractions from the TSKgel DEAE-5PW anion-exchange column (#4-18) with the highest purity (as determined by SDS-PAGE) were pooled and concentrated to ~20 mL using an Amicon stirred cell equipped with a YM10 (10,000 MW cutoff) ultrafiltration membrane. Fractions from the TSKgel Phenyl-5PW column (#9-12) with the highest purity (as determined by SDS-PAGE) were pooled and concentrated to ~4.5 mL using an Amicon stirred cell equipped with a YM10 (10,000 MW cutoff) ultrafiltration membrane and stored at 4 °C. This purification resulted in ~70 mg of 95% pure protein as assessed by ESI mass spectroscopy and SDS-PAGE. The observed monomer mass for P1A-*cis*-CaaD was 16,595 Da.

Expression and Purification of H28A-cis-CaaD. The pCC5 plasmid containing the H28A-*cis*-CaaD gene (11) was transformed as described in the parent chapter for the wild type *cis*-CaaD gene into *E. coli* BL21-Gold(DE3) cells for protein expression. The gene product was expressed using the T7 expression system as described for wild type. Typically 1 L of culture yields 5 g of cells which were frozen until ready for use. The cells (~10g) were thawed and processed following the protocol described for lysis of wild type cells and subsequent protein purification. Fractions from the TSKgel DEAE-5PW anion-exchange column (#12-34) with the highest purity (as determined by SDS-PAGE) were pooled and concentrated to ~20 mL using an Amicon stirred cell equipped with a YM10 (10,000 MW cutoff) ultrafiltration membrane. Fractions from the TSKgel Phenyl-5PW column (#22-25) with the highest purity (as determined by SDS-PAGE) were

pooled and concentrated to ~2 mL using an Amicon stirred cell equipped with a YM10 (10,000 MW cutoff) ultrafiltration membrane and stored at 4 °C. This purification resulted in ~25 mg of 90% pure protein as assessed by ESI mass spectroscopy and SDS-PAGE. The observed monomer mass for H28A-*cis*-CaaD was 16,554 Da.

Expression and Purification of R70A-cis-CaaD. The pCC5 plasmid containing the R70A-*cis*-CaaD gene (9) was transformed as described in the parent chapter for the wild type *cis*-CaaD gene into *E. coli* BL21-Gold(DE3) cells for protein expression. The gene product was expressed using the T7 expression system as described for wild type. Typically 1 L of culture yields 5 g of cells which were frozen until ready for use. The cells (~10g) were thawed and processed following the protocol described for lysis of wild type cells and subsequent protein purification. Fractions from the TSKgel DEAE-5PW anion-exchange column (#12-34) with the highest purity (as determined by SDS-PAGE) were pooled and concentrated to ~20 mL using an Amicon stirred cell equipped with a YM10 (10,000 MW cutoff) ultrafiltration membrane. Fractions from the TSKgel Phenyl-5PW column (#20-22) with the highest purity (as determined by SDS-PAGE) were pooled and concentrated to ~4.5 mL using an Amicon stirred cell equipped with a YM10 (10,000 MW cutoff) ultrafiltration membrane and stored at 4 °C. This purification resulted in ~70 mg of 95% pure protein as assessed by ESI mass spectroscopy and SDS-PAGE. The observed monomer mass for R70A-*cis*-CaaD was 16,534 Da.

Expression and Purification of R73A-cis-CaaD. The pCC5 plasmid containing the R73A-*cis*-CaaD gene (9) was transformed as described in the parent chapter for the wild type *cis*-CaaD gene into *E. coli* BL21-Gold(DE3) cells for protein expression. The

gene product was expressed using the T7 expression system as described for wild type. Typically 1 L of culture yields 5 g of cells which were frozen until ready for use. The cells (~10g) were thawed and processed following the protocol described for lysis of wild type cells and subsequent protein purification. Fractions from the TSKgel DEAE-5PW anion-exchange column (#12-34) with the highest purity (as determined by SDS-PAGE) were pooled and concentrated to ~20 mL using an Amicon stirred cell equipped with a YM10 (10,000 MW cutoff) ultrafiltration membrane. Fractions from the TSKgel Phenyl-5PW column (#19-21) with the highest purity (as determined by SDS-PAGE) were pooled and concentrated to ~6 mL using an Amicon stirred cell equipped with a YM10 (10,000 MW cutoff) ultrafiltration membrane and stored at 4 °C. This purification resulted in ~120 mg of 90% pure protein as assessed by ESI mass spectroscopy and SDS-PAGE. The observed monomer mass for R73A-*cis*-CaaD was 16,534 Da.

Expression and Purification of Y103F-cis-CaaD. The pCC5 plasmid containing the Y103F-*cis*-CaaD gene (11) was transformed as described in the parent chapter for the wild type *cis*-CaaD gene into *E. coli* BL21-Gold(DE3) cells for protein expression. The gene product was expressed using the T7 expression system as described for wild type. Typically 1 L of culture yields 5 g of cells which were frozen until ready for use. The cells (~10g) were thawed and processed following the protocol described for lysis of wild type cells and subsequent protein purification. Fractions from the TSKgel DEAE-5PW anion-exchange column (#18-30) with the highest purity (as determined by SDS-PAGE) were pooled and concentrated to ~20 mL using an Amicon stirred cell equipped with a YM10 (10,000 MW cutoff) ultrafiltration membrane. Fractions from the TSKgel Phenyl-

5PW column (#20-22) with the highest purity (as determined by SDS-PAGE) were pooled and concentrated to ~15 mL using an Amicon stirred cell equipped with a YM10 (10,000 MW cutoff) ultrafiltration membrane and stored at 4 °C. This purification resulted in ~300 mg of 95% pure protein as assessed by ESI mass spectroscopy and SDS-PAGE. The observed monomer mass for Y103F-*cis*-CaaD was 16,605 Da.

Expression and Purification of E114Q-cis-CaaD. The pCC5 plasmid containing the E114Q-*cis*-CaaD gene (9) was transformed as described in the parent chapter for the wild type *cis*-CaaD gene into *E. coli* BL21-Gold(DE3) cells for protein expression. The gene product was expressed using the T7 expression system as described for wild type. Typically 1 L of culture yields 5 g of cells which were frozen until ready for use. The cells (~10g) were thawed and processed following the protocol described for lysis of wild type cells and subsequent protein purification. Fractions from the TSKgel DEAE-5PW anion-exchange column (#11-32) with the highest purity (as determined by SDS-PAGE) were pooled and concentrated to ~20 mL using an Amicon stirred cell equipped with a YM10 (10,000 MW cutoff) ultrafiltration membrane. Fractions from the TSKgel Phenyl-5PW column (#10-15) with the highest purity (as determined by SDS-PAGE) were pooled and concentrated to ~6 mL using an Amicon stirred cell equipped with a YM10 (10,000 MW cutoff) ultrafiltration membrane and stored at 4 °C. This purification resulted in ~130 mg of 95% pure protein as assessed by ESI mass spectroscopy and SDS-PAGE. The observed monomer mass for E114Q-*cis*-CaaD was 16,619 Da.

S.2.2.2 Steady-State Kinetic Parameters for *cis*-CaaD Mutants

The steady-state kinetic parameters for the E114Q and Y103F mutants of *cis*-CaaD were measured as described for wild type in the parent chapter using *cis*-3-chloro- and *cis*-3-bromoacrylic acid. The assay was initiated by the addition of substrate (10-700 μM for E114Q-*cis*-CaaD and 1.5-100 μM for Y103F-*cis*-CaaD). The data were analyzed as described for wild type in the parent chapter.

S.2.2.3 Stopped Flow Experiments With *cis*-CaaD Mutants

Stopped Flow Experiments With the E114Q Mutant of cis-CaaD. The stopped flow experiments with the E114Q mutant of *cis*-CaaD were carried out as described in the parent chapter for wild type *cis*-CaaD in 20 mM Na_2HPO_4 buffer, pH 9.0. *cis*-3-Chloro- and *cis*-3-bromoacrylic acid (100-50,000 μM before mixing) were made up as described for wild type. In order to reduce photobleaching, the slit width on the xenon light source and the light filter were set at 3.16 mm. The high voltage output was set at 600 volts. Three time intervals (3.5, 15, and 30s) were recorded for each substrate concentration. Each experiment was repeated 5 times.

Stopped Flow Experiments With the Y103F Mutant of cis-CaaD. The stopped flow experiments with the Y103F mutant of *cis*-CaaD were carried out as described in the parent chapter for wild type *cis*-CaaD in 20 mM Na_2HPO_4 buffer, pH 9.0. *cis*-3-Chloro- and *cis*-3-bromoacrylic acid (25-15,000 μM before mixing) were made up as described for wild type. In order to reduce photobleaching, the slit width on the xenon light source and the light filter were set at 1.56 mm. The high voltage output was set at 753 volts.

Three time intervals (1, 2, and 10s) were recorded for each substrate concentration. Each experiment was repeated 5 times.

Stopped Flow Experiments With the P1A Mutant of cis-CaaD. The stopped flow experiments with the P1A mutant of *cis*-CaaD were carried out as described in the parent chapter for wild type *cis*-CaaD in 20 mM Na_2HPO_4 buffer, pH 9.0. *cis*-3-Chloro- and *cis*-3-bromoacrylic acid (25-100,000 μM before mixing) were made up as described for wild type. In order to reduce photobleaching, the slit width on the xenon light source and the light filter were set at 1.56 mm. The high voltage output was set at 710 volts. Three time intervals (2, 20, and 600s) were recorded for each substrate concentration. Each experiment was repeated 5 times.

Stopped Flow Experiments With the H28A, R70A, and R73A Mutants of cis-CaaD. The stopped flow experiments with the H28A, R70A, and R73A mutants of *cis*-CaaD were carried out as described in the parent chapter for wild type *cis*-CaaD in 20 mM Na_2HPO_4 buffer, pH 9.0, using 20 and 50 μM enzyme. *cis*-3-Chloro- and *cis*-3-bromoacrylic acid (25-100,000 μM before mixing) were made up as described for wild type. Various combinations of the slit width on the light source and light filter, along with the HV settings, were used in order to detect a fluorescence signal.

S.2.2.4 Rapid Chemical-Quench Experiment With E114Q-*cis*-CaaD

Rapid Chemical-Quench Flow Measurements Using E114Q-cis-CaaD and cis-3-Bromoacrylic Acid. The rapid quench experiments were carried using a quench-flow apparatus (RQF-3 Rapid Quench Flow) from Kintek Corp (http://www.kintek-corp.com). These reactions were carried out at 22 °C. Typcially, one syringe was loaded with

E114Q-*cis*-CaaD (2000 μM made up in 20 mM $NaCO_3$-NaOH buffer, pH 9.0). Another syringe was loaded with freshly prepared 50,000 μM *cis*-3-bromoacrylic acid (made up in 50 mM $NaHCO_3$-NaOH buffer, pH 10.0). Each reaction was initiated by the rapid mixing of aliquots (15 μL) of the reactants from both syringes. The reaction mixture was quenched at various intervals ranging from 10 ms – 4 min with 80 μL of 0.6 M H_2SO_4. The amount of bromide formed was then quantified using ion chromatography. Kinetic parameters were derived as described in the parent chapter.

S.2.3 Data and Results

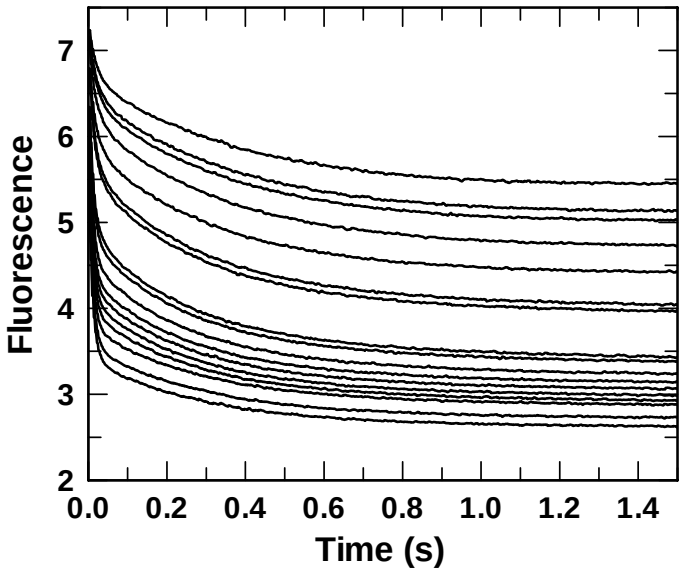

Figure S.2.3.1. Traces from 17 stopped-flow experiments in which *cis*-CaaD (10 μM) in 20 mM Na_2HPO_4 buffer, pH 9.0, was mixed with an equal volume of *cis*-3-chloroacrylic acid (50-4500 μM, top to bottom) at 22 °C. The decrease in fluorescence was fit to an equation for a double exponential. The signals return to the initial fluorescence value at times ranging from 10-180 s. The reported concentrations are those after mixing enzyme and substrate. Only the first 1.5 s of the reaction is shown.

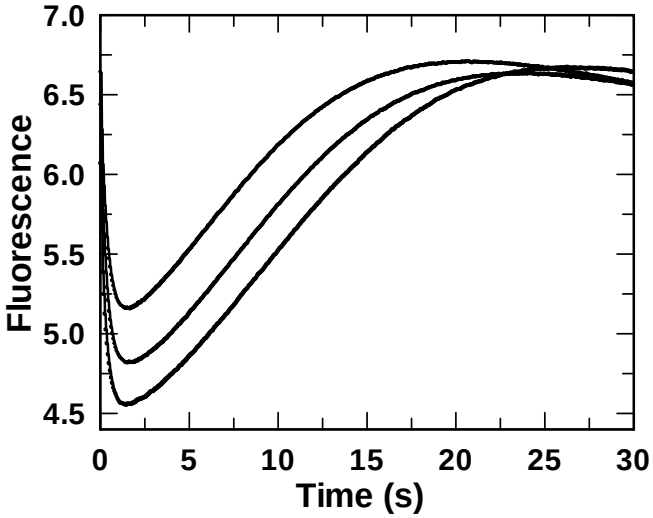

Figure S.2.3.2. Three representative traces from a total of 17 stopped-flow experiments in which *cis*-CaaD (10 μM) in 20 mM Na_2HPO_4 buffer, pH 9.0, was mixed with an equal volume of *cis*-3-chloroacrylic acid (150 μM, 200 μM, and 250 μM, top to bottom) at 22 °C. These reactions were monitored for 30 s to show the return to the initial fluorescence value. The reported concentrations are those after mixing enzyme and substrate.

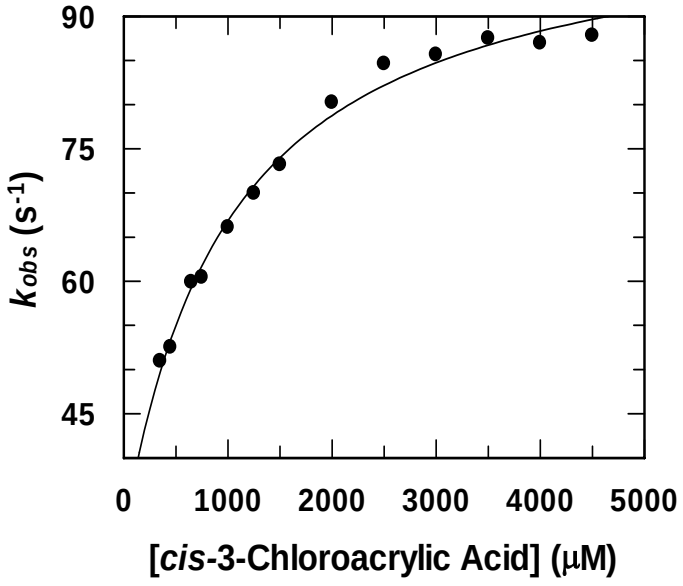

Figure S.2.3.3. Concentration dependence of k_{obs} for binding of *cis*-3-chloroacrylic acid (50–4500 μM) to *cis*-CaaD (10 μM) in 20 mM Na_2HPO_4 buffer, pH 9.0, at 22 °C. The concentration dependence of the fast phase was fit to an equation for a hyperbola. The reported concentrations are those after mixing enzyme and substrate.

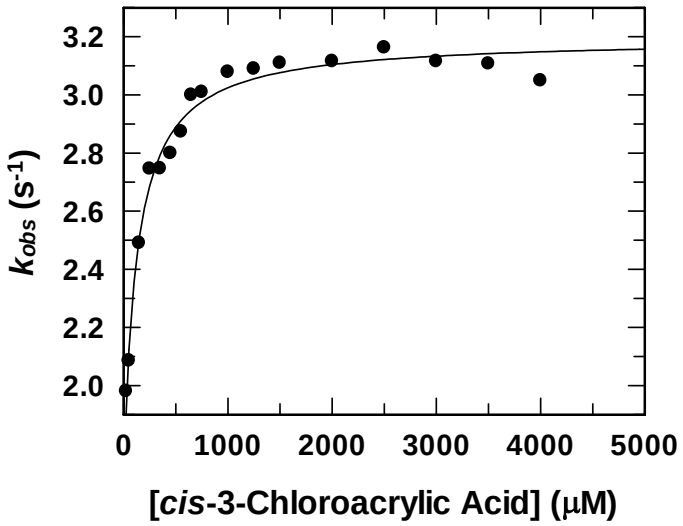

Figure S.2.3.4. Concentration dependence of k_{obs} for binding of *cis*-3-chloroacrylic acid (50–4000 μM) to *cis*-CaaD (10 μM) in 20 mM Na_2HPO_4 buffer, pH 9.0, at 22 °C. The concentration dependence of the slow phase was fit to an equation for a hyperbola. The reported concentrations are those after mixing enzyme and substrate.

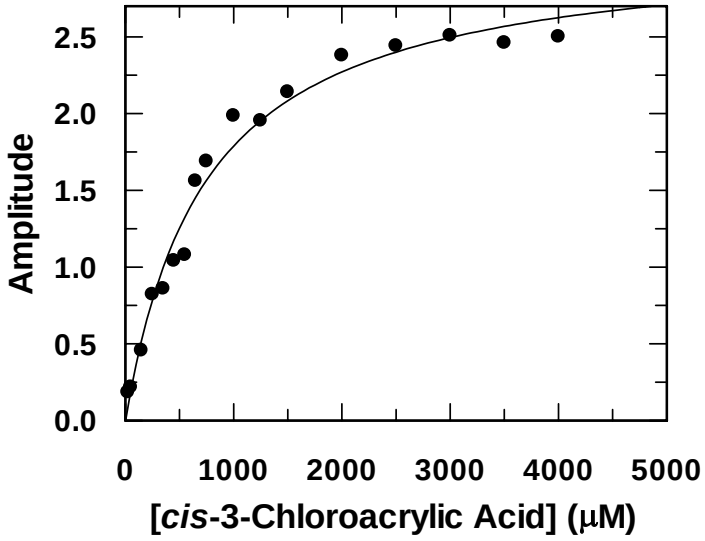

Figure S.2.3.5. Concentration dependence of the amplitude for the fast phase binding of *cis*-3-chloroacrylic acid (50–4000 μM) to *cis*-CaaD (10 μM) in 20 mM Na_2HPO_4 buffer, pH 9.0, at 22 °C. The concentration dependence of the amplitude was fit to an equation for a hyperbola. The reported concentrations are those after mixing enzyme and substrate.

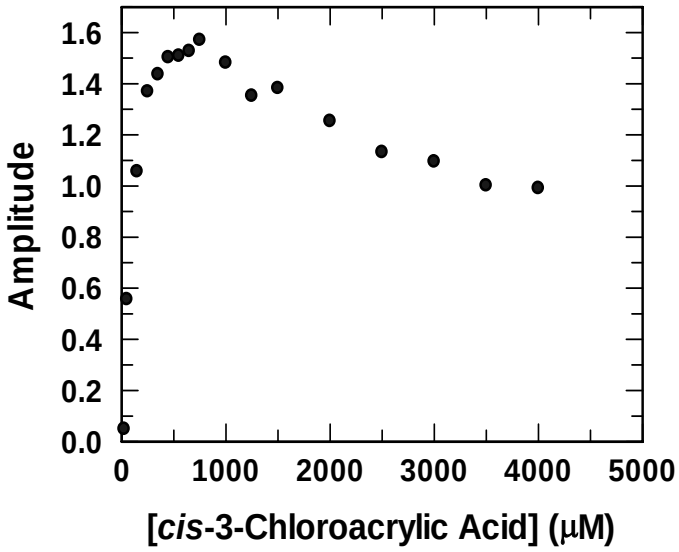

Figure S.2.3.6. Concentration dependence of the amplitude for the slow phase binding of *cis*-3-chloroacrylic acid (50–4000 μM) to *cis*-CaaD (10 μM) in 20 mM Na_2HPO_4 buffer, pH 9.0, at 22 °C. The concentration dependence could not be fit. The reported concentrations are those after mixing enzyme and substrate.

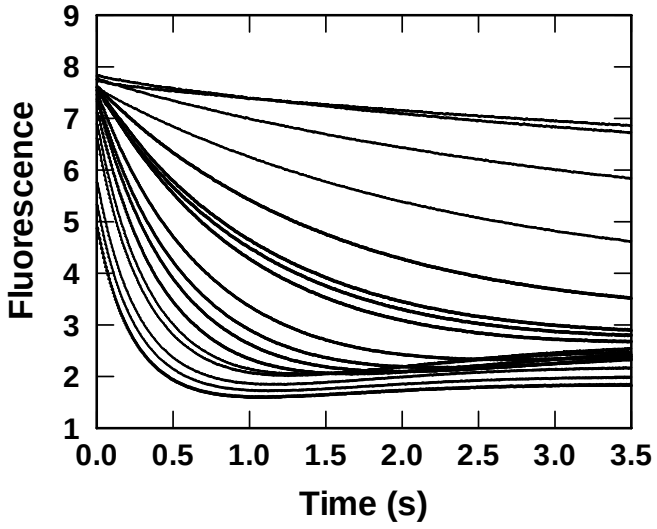

Figure S.2.3.7. Traces from 17 stopped-flow experiments in which E114Q-*cis*-CaaD (10 μM) in 20 mM Na_2HPO_4 buffer, pH 9.0, was mixed with an equal volume of *cis*-3-chloroacrylic acid (50-25,000 μM, top to bottom) at 22 °C. The decrease in fluorescence was fit to either a single exponential (50-3,500 μM) or a double exponential (3,500-25,000 μM). The signal does not return to the initial fluorescence reading. The reported concentrations are those after mixing enzyme and substrate. The individual reactions were monitored for 3.5 s.

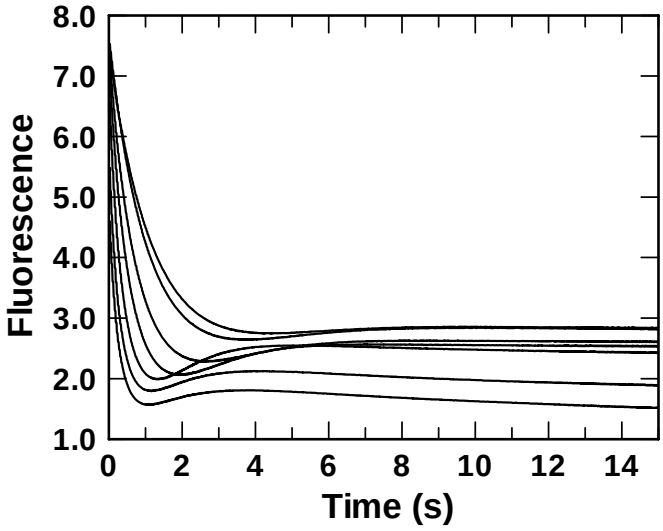

Figure S.2.3.8. Seven representative traces from 17 stopped-flow experiments in which E114Q-*cis*-CaaD (10 μM) in 20 mM Na_2HPO_4 buffer, pH 9.0, was mixed with an equal volume of *cis*-3-chloroacrylic acid (300 μM, 500 μM, 750 μM, 1500 μM, 5000 μM, 15,000 μM, and 25,000 μM, top to bottom) at 22 °C. The reported concentrations are those after mixing enzyme and substrate. The individual reactions were monitored for 15 s, showing that the signals do not return to the initial fluorescence values.

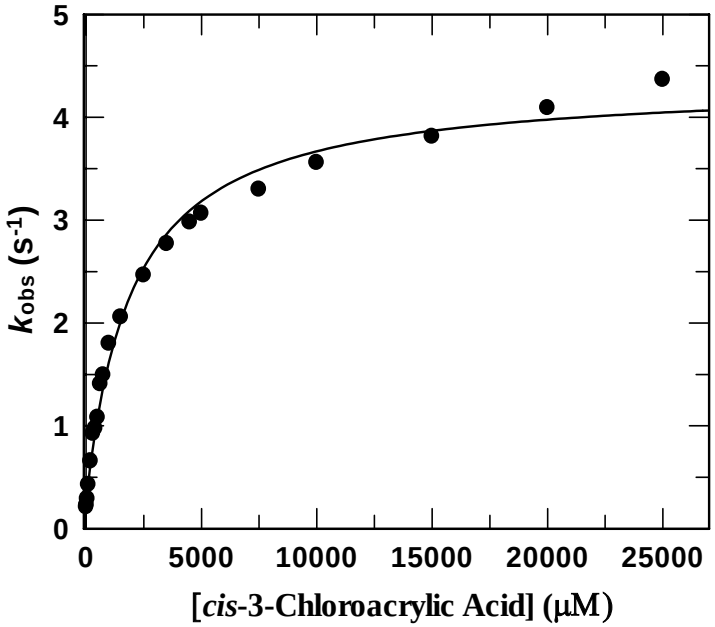

Figure S.2.3.9. Concentration dependence of k_{obs} for binding of *cis*-3-chloroacrylic acid (50–25,000 μM) to E114Q-*cis*-CaaD (10 μM) in 20 mM Na_2HPO_4 buffer, pH 9.0, at 22 °C. The concentration dependence of the fast phase was fit to an equation for a hyperbola. The reported concentrations are those after mixing enzyme and substrate.

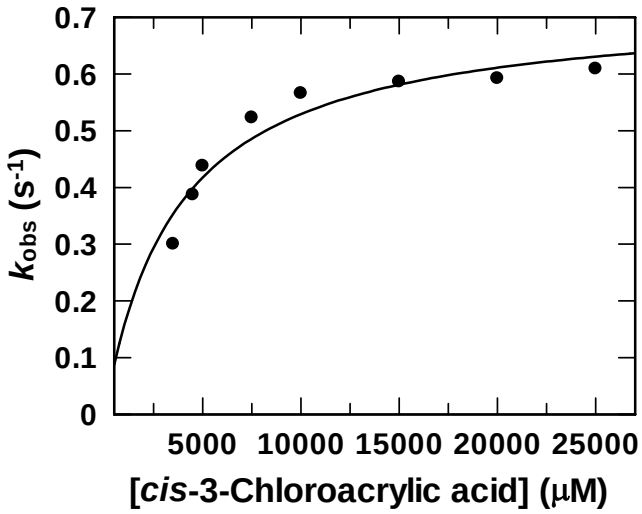

Figure S.2.3.10. Concentration dependence of k_{obs} for binding of *cis*-3-chloroacrylic acid (50–25,000 μM) to E114Q-*cis*-CaaD (10 μM) in 20 mM Na_2HPO_4 buffer, pH 9.0, at 22 °C. The concentration dependence of the slow phase was fit to an equation for a hyperbola. The reported concentrations are those after mixing enzyme and substrate.

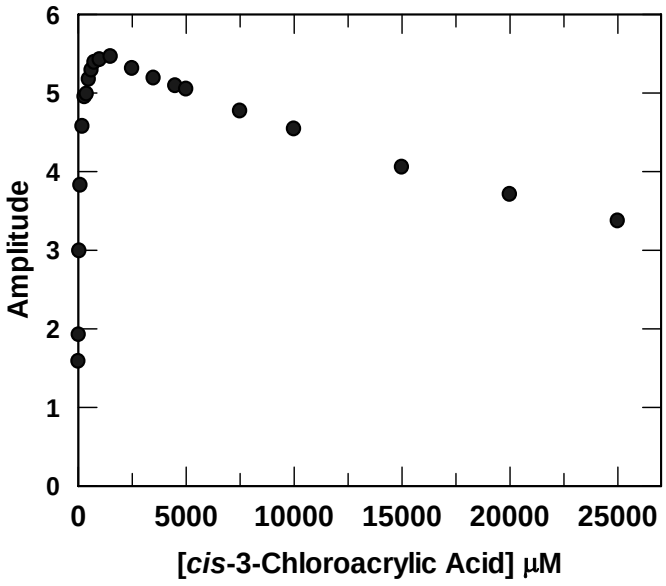

Figure S.2.3.11. Concentration dependence of the amplitude for the fast phase binding of *cis*-3-chloroacrylic acid (50–25,000 μM) to E114Q-*cis*-CaaD (10 μM) in 20 mM Na_2HPO_4 buffer, pH 9.0, at 22 °C. The data could not be fit. The reported concentrations are those after mixing enzyme and substrate.

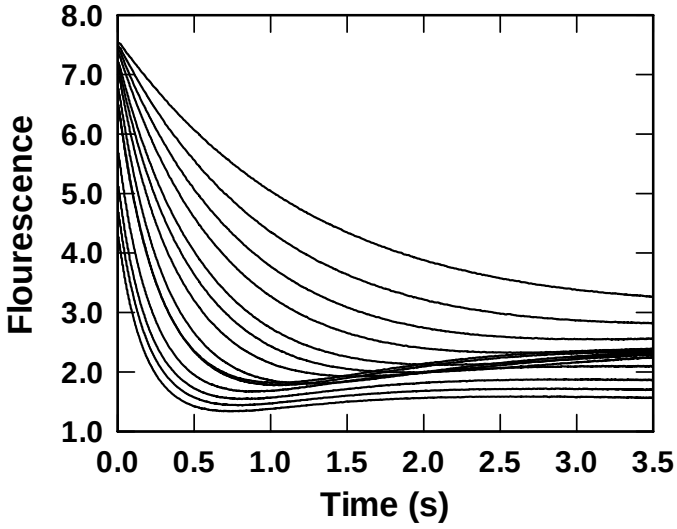

Figure S.2.3.12. Traces from 13 stopped-flow experiments in which E114Q-*cis*-CaaD (10 μM) in 20 mM Na_2HPO_4 buffer, pH 9.0, was mixed with an equal volume of *cis*-3-bromoacrylic acid (50-25,000 μM, top to bottom) at 22 °C. The decrease in fluorescence was fit to a double exponential. The signals do not return to the initial fluorescence value. The reported concentrations are those after mixing enzyme and substrate. The individual reactions were monitored for 3.5 s.

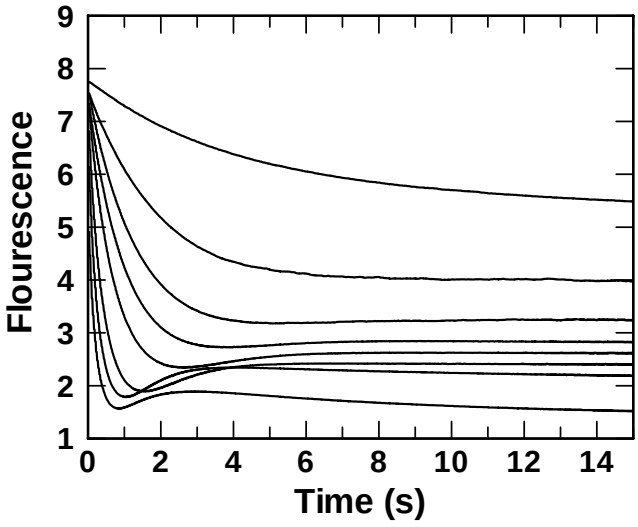

Figure S.2.3.13. Traces from 8 stopped-flow experiments in which E114Q-*cis*-CaaD (10 μM) in 20 mM Na_2HPO_4 buffer, pH 9.0, was mixed with an equal volume of *cis*-3-bromoacrylic acid (50 μM, 100 μM, 200 μM, 300 μM, 500 μM, 1500 μM, 5000 μM and 15,000 μM, top to bottom) at 22 °C. The decrease in fluorescence was fit to a double exponential. The reported concentrations are those after mixing enzyme and substrate. The individual reactions were monitored for 15 s, showing that the signals do not return to the initial fluorescence value.

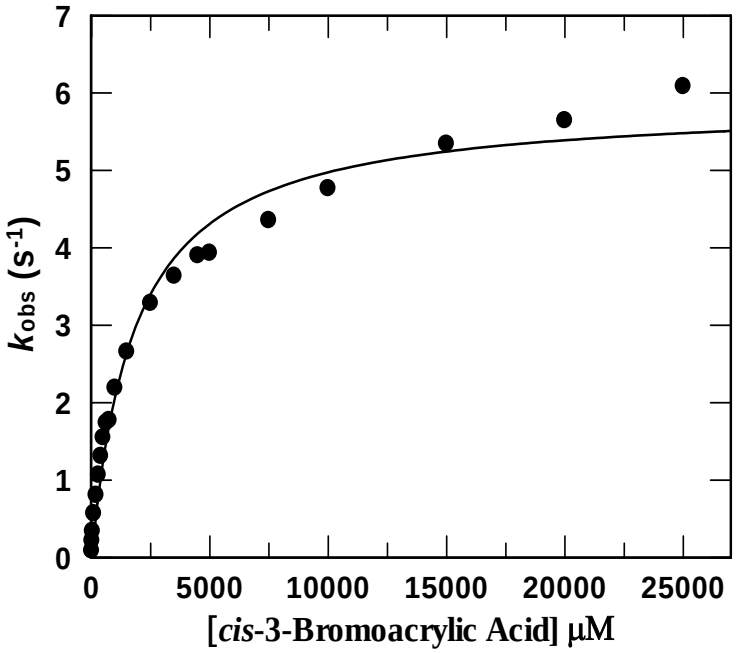

Figure S.2.3.14. Concentration dependence of k_{obs} for binding of *cis*-3-bromoacrylic acid (50–25,000 μM) to E114Q-*cis*-CaaD (10 μM) in 20 mM Na_2HPO_4 buffer, pH 9.0, at 22 °C. The concentration dependence of the fast phase was fit to an equation for a hyperbola. The reported concentrations are those after mixing enzyme and substrate.

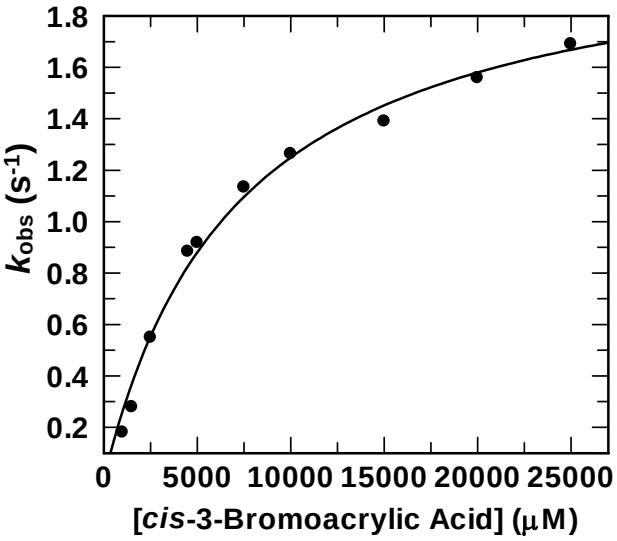

Figure S.2.3.15. Concentration dependence of k_{obs} for binding of *cis*-3-bromoacrylic acid (50–25,000 μM) to E114Q-*cis*-CaaD (10 μM) in 20 mM Na_2HPO_4 buffer, pH 9.0, at 22 °C. The concentration dependence of the slow phase was fit to an equation for a hyperbola. The reported concentrations are those after mixing enzyme and substrate.

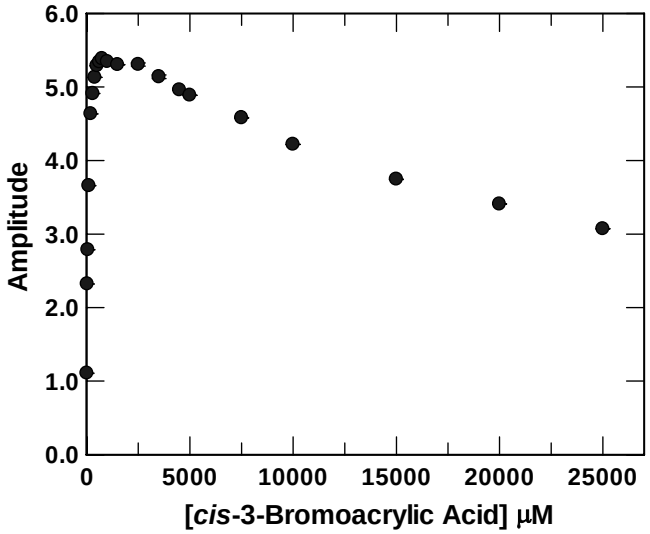

Figure S.2.3.16. Concentration dependence of the amplitude for the fast phase binding of *cis*-3-bromoacrylic acid (50–25,000 μM) to E114Q-*cis*-CaaD (10 μM) in 20 mM Na_2HPO_4 buffer, pH 9.0, at 22 °C. The data could not be fit. The reported concentrations are those after mixing enzyme and substrate.

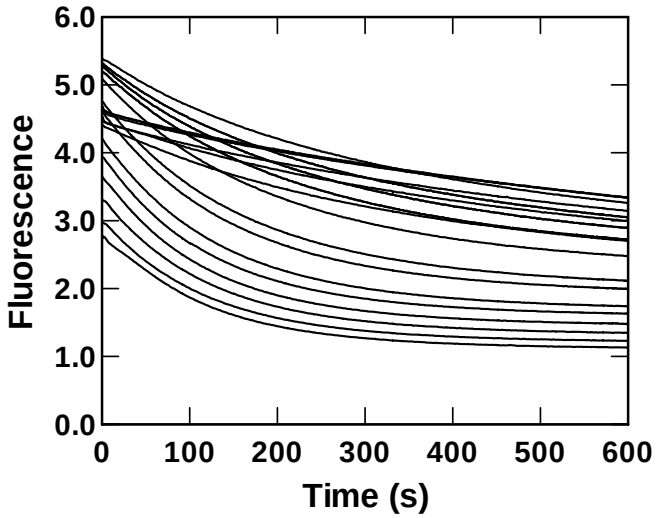

Figure S.2.3.17. Traces from 18 stopped-flow experiments in which P1A-*cis*-CaaD (10 μM) in 20 mM Na_2HPO_4 buffer, pH 9.0, was mixed with an equal volume of *cis*-3-chloroacrylic acid (12.5-25,000 μM, top to bottom) at 22 °C. The reported concentrations are those after mixing enzyme and substrate. The data could not be fit. The individual reactions were monitored for 600 s.

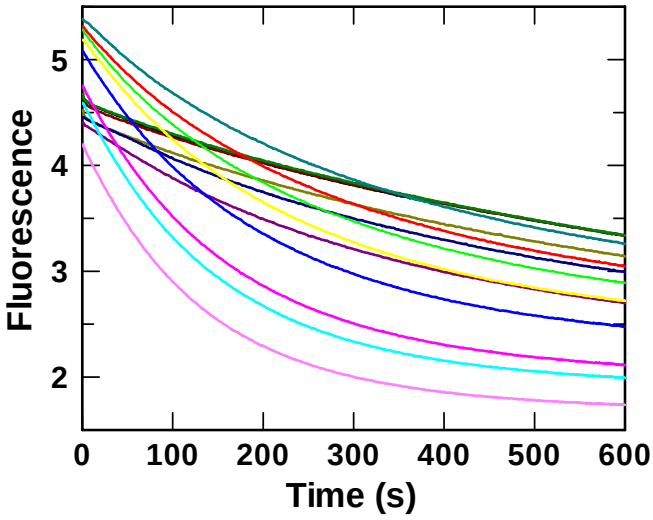

Figure S.2.3.18. Traces from 14 stopped-flow experiments in which P1A-*cis*-CaaD (10 μM) in 20 mM Na_2HPO_4 buffer, pH 9.0, was mixed with an equal volume of *cis*-3-chloroacrylic acid [12.5 μM (black), 25 μM (maroon), 50 μM (green), 100 μM (olive), 200 μM (navy), 400 μM (purple), 500 μM (teal), 625 μM (red), 750 μM (lime), 1000 μM (yellow), 1500 μM (blue), 2500 μM (fuchsia), 3500 μM (aqua), and 5000 μM (pink)] at 22 °C. The data could not be fit. The reported concentrations are those after mixing enzyme and substrate. The individual reactions were monitored for 600 s.

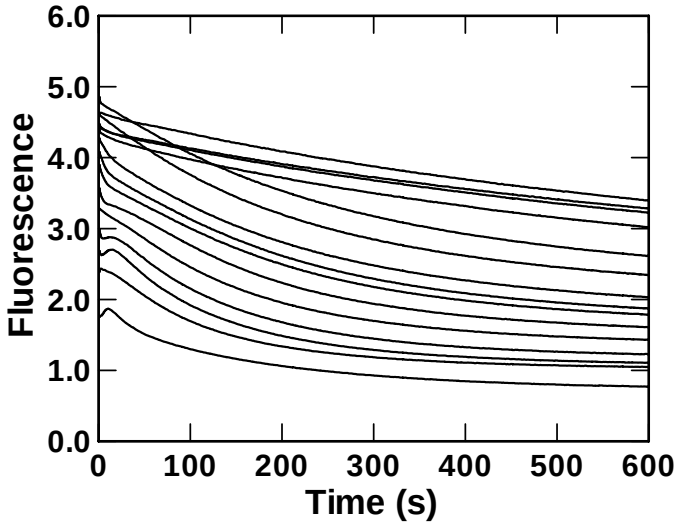

Figure S.2.3.19. Representative traces from 15 stopped-flow experiments in which P1A-*cis*-CaaD (10 μM) in 20 mM Na_2HPO_4 buffer, pH 9.0, was mixed with an equal volume of *cis*-3-bromoacrylic acid (12.5-25,000 μM, top to bottom) at 22 °C. The reported concentrations are those after mixing enzyme and substrate. The data could not be fit. The individual reactions were monitored for 600 s.

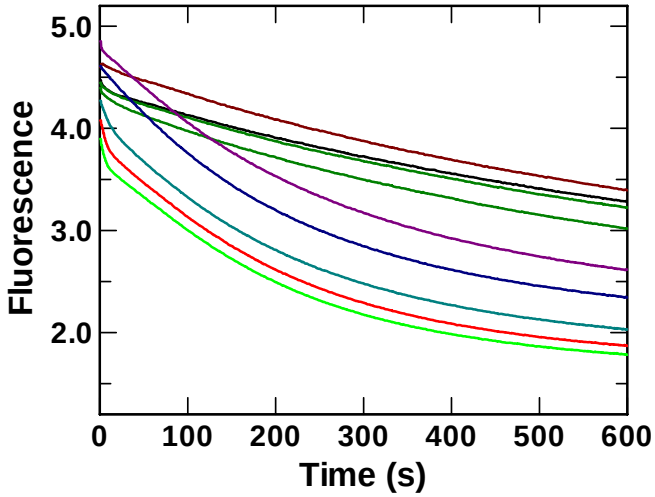

Figure S.2.3.20. Representative traces from 9 stopped-flow experiments in which P1A-*cis*-CaaD (10 μM) in 20 mM Na_2HPO_4 buffer, pH 9.0, was mixed with an equal volume of *cis*-3-bromoacrylic acid [12.5 μM (black), 50 μM (maroon), 100 μM (green), 300 μM (olive), 1500 μM (navy), 2500 μM (purple), 3500 μM (teal), 4500 μM (red), and 5000 μM (lime)] at 22 °C. The data could not be fit. The reported concentrations are those after mixing enzyme and substrate. The individual reactions were monitored for 600 s.

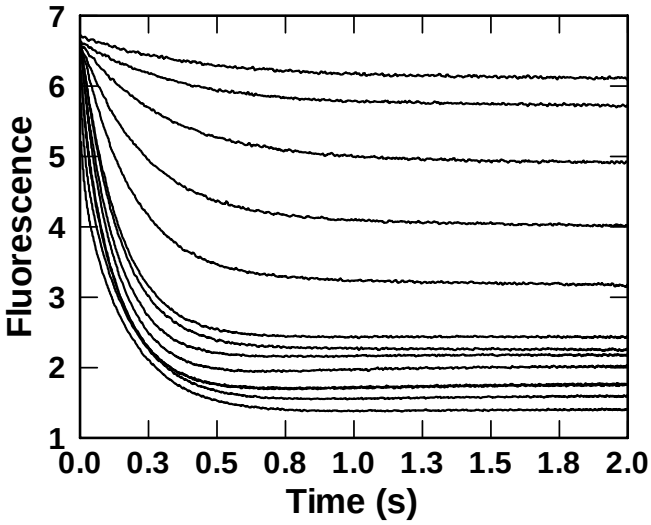

Figure S.2.3.21. Traces from 12 stopped-flow experiments in which Y103F-*cis*-CaaD (10 μM) in 20 mM Na_2HPO_4 buffer, pH 9.0, was mixed with an equal volume of *cis*-3-chloroacrylic acid (12.5-7,500 μM, top to bottom) at 22 °C. The decrease in fluorescence was fit to a single exponential. The reported concentrations are those after mixing enzyme and substrate. The individual reactions were monitored for 2 s. The signals do not return to the initial fluorescence readings.

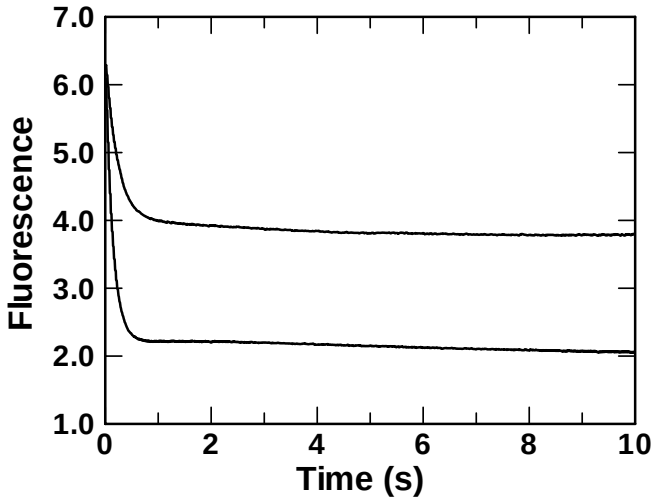

Figure S.2.3.22. Two representative traces from a total of 23 stopped-flow experiments in which Y103-*cis*-CaaD (10 μM) in 20 mM Na_2HPO_4 buffer, pH 9.0, was mixed with an equal volume of *cis*-3-chloroacrylic (100 μM and 500 μM, top to bottom) at 22 °C. The reported concentrations are those after mixing enzyme and substrate. The individual reactions were monitored for 10 s, showing that the signals do not return to the initial fluorescence readings.

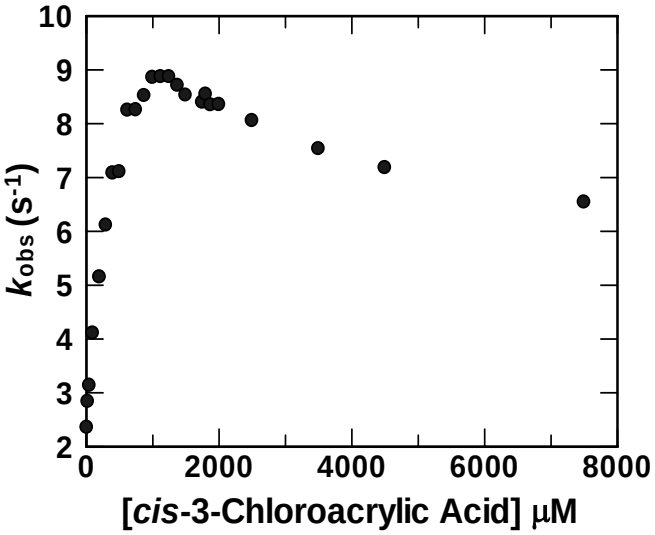

Figure S.2.3.23. Concentration dependence of k_{obs} for the fast phase binding of *cis*-3-chloroacrylic acid (12.5–7,500 μM) to Y103F-*cis*-CaaD (10 μM) in 20 mM Na_2HPO_4 buffer, pH 9.0, at 22 °C. The data for 1400-7500 μM could not be fit. The reported concentrations are those after mixing enzyme and substrate.

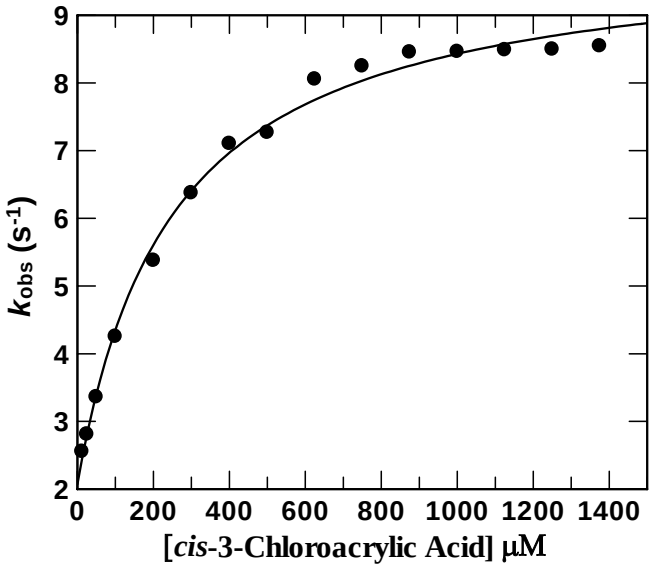

Figure S.2.3.24. Concentration dependence of k_{obs} for binding of *cis*-3-chloroacrylic acid (12.5–1,400 μM) to Y103F-*cis*-CaaD (10 μM) in 20 mM Na_2HPO_4 buffer, pH 9.0, at 22 °C. The concentration dependence of the fast phase up to 1400 μM was fit to an equation for a hyperbola. The reported concentrations are those after mixing enzyme and substrate.

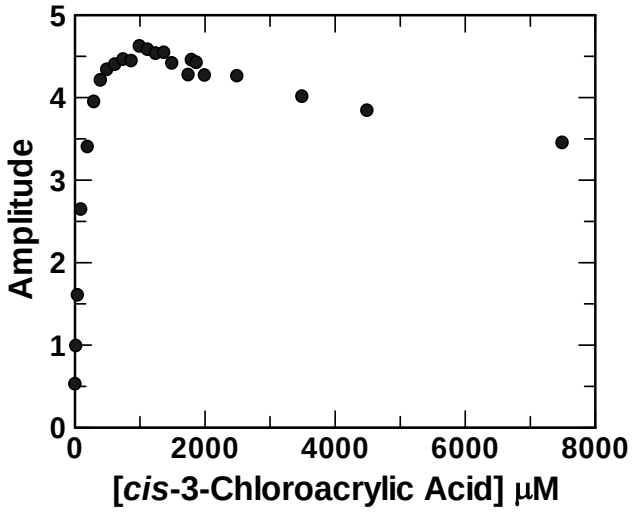

Figure S.2.3.25. Concentration dependence of the amplitude for the fast phase binding of *cis*-3-chloroacrylic acid (12.5–7,500 μM) to Y103F-*cis*-CaaD (10 μM) in 20 mM Na_2HPO_4 buffer, pH 9.0, at 22 °C. The data from 1400-7500 μM could not be fit. The reported concentrations are those after mixing enzyme and substrate.

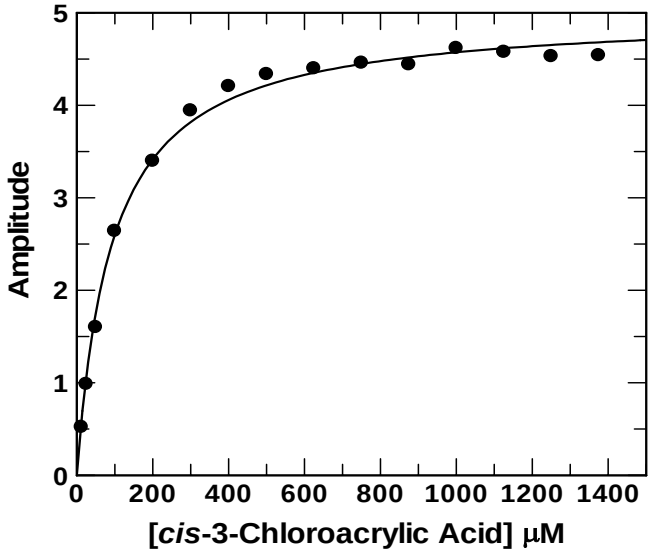

Figure S.2.3.26. Concentration dependence of the amplitude for the fast phase binding of *cis*-3-chloroacrylic acid (12.5–1,400 μM) to Y103F-*cis*-CaaD (10 μM) in 20 mM Na_2HPO_4 buffer, pH 9.0, at 22 °C. The concentration dependence of the amplitude for the fast phase up to 1400 μM substrate concentration was fit to an equation for a hyperbola.

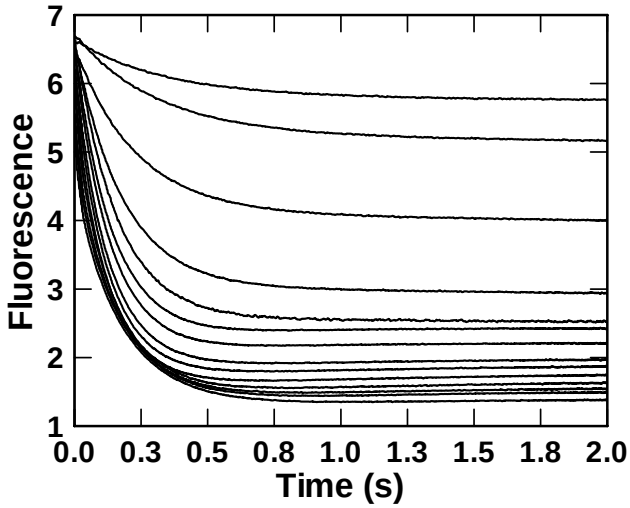

Figure S.2.3.27. Traces from 14 stopped-flow experiments in which Y103F-*cis*-CaaD (10 μM) in 20 mM Na_2HPO_4 buffer, pH 9.0, was mixed with an equal volume of *cis*-3-bromoacrylic acid (12.5-7,500 μM, top to bottom) at 22 °C. The decrease in fluorescence was fit to a single exponential. The signal does not return to the initial fluorescence reading. The reported concentrations are those after mixing enzyme and substrate. The individual reactions were monitored for 2 s.

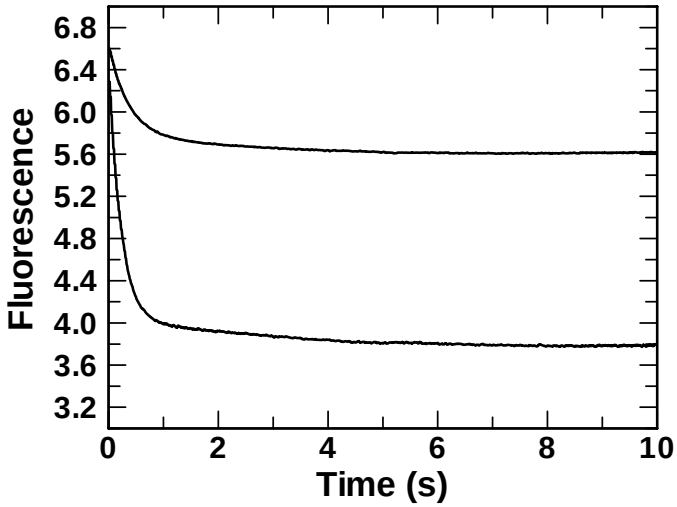

Figure S.2.3.28. Two representative traces from a total of 21 stopped-flow experiments in which Y103-*cis*-CaaD (10 μM) in 20 mM Na_2HPO_4 buffer, pH 9.0, was mixed with an equal volume of *cis*-3-bromoacrylic (25 μM and 100 μM, top to bottom) at 22 °C. The reported concentrations are those after mixing enzyme and substrate. The individual reactions were monitored for 10 s, showing that the signal does not return to the initial fluorescence value.

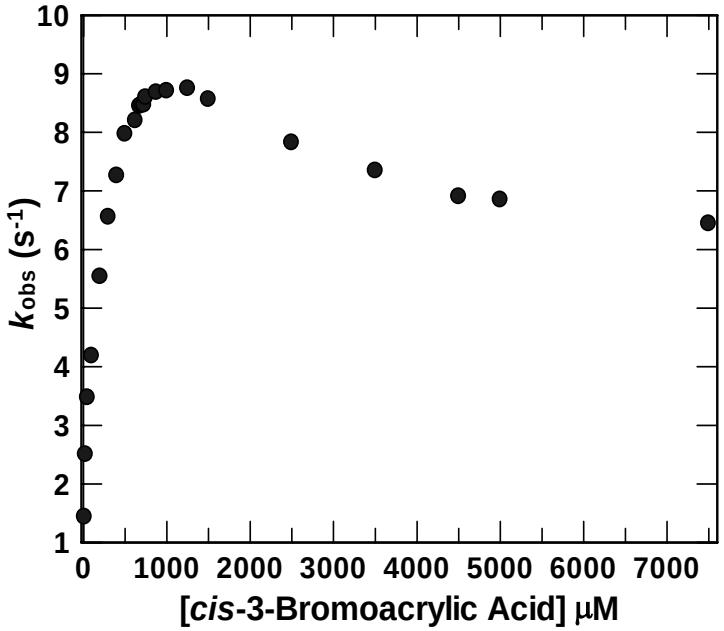

Figure S.2.3.29. Concentration dependence of k_{obs} for the fast phase binding of *cis*-3-bromoacrylic acid (12.5–7,500 μM) to Y103F-*cis*-CaaD (10 μM) in 20 mM Na_2HPO_4 buffer, pH 9.0, at 22 °C. The data from 1400-7500 μM could not be fit. The reported concentrations are those after mixing enzyme and substrate.

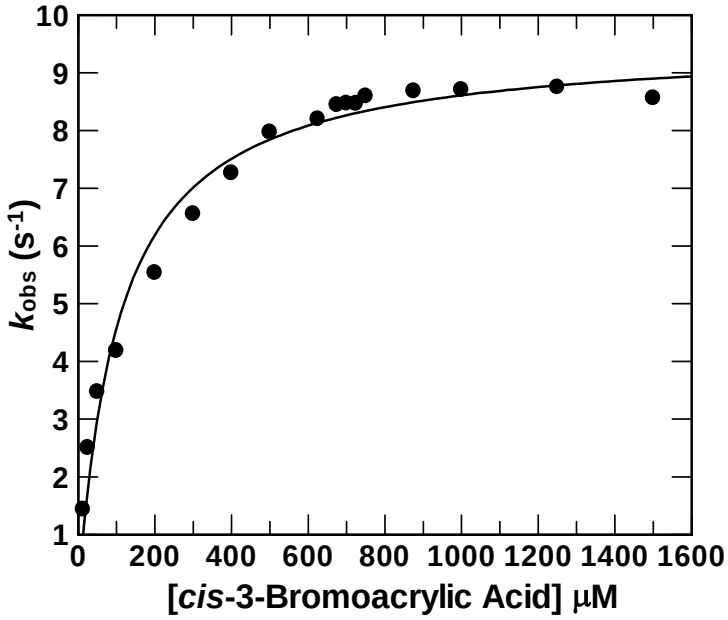

Figure S.2.3.30. Concentration dependence of k_{obs} for the fast phase binding of *cis*-3-bromoacrylic acid (12.5–1,500 μM) to Y103F-*cis*-CaaD (10 μM) in 20 mM Na_2HPO_4 buffer, pH 9.0, at 22 °C. The concentration dependence of the fast phase up to 1400 μM was fit to an equation for a hyperbola. The reported concentrations are those after mixing enzyme and substrate.

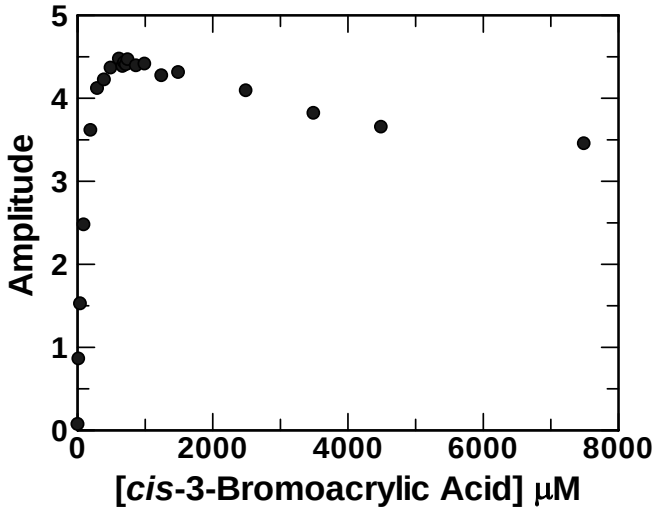

Figure S.2.3.31. Concentration dependence of the amplitude for the fast phase binding of *cis*-3-bromoacrylic acid (12.5–7,500 μM) to Y103-*cis*-CaaD (10 μM) in 20 mM Na_2HPO_4 buffer, pH 9.0, at 22 °C. The data for 1400-7500 μM could not be fit. The reported concentrations are those after mixing enzyme and substrate.

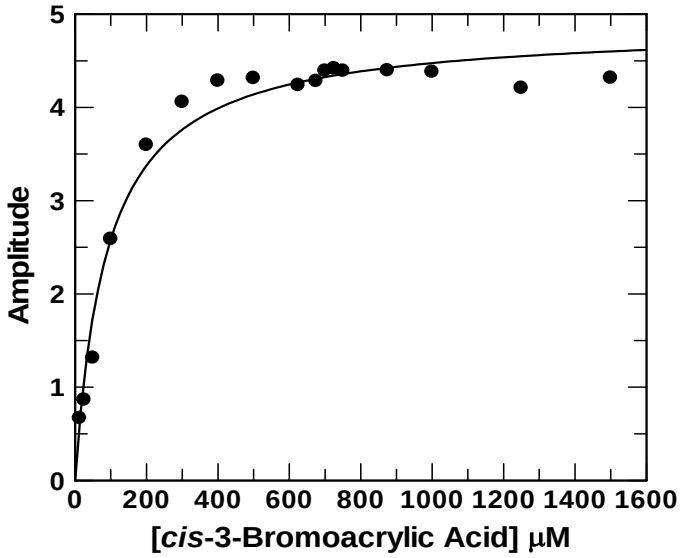

Figure S.2.3.32. Concentration dependence of the amplitude for the fast phase binding of *cis*-3-bromoacrylic acid (12.5–1,500 μM) to Y103F-*cis*-CaaD (10 μM) in 20 mM Na_2HPO_4 buffer, pH 9.0, at 22 °C. The concentration dependence of the amplitude up to 1400 μM was fit to an equation for a hyperbola. The reported concentrations are those after mixing enzyme and substrate.

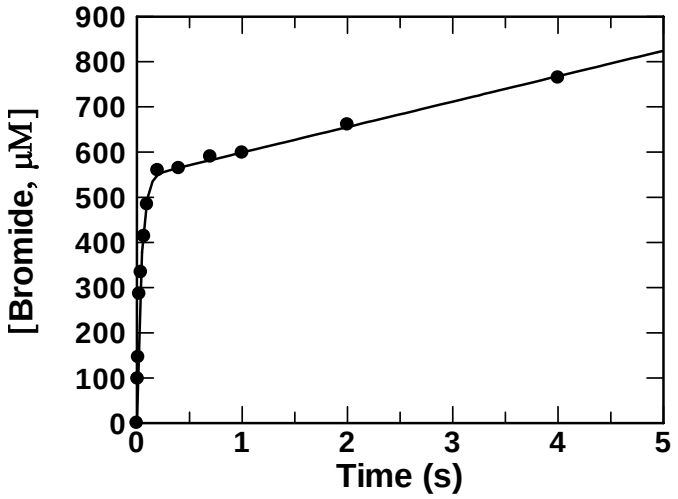

Figure S.2.3.33. Rapid quench experiment using 1000 μM E114Q-*cis*-CaaD with 25,000 μM *cis*-3-bromoacrylic acid in 20 mM $NaHCO_3$-NaOH buffer, pH 9.0, at 22 °C. The reported concentrations are those after mixing enzyme and substrate. The reaction shows a burst of bromide (24 ± 2 s^{-1}) formation followed by a slow rate (56 ± 6 μM s^{-1}) with an amplitude of 543 ± 11 μM.

Table S.1. Steady-State Kinetic Parameters for E114Q-*cis*-CaaD

substrate	k_{cat} (s^{-1})	K_m (μM)	k_{cat}/K_m (M^{-1} s^{-1})
cis-3-Chloroacrylic Acid[a]	.052 ± .001	30.6 ± 2.9	1.7×10^3
cis-3-Bromoacrylic Acid[a]	.056 ± .001	24.5 ± 4.0	2.3×10^3
cis-3-Bromoacrylic Acid[b]	-[c]	-	-

[a]The steady-state kinetic parameters were determined in 20 mM sodium phosphate buffer (pH 9.0) at 22 °C. Errors are standard deviations.

[b]The steady-state kinetic parameters were determined in 20 mM sodium bicarbonate buffer (pH 9.0) at 22 °C. Errors are standard deviations.

[c]There was not detectable decay in the absorbance at 224 nm after 5 min.

Table S.2. Steady-State Kinetic Parameters for Y103F-*cis*-CaaD

substrate	k_{cat} (s^{-1})	K_m (μM)	k_{cat}/K_m (M^{-1} s^{-1})
cis-3-Bromoacrylic Acid[a]	0.31 ± 0.06	7.5 ± 0.8	4.1×10^4
cis-3-Bromoacrylic Acid[b]	0.06 ± 0.01	13.7 ± 2.0	4.4×10^3

[a]The steady-state kinetic parameters were determined in 20 mM sodium phosphate buffer (pH 9.0) at 22 °C. Errors are standard deviations.

[b]The steady-state kinetic parameters were determined in 20 mM sodium bicarbonate buffer (pH 9.0) at 22 °C. Errors are standard deviations.

Table S.3. Pre-Steady State Kinetic Parameters Obtained for *cis*-CaaD and Mutants with *cis*-3-Chloroacrylic Acid in 20 mM Na_2HPO_4 buffer, pH 9.0, (Fast Phase).

Enzyme	K_d [a] (μM)	k_{rev} [a] (s^{-1})	k_{for} [a] (s^{-1})	A_o [b]	ΔA [b]	$K_{d,app}$ [b] (μM)
Wild type	1015 ± 210	31 ± 4	71 ± 3	0	3.1 ± 0.1	736 ± 120
E114Q	2000 ± 200	0.3 ± 0.1	4.1 ± 0.1	n/a	n/a	n/a
Y103F	250 ± 28	2.1 ± 0.2	7.9 ± 0.2	0	5.0 ± 0.1	93 ± 6

[a]The pre-steady state kinetic parameters were determined by non-linear regression analysis. The data (k_{obs} vs [*cis*-3-chloroacrylic acid]) from stopped flow experiments were fit to an equation for a hyperbola: $k_{obs} = \frac{k_{for}[S]}{(K_d + [S])} + k_{rev}$, where k_{obs} is the rate of the fast phase fluorescence decrease, k_{for} is the forward reaction rate of the conformational change, k_{rev} is the reverse reaction rate of the conformational change, [S] is the concentration of substrate, and K_d is the binding constant. Errors are standard deviations.

[b]The pre-steady state kinetic parameters were determined by non-linear regression analysis. The data (A vs [*cis*-3-chloroacrylic acid]) from stopped flow experiments were fit to an equation for a hyperbola: $A = \frac{\Delta A\ [S]}{(K_{d,app} + [S])} + A_o$, where A is the amplitude of the fast phase fluorescence decrease, ΔA is the change in amplitude, A_o is the starting amplitude value, [S] is the concentration of substrate, and $K_{d,app}$ is the net K_d. Errors are standard deviations.

.

Table S.4. Pre-Steady State Kinetic Parameters Obtained for *cis*-CaaD and Mutants with *cis*-3-Bromoacrylic Acid in 20 mM Na_2HPO_4 buffer, pH 9.0, (Fast Phase).

Enzyme	K_d [a] (μM)	k_{rev} [a] (s^{-1})	k_{for} [a] (s^{-1})	A_o [b]	ΔA [b]	$K_{d,app}$ [b] (μM)
Wild type	1400 ± 300	47 ± 3	89 ± 5	0	2.7 ± 0.1	690 ± 49
E114Q	1817 ± 192	0	5.9 ± 0.2	n/a	n/a	n/a
Y103F	108 ± 13	0	9.5 ± 0.2	0	4.9 ± 0.1	88 ± 11

[a]The pre-steady state kinetic parameters were determined by non-linear regression analysis. The data (k_{obs} vs [*cis*-3-bromoacrylic acid]) from stopped flow experiments were fit to an equation for a hyperbola: $k_{obs} = \frac{k_{for}[S]}{(K_d + [S])} + k_{rev}$, where k_{obs} is the rate of the fast phase fluorescence decrease, k_{for} is the forward reaction rate of the conformational change, k_{rev} is the reverse reaction rate of the conformational change, [S] is the concentration of substrate, and K_d is the binding constant. Errors are standard deviations.

[b]The pre-steady state kinetic parameters were determined by non-linear regression analysis. The data (A vs [*cis*-3-bromoacrylic acid]) from stopped flow experiments were fit to an equation for a hyperbola: $A = \frac{\Delta A\ [S]}{(K_{d,app} + [S])} + A_o$, where A is the amplitude of the fast phase fluorescence decrease, ΔA is the change in amplitude, A_o is the starting amplitude value, [S] is the concentration of substrate, and $K_{d,app}$ is the net K_d. Errors are standard deviations.

Table S.5. Pre-Steady State Kinetic Parameters Obtained for *cis*-CaaD and Mutants with *cis*-3-Chloroacrylic Acid in 20 mM Na_2HPO_4 buffer, pH 9.0, (Slow Phase).

Enzyme	K_d [a] (μM)	k_{rev} [a] (s^{-1})	k_{for} [a] (s^{-1})	A_o [b]	ΔA [b]	$K_{d,app}$ [b] (μM)
Wild type	130 ± 21	1.7 ± 0.1	1.5 ± 0.1	n/a	n/a	n/a
E114Q	3660 ± 770	0	0.7 ± 0.1	n/a	n/a	n/a
Y103F	n/a	n/a	n/a	n/a	n/a	n/a

[a]The pre-steady state kinetic parameters were determined by non-linear regression analysis. The data (k_{obs} vs [*cis*-3-chloroacrylic acid]) from stopped flow experiments were fit to an equation for a hyperbola: $k_{obs} = \frac{k_{for}[S]}{(K_d + [S])} + k_{rev}$, where k_{obs} is the rate of the slow phase fluorescence decrease, k_{for} is the forward reaction rate of the conformational change, k_{rev} is the reverse reaction rate of the conformational change, [S] is the concentration of substrate, and K_d is the binding constant. Errors are standard deviations.

[b]The pre-steady state kinetic parameters were determined by non-linear regression analysis. The data (A vs [*cis*-3-chloroacrylic acid]) from stopped flow experiments were fit to an equation for a hyperbola: $A = \frac{\Delta A\ [S]}{(K_{d,app} + [S])} + A_o$, where A is the amplitude of the slow phase fluorescence decrease, ΔA is the change in amplitude, A_o is the starting amplitude value, [S] is the concentration of substrate, and $K_{d,app}$ is the net K_d. Errors are standard deviations.

Table S.6. Pre-Steady State Kinetic Parameters Obtained for *cis*-CaaD and Mutants with *cis*-3-Bromoacrylic Acid in 20 mM Na_2HPO_4 buffer, pH 9.0, (Slow Phase).

Enzyme	K_d [a] (μM)	k_{rev} [a] (s^{-1})	k_{for} [a] (s^{-1})	A_o [b]	ΔA [b]	$K_{d,app}$ [b] (μM)
Wild type	151 ± 21	1.9 ± 0.1	1.5 ± 0.1	n/a	n/a	n/a
E114Q	7200 ± 820	0	2.2 ± 0.1	n/a	n/a	n/a
Y103F	n/a	n/a	n/a	n/a	n/a	n/a

[a]The pre-steady state kinetic parameters were determined by non-linear regression analysis. The data (k_{obs} vs [*cis*-3-bromoacrylic acid]) from stopped flow experiments were fit to an equation for a hyperbola: $k_{obs} = \frac{k_{for}[S]}{(K_d + [S])} + k_{rev}$, where k_{obs} is the rate of the slow phase fluorescence decrease, k_{for} is the forward reaction rate of the conformational change, k_{rev} is the reverse reaction rate of the conformational change, [S] is the concentration of substrate, and K_d is the binding constant. Errors are standard deviations.

[b]The pre-steady state kinetic parameters were determined by non-linear regression analysis. The data (A vs [*cis*-3-bromoacrylic acid]) from stopped flow experiments were fit to an equation for a hyperbola: $A = \frac{\Delta A\ [S]}{(K_{d,app} + [S])} + A_o$, where A is the amplitude of the slow phase fluorescence decrease, ΔA is the change in amplitude, A_o is the starting amplitude value, [S] is the concentration of substrate, and $K_{d,app}$ is the net K_d. Errors are standard deviations.

Chapter 3: A Pre-steady State Kinetic Analysis of *trans*-3-Chloroacrylic Acid Dehalogenase (CaaD)

3.1 Introduction

trans-3-Chloroacrylic acid dehalogenase (CaaD) catalyzes the hydrolytic dehalogenation of *trans*-3-haloacrylates (e.g., *trans*-3-chloro- and 3-bromoacrylate, **2** and **3**, respectively in Scheme 1) to afford malonate semialdehyde (**4**) and the corresponding hydrohalic acid (1,2). The CaaD-catalyzed reaction (using **2**) represents one step in the bacterial catabolism of the nematocide, 1,3-dichloropropene (**1**, Scheme 1) in various soil organisms such as *Pseudomonas pavonaceae* 170 and coryneform bacterium strain FG41 (3). Although CaaD was first identified and partially purified in 1992 (3), mechanistic studies of the enzyme began just over 5 years ago (1,2,4,5).

Scheme 1

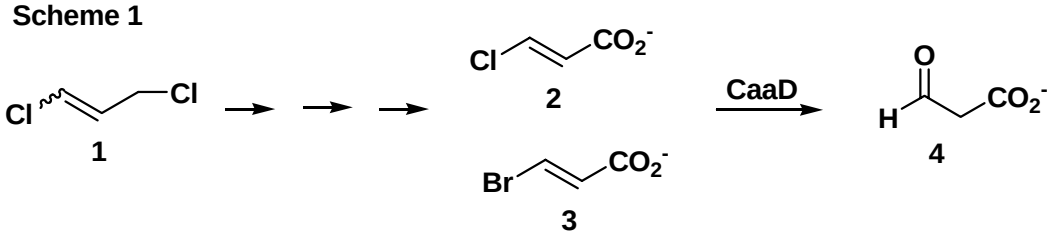

CaaD is a heterohexamer composed of 3 α-subunits and 3 β-subunits (4). The small size of these subunits (70 and 75 amino acids, respectively) and sequence analysis initially placed CaaD in the tautomerase supeerfamily (1), a group of structurally

homologous proteins characterized by a common β–α–β building block and a catalytic amino-terminal proline (6-8). Subsequently, mechanistic, inhibition, mutagenesis, crystallographic, and NMR studies elucidated key details of the enzyme-catalyzed reaction, resulting in the current working hypothesis for the mechanism shown in Scheme 2 (1,2,4,5). In the proposed mechanism, αGlu-52 activates water for attack at C-3 of **2** or **3** by abstraction of a hydrogen. A pair of arginines (αArg-8 and αArg-11) concomitantly interacts with the C-1 carboxylate group to bind and polarize the substrate for attack. The CaaD-catalyzed addition of water to the double bond of **2** (or **3**) is completed by protonation at C-2, which is effected by βPro-1, functioning as a general acid catalyst.

Our understanding of the CaaD mechanism is still rudimentary. For example, it is not known if the reaction proceeds through a halohydrin intermediate (e.g., **5**, Scheme 2) or an enol intermediate (e.g., **6**, Scheme 2) (4,8). In addition to the mechanistic significance, a determination of which intermediate is operative has evolutionary implications. The presence of the halohydrin intermediate could suggest that CaaD is an "accidental" dehalogenase. The enzyme may be a physiological hydratase that catalyzes the addition of water across the double bonds of unknown α,β-unsaturated acids (4,8). In the case of **2** or **3**, this reaction generates a halohydrin intermediate that undergoes rapid decay to **4**. The formation of **6** in the reaction, and the presence of a halide binding pocket, could suggest that CaaD evolved to carry out a dehalogenation reaction.

Scheme 2

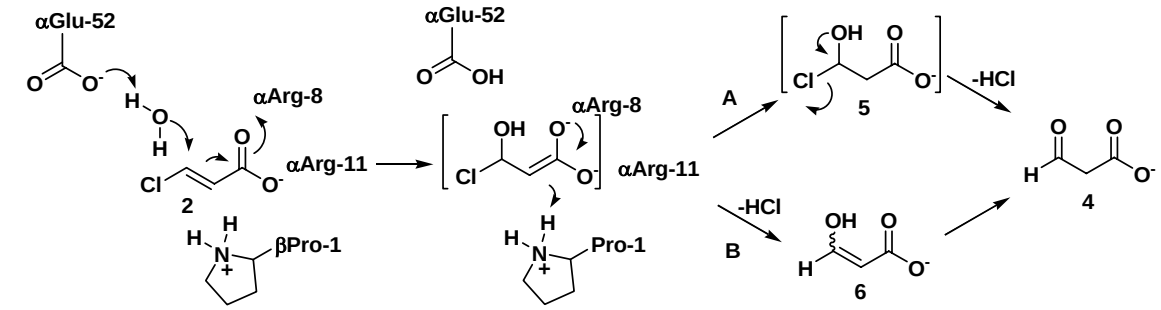

As part of an effort to understand the mechanism of CaaD more completely, a pre-steady state kinetic analysis of the reaction was initiated. For this analysis, it was necessary to construct a mutant of CaaD where αPhe-39, a residue located in the active site (4), was replaced with a tryptophan residue. The resulting αF39W mutant introduces the only fluorophore in the enzyme. A series of stopped flow experiments was then carried out on the enzyme using **2** and **3**. For both, there is a decrease in fluorescence that can be fit to a double exponential. The fluorescence signal does not return to its initial value. Analysis of the double exponential for **2** yields the apparent K_d for substrate binding. It was not possible to analyze the rate constants from the double exponential observed for **3**. The completion of these studies, the formulation of a kinetic model, and a comparison of the results to those obtained for various mutants will provide more insight into the individual steps in the CaaD-catalyzed reaction and how mutations impact these steps. Finally, a comparison of this analysis with that carried out on *cis*-3-chloroacrylic acid dehalogenase, which is in a different family in the tautomerase superfamily (9), will underscore similarities and differences between these two enzymes.

3.2 Materials and Methods

Materials. All reagents, buffers, and solvents were obtained from Sigma Aldrich Chemical Co. (St. Louis, MO), Fisher Scientific Inc. (Pittsburgh, PA), Spectrum Laboratory Products, Inc. (New Brunswick, NJ), or EM Science (Cincinnati, OH), unless noted otherwise. Pre-packed PD-10 Sephadex G-25 columns were purchased from Biosciences AB (Uppsala, Sweden). *E. coli* BL21-Gold(DE3) cells were purchased from Stratagene (La Jolla, CA). The components of LB, SOB, and SOC medium were obtained from sources reported elsewhere (2,10).

General Methods. Protein was analyzed by SDS-PAGE under denaturing conditions on gels containing 15% polyacrylamide (11). The gels were stained with Coomassie brilliant blue. Protein concentrations were determined by the method of Waddell (12). Absorbance data were obtained on a Hewlett Packard 8452A Diode Array spectrophotometer. The steady-state kinetic data were fitted by nonlinear regression data analysis using the Grafit program (Erithacus Software Ltd., Horley, U.K.) obtained from Sigma Chemical Co**.** The pre-steady state kinetic data were fit and simulated using KinTekSim (Austin, TX). The stopped flow experiments were carried out on a SF 2004 series stopped flow apparatus from Kintek Corp. (Austin, TX).

Composition of SOB and SOC Media. The SOB medium was made by mixing tryptone (4 g) and yeast extract (1 g) in 100 mL of deionized water (10). The mixture was then autoclaved for 45 min and stored in a sealed glass bottle at 22 °C until ready to use. The SOC medium (10 mL) was made by mixing 4.7 mL of deionized water with SOB medium (5 mL). To this mixture, $MgSO_4$ (0.1 mL of a 1 mg/mL stock solution),

NaCl/KCl (0.1 mL of a 1 mg/mL stock solution), and glucose (0.1 mL of a 1 mg/mL stock solution) were added (10). The solution was mixed at 22 °C and used immediately after being made.

3.2.1 Transformation, Expression, and Purification of CaaD and the αF39W Mutant

Transformation of Expression Cells for CaaD. *E. coli* BL21-Gold(DE3) competent cells were thawed and stored on ice. Competent cells (~100 μL) were pipetted into a pre-chilled 15-mL Falcon 2059 tube along with the expression vector for CaaD, designated pET 44T2 (~50 ng) (1). The reaction mixture was gently incubated on ice for 30 min. During this time, a 900-μL aliquot of SOC medium was preheated in a water bath to 42 °C. The reaction mixture was heat-pulsed for 20 s in a water bath at 42 °C and then incubated on ice for 2 min. Subsequently, the 900-μL aliquot of SOC medium was added to the reaction mixture. The cells were incubated at 37 °C for 1 h in an environmental shaker at 225 rpm. The cells were then concentrated by centrifugation (500 rpm for 5 min), and a 600-μL portion of the supernatant was removed. The cells were resuspended in the remaining supernatant. A portion of the resulting transformation reaction mixture (200 μL) was plated, using a sterile spreader, onto two LB/Ap (50 μg/mL) agar plates. The plates were then incubated overnight (~ 16 h) at 37 °C.

Overexpression and Purification of CaaD. Wild-type CaaD was produced in *E. coli* BL21-Gold(DE3) cells using the T7 expression system (1). The freshly transformed cells, with the plasmid containing the genes for the α- and β- subunit of CaaD (1), were collected from a plate and used to inoculate three 2-liter flasks containing 1L of LB/Ap

(100 mg/L). After overnight growth at 30 °C in an environmental shaker at 225 rpm, cells were harvested by centrifugation (15 min at 7,000 rpm) and stored at -20 °C until further use. Typically, 1 L of culture yields 7 g of cells.

Cells (~21 g) were thawed and suspended in 11 mL of 10 mM Tris-SO_4 buffer, pH 8.0, and placed on ice. Cells were disrupted, while stirring on ice, by sonication at 60 W output (in a W385 sonicator of Heat Systems-Ultrasonics, Inc.) for ten 2-min intervals using 5-s pulses with a cycle time of 50%. After each 2-min interval, cells were allowed to sit for 5 min. DNase (10 μL of a 10 Units/μL solution) and RNase (10 mL of a 500 μg/mL solution) were added to the solution and allowed to stir on ice for 1 h. The lysed cells were then centrifuged at 17,000 rpm for 45 min. The supernatant was retained and centrifuged at 60,000 rpm for 1 h (1,2).

Subsequently, the supernatant was filtered through a 0.2 μm-pore diameter filter and applied to a TSKgel DEAE-5PW anion-exchange column (150 × 21.5 mm), which had been previously equilibrated with 10 mM Tris-SO_4 buffer, pH 8.0. The column was washed with 10 mM Tris-SO_4 buffer, pH 8.0, containing 0.5 M Na_2SO_4 for 20 min and the protein was eluted using a linear gradient (0-0.5 M Na_2SO_4) at a flow rate of 5 mL/min over a 90 min period. Fractions were collected at 1.75 min intervals (8.75 mL). Fractions (#4-14) with the highest purity (as determined by SDS PAGE) were pooled and concentrated to ~16 mL using an Amicon stirred cell equipped with an YM10 (10,000 MW cutoff) ultrafiltration membrane (1,2).

Solid $(NH_4)_2SO_4$ was added to the concentrate to make a final concentration of 1.6 M and the resulting solution was stirred for 1 h at 4 °C. The solution was centrifuged

at 11,000 rpm for 15 min and the supernatant was filtered through a 0.2 μm-pore diameter filter and applied to a TSKgel Phenyl-5PW column (150 × 21.5 mm) which had been previously equilibrated with 10 mM Tris-SO_4 buffer, pH 8.0, containing 1.0 M $(NH_4)_2SO_4$. The protein was eluted with a decreasing linear gradient [1.0 to 0 M $(NH_4)_2SO_4$] at a flow rate of 5 mL/min. Fractions were collected at 1.75 min intervals (8.75 mL) over a 90-min period. The fractions (#10-16) with the highest purity (as determined by SDS-PAGE) were concentrated to ~6 mL using an Amicon stirred cell equipped with an YM10 (10,000 MW cutoff) ultrafiltration membrane and stored at 4 °C. This purification resulted in ~120 mg of 95% pure as assessed by ESI mass spectroscopy protein (α-subunit MW 8,342, β-subunit MW 7,505) and SDS-PAGE.

Expression and Purification of the αF39W Mutant of CaaD. The plasmid containing the αF39W mutant of CaaD was transformed as described for the wild type CaaD gene into *E. coli* BL21-Gold(DE3) cells for protein expression. The plasmid was constructed by Dr. Linette Watkins. The gene product was expressed using the T7 expression system as described for wild type. Typically, 1 L of culture yields 7 g of cells which were frozen until ready for use. The cells (~21 g) were thawed and processed following the protocol described for lysis of wild type cells and subsequent protein purification. Fractions (#6-22) from the TSKgel DEAE-5PW anion-exchange column with the higest purity (as determined by SDS-PAGE) were pooled and concentrated to ~16 mL using an Amicon stirred cell equipped with an YM10 (10,000 MW cutoff) ultrafiltration membrane. Fractions (#19-20) from the TSKgel Phenyl-5PW column with the highest purity (as determined by SDS-PAGE) and activity (as determined by an

activity assay) were concentrated to ~6 mL using an Amicon equipped with an YM10 (10,000 MW cutoff) ultrafiltration membrane and stored at 4 °C. This purification resulted in ~100 mg of 95% pure protein as assessed by ESI mass spectroscopy (α-subunit MW 8,381, β-subunit MW 7,505) and SDS-PAGE.

3.2.2 Activity Assay for αF39W-CaaD

Activity Assay for αF39W-CaaD. A sample of protein (20 μL) from each fraction was placed in a cuvette containing 1 mL of 20 mM Na_2HPO_4 buffer, pH 9.0. The solution was gently mixed and allowed to sit at 22 °C for 30 min. Subsequently, the sample was used to blank the spectrophotometer at 224 nm. A 4-μL aliquot of 50 mM *trans*-3-chloroacrylic acid in 20 mM Na_2HPO_4 buffer, pH 9.0, was then added and the absorbance decrease was monitored at 224 nm (2). Absorbance readings were recorded every min for a 5 min period. Fractions showing the largest change in absorbance were collected and concentrated.

3.2.3 Steady-State Kinetic Parameters for CaaD

The Steady-State Kinetic Parameters for CaaD. The steady-state parameters for CaaD were measured using *trans*-3-chloro- and *trans*-3-bromoacrylic acid. The assays were carried out at 22 °C in 20 mM Na_2HPO_4 buffer, pH 9.0 (2). A 25 mL solution of CaaD (2 μM based on monomeric mass) was made up in buffer and allowed to equilibrate at 22 °C for 1 h. The assay was initiated by the addition of *trans*-3-chloro- or *trans*-3-bromoacrylic acid (10 μM - 500 μM) from a 10 mM or 50 mM stock solution (in 100 mM Na_2HPO_4 buffer, pH 9.0). The addition of substrate to a 100 mM Na_2HPO_4 buffer, pH 9.0, adjusted the pH of the stock solution from 9.0 to a final pH of 7.3. The 10

mM stock solution was made by diluting an aliquot of the 50 mM stock solution into 100 mM Na_2HPO_4 buffer, pH 7.3. The decrease in absorbance at 224 nm, corresponding to the hydration of *trans*-3-chloroacrylate (ε = 4900 M^{-1} cm^{-1}) (2) or *trans*-3-bromoacrylate (ε = 9700 M^{-1} cm^{-1}) (2), was monitored over a 60-s time interval, recording readings every 1.5 s. The rates of substrate depletion over the first 40 s were then plotted versus the corresponding substrate concentrations. The hyperbolic curve was fit by nonlinear regression analysis to the Michaelis-Menten equation, provided in the Grafit program (Erithacus Software Ltd., Horley, U.K.) to determine the values of k_{cat} and K_m.

3.2.4 Steady-State Parameters for the αF39W Mutant of CaaD

Steady-State Kinetic Parameters for αF39W-CaaD. The steady-state kinetic parameters for αF39W-CaaD were measured using *trans*-3-chloro- and *trans*-3-bromoacrylic acid. The assays were carried out at 22 °C in 20 mM Na_2HPO_4 buffer, pH 9.0. A 25 mL solution of αF39W-CaaD (2 μM based on monomeric mass) was made up in buffer and allowed to equilibrate at 22 °C for 1 h. The assay was initiated by the addition of *trans*-3-chloro- or *trans*-3-bromoacrylic acid (5 μM – 400 μM) which were made from 10 mM or 50 mM stock solutions (in 100 mM Na_2HPO_4 buffer, pH 9.0). The addition of substrate to a 100 mM Na_2HPO_4 buffer, pH 9.0, adjusted the pH of the stock solution from 9.0 to a final pH of 7.3. The 10 mM stock solution was made by diluting an aliquot of the 50 mM stock solution into 100 mM Na_2HPO_4 buffer, pH 7.3. The decrease in absorbance at 224 nm, corresponding to the hydration of *trans*-3-chloroacrylate (ε = 4900 M^{-1} cm^{-1}) (2) or *trans*-3-bromoacrylate (ε = 9700 M^{-1} cm^{-1}) (2) was monitored over

a 60-s time interval, recording readings every 1.5 s. The rates of substrate depletion over the first 30 s were then plotted versus the corresponding substrate concentrations. The hyperbolic curve was fit by nonlinear regression analysis to the Michaelis-Menten equation, provided in the Grafit program (Erithacus Software Ltd., Horley, U.K.) to determine the values of k_{cat} and K_m.

3.2.5 Stopped Flow Experiments Using αF39W-CaaD

Stopped Flow Experiments Using αF39W-CaaD. All stopped flow experiments and measurements were carried out using a SF 2004 series stopped flow apparatus from Kintek Corp. (http://www.kintek-corp.com). αF39W-CaaD (20 μM based on monomer molecular mass) was made up in 20 mM Na_2HPO_4 buffer, pH 9.0, and allowed to equilibrate at 22 °C for 1 h. Various concentrations of *trans*-3-chloro- or *trans*-3-bromoacrylic acid (50-50,000 μM before mixing) were made up in 100 mM Na_2HPO_4 buffer, pH 9.0. The addition of *trans*-3-chloro- or *trans*-3-bromoacrylic acid to the buffer adjusted the pH to ~7.8. The enzyme (10 μM after mixing) and substrate (25-25,000 μM after mixing) solutions were then mixed in the stopped flow apparatus at 22 °C. The pH after mixing was 7.8. The samples were excited at 280 nm and fluorescence emission was monitored using a photomultiplier tube equipped with a 340 nm long pass Corion filter. In order to reduce photobleaching, the slit width on the xenon light source and the light filter were set at 3.16 mm. The high voltage output was set at 717 volts. Three time courses (0.2 s, 2.5 s, and 10 s) consisting of five runs per time course were recorded for each substrate concentration. Rate constants were obtained by analyzing the fluorescence

signals collected in the stopped-flow experiments by non-linear regression. (The traces for the 0.2 time course are not shown.)

3.3 Results

3.3.1 Steady-State Parameters for CaaD and αF39W-CaaD

Steady-State Kinetic Parameters for CaaD and the αF39W mutant of CaaD. The steady state kinetic parameters for CaaD and the αF39W mutant using *trans*-3-chloro or *trans*-3-bromoacrylate were measured in 20 mM Na_2HPO_4 buffer, pH 9.0 (2). The results of these experiments provide the necessary background for pre-steady state kinetic analysis experiments. The values of K_m and k_{cat} (Table 1) for CaaD with *trans*-3-chloro- and *trans*-3-bromoacrylic acid differ from those of αF39W-CaaD but not significantly (Table 2). For αF39W-CaaD with *trans*-3-chloroacrylate, the values of K_m and k_{cat} showed a 4.8-fold increase and a 5.2-fold decrease, respectively, when compared to wild type CaaD. This resulted in a 2.6-fold decrease in the value of k_{cat}/K_m. For *cis*-3-bromoacrylate the values of K_m and k_{cat} showed a 5-fold increase and a 5.5-fold decrease, respectively. This resulted in a 2.7-fold decrease in the value of k_{cat}/K_m. The kinetic parameters did not change significantly for either enzyme using *trans*-3-chloro- or *trans*-3-bromoacrylic acid.

Table 1. Steady-State Kinetic Parameters for CaaD

substrate	k_{cat} (s^{-1})	K_m (μM)	k_{cat}/K_m ($M^{-1}\ s^{-1}$)
trans-3-Chloroacrylic Acid[a]	2.2 ± 0.1	21 ± 1	1.1×10^4
trans-3-Bromoacrylic Acid[a]	2.4 ± 0.1	20 ± 2	1.2×10^4

[a]The steady-state kinetic parameters were determined in 20 mM sodium phosphate buffer (pH 9.0) at 22 °C. Errors are standard deviations.

Table 2. Steady-State Kinetic Parameters for αF39W-CaaD

substrate	k_{cat} (s^{-1})	K_m (μM)	k_{cat}/K_m ($M^{-1}\ s^{-1}$)
trans-3-Chloroacrylic Acid[a]	$0.42 \pm .01$	100 ± 2	4.2×10^3
trans-3-Bromoacrylic Acid[a]	$0.44 \pm .01$	100 ± 2	4.4×10^3

[a]The steady-state kinetic parameters were determined in 20 mM sodium phosphate buffer (pH 9.0) at 22 °C. Errors are standard deviations.

3.3.2 Stopped Flow Kinetic Experiments Using αF39W-CaaD

In order to examine the ground-state binding of CaaD with *trans*-3-chloro- and *trans*-3-bromoacrylic acid by stopped flow fluorescence, it was first necessary to introduce a fluorophore into CaaD. αPhe-39 was selected for site-specific mutagenesis because the available crystal structure showed that it was in the active site (3). Hence, αPhe-39 was mutated to αTrp-39, therefore introducing a fluorophore that can monitor events at the active site such as a conformational change of the enzyme upon substrate binding and/or chemistry. The *α*F39W mutant of CaaD was used in subsequent stopped flow experiments where the enzyme was mixed with *trans*-3-chloro- or *trans*-3-bromoacrylic acid. A series of decreasing fluorescent signals was collected, using a stopped-flow apparatus, at increasing concentrations of *trans*-3-chloro- or *trans*-3-bromoacrylic acid (Figures 3.1-3.2 and Figures 3.3-3.4, respectively). The stopped-flow traces were analyzed using non-linear regression and fit to a double exponential equation to yield rates (k_{obs}) and amplitudes for the fast and slow phases (15). The observed rate constants were then plotted versus the corresponding *trans*-3-chloroacrylic acid concentrations (Figures 3.5-3.8) and resulting curve was fit to a hyperbola (equation 1),

$$k_{obs} = \frac{k_{max} \times [S]}{K_d + [S]} \qquad (1)$$

where k_{obs} is the observed rate, k_{max} is the maximum observed rate, [S] is substrate concentration, and K_d is the ground-state binding constant. The resulting curves for the fast phase and slow phase are shown in Figures 3.5 and 3.6. The non-linear regression

analysis suggests weak ground state binding of substrate where K_d is 3500 ± 400 μM, followed by a second step with a k_{max} of 13.5 ± 0.4 s^{-1} (Figure 3.5) (15).

The stopped-flow fluorescence traces for αF39W-CaaD with *trans*-3-bromoacrylic acid were also fit to a double exponential and the k_{obs} values were plotted against the corresponding substrate concentrations (Figures 3.9-3.12). However, the concentration dependence of the k_{obs} and the amplitude for the fast phase and the concentration dependence of the amplitude for the slow phase could not be fit. The concentration dependence of k_{obs} for the slow phase could be fit to the equation for a hyperbola. The resulting K_d was 2500 ± 2000 μM (Figure 3.10). The magnitude of the error is such that firm conclusions can not be made.

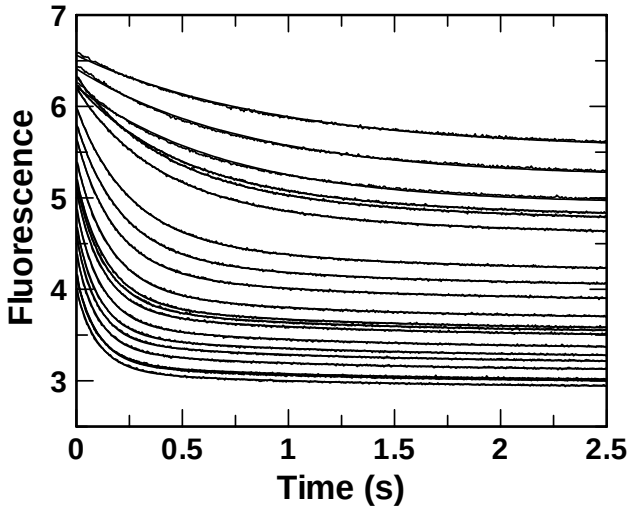

Figure 3.1. Traces from 19 stopped-flow experiments in which αF39W-CaaD (10 μM) in 20 mM Na_2HPO_4 buffer, pH 9.0, was mixed with an equal volume of *trans*-3-chloroacrylic acid (25-11,000 μM, top to bottom) at 22 °C. The decrease in fluorescence was fit to a double exponential. The reported concentrations are those after mixing enzyme and substrate. The individual reactions were monitored for 2.5 s.

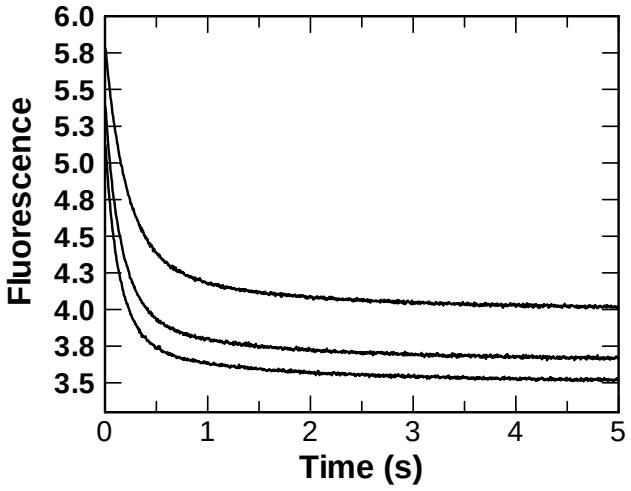

Figure 3.2. Three representative traces from a total of 19 stopped-flow experiments in which αF39W-CaaD (10 μM) in 20 mM Na_2HPO_4 buffer, pH 9.0, was mixed with an equal volume of *trans*-3-chloroacrylic acid (2000 μM, 3000 μM, and 4000 μM, top to bottom) at 22 °C. The data were fit to a double exponential and the rates are 4.79 ± 0.01 s^{-1} (k_1) and 0.824 ± 0.001 s^{-1} (k_2); 6.31 ± 0.01 s^{-1} (k_1) and 0.887 ± 0.001 s^{-1} (k_2); 7.27 ± 0.01 s^{-1} (k_1) and 0.875 ± 0.011 s^{-1} (k_2), respectively. The reported concentrations are those after mixing enzyme and substrate. The reactions were monitored for 10 s but only the first 5 s are shown as there was no significant change after 5 s.

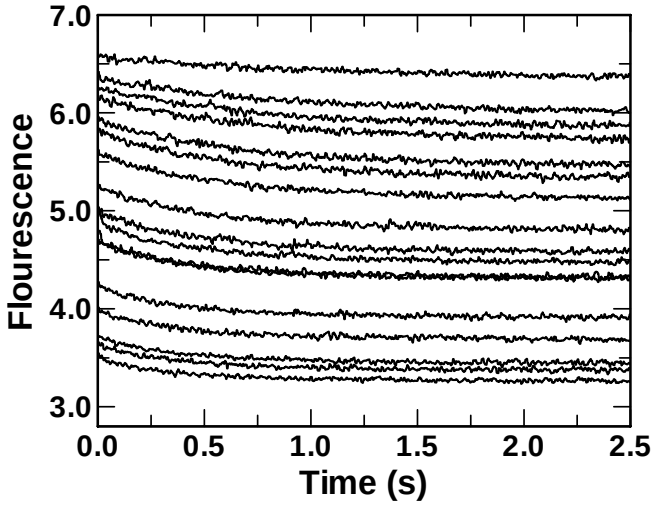

Figure 3.3. Traces from 16 stopped-flow experiments in which αF39W-CaaD (10 μM) in 20 mM Na_2HPO_4 buffer, pH 9.0, was mixed with an equal volume of *trans*-3-bromoacrylic acid (150-25,000 μM, top to bottom) at 22 °C. The decrease in fluorescence was fit to a double exponential. The reported concentrations are those after mixing enzyme and substrate. The individual reactions were monitored for 2.5 s.

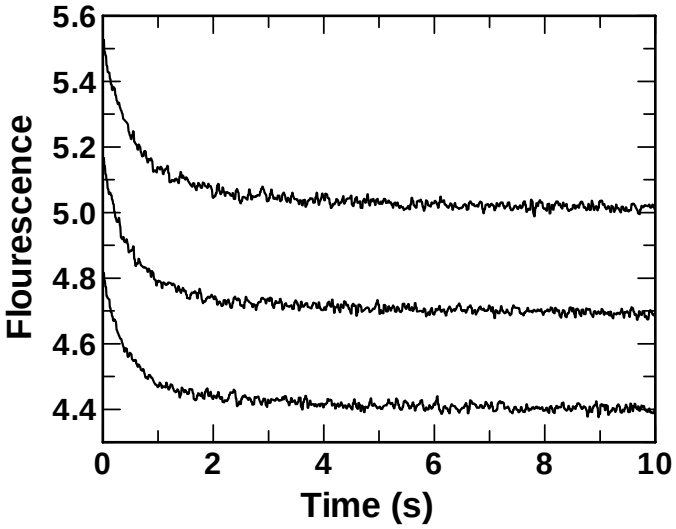

Figure 3.4. Three representative traces from a total of 16 stopped-flow experiments in which αF39W-CaaD (10 μM) in 20 mM Na_2HPO_4 buffer, pH 9.0, was mixed with an equal volume of *trans*-3-bromoacrylic acid (2000 μM, 3000 μM, and 4000 μM, top to bottom) at 22 °C. The data was fit to a double exponential and their rates are 10.39 ± 0.01 s^{-1} (k_1) and 1.591 ± 0.001 s^{-1} (k_2); 5.92 ± 0.01 s^{-1} (k_1) and 1.747 ± 0.001 s^{-1} (k_2); 41.9 ± 5.1 s^{-1} (k_1) and 1.957 ± 0.001 s^{-1} (k_2), respectively. The reported concentrations are those after mixing enzyme and substrate. The reactions were monitored for 10 s.

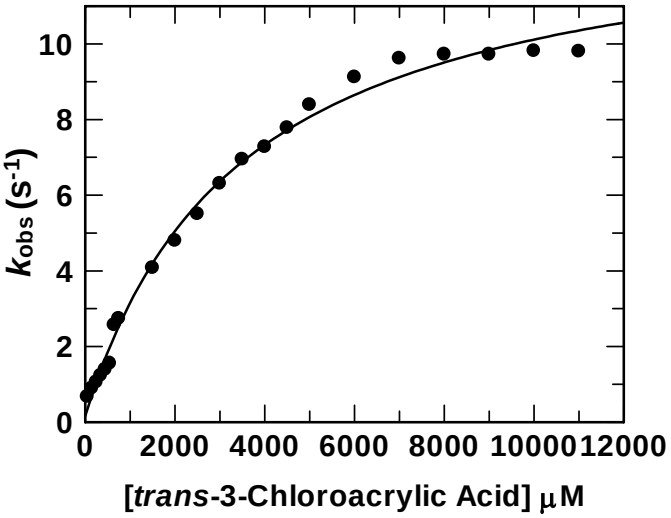

Figure 3.5. Concentration dependence of k_{obs} for binding of *trans*-3-chloroacrylic acid (25–11,000 μM) to αF39W-CaaD (10 μM) in 20 mM Na_2HPO_4 buffer, pH 9.0, at 22 °C. The concentration dependence of the fast phase was fit to a hyperbolic equation using non-linear regression to derive a ground-state binding constant (K_d) of 3500 ± 400 μM and a maximum rate of 13.4 ± 0.4 s^{-1} for a subsequent step. The reported concentrations are those after mixing enzyme and substrate.

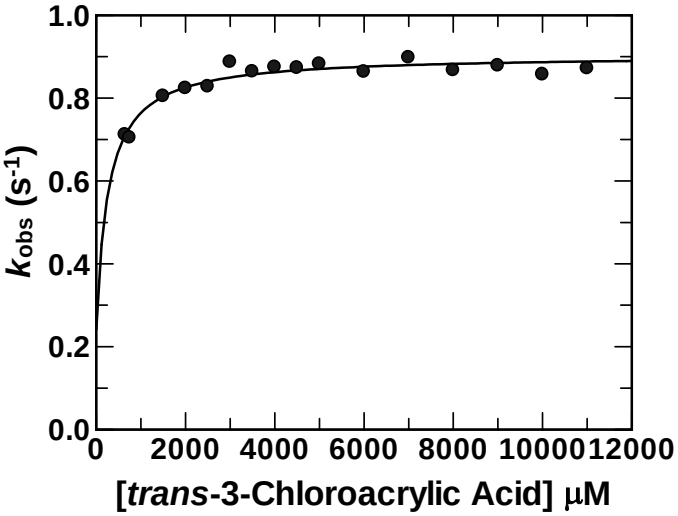

Figure 3.6. Concentration dependence of k_{obs} for binding of *trans*-3-chloroacrylic acid (25–11,000 μM) to αF39W-CaaD (10 μM) in 20 mM Na_2HPO_4 buffer, pH 9.0, at 22 °C. The concentration dependence of the slow phase was fit to a hyperbolic equation using non-linear regression analysis to derive a maximum rate of 0.90 ± 0.10 s^{-1}. The reported concentrations are those after mixing enzyme and substrate.

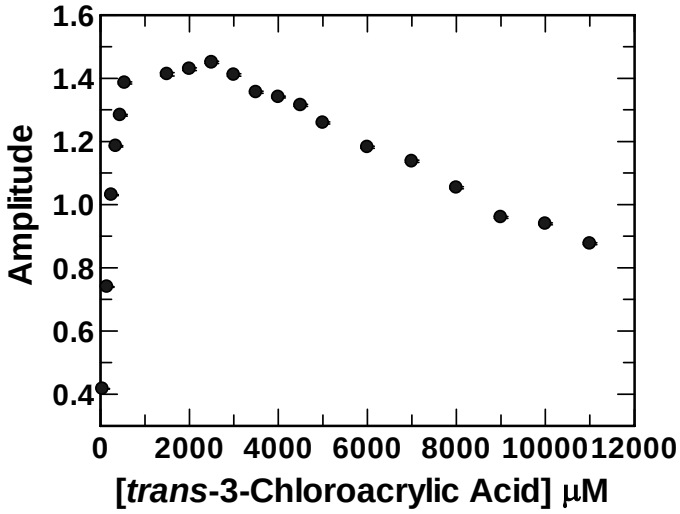

Figure 3.7. Concentration dependence of the amplitude for the fast phase binding of *trans*-3-chloroacrylic acid (25–11,000 μM) to αF39W-CaaD (10 μM) in 20 mM Na_2HPO_4 buffer, pH 9.0, at 22 °C. The data could not be fit. The reported concentrations are those after mixing enzyme and substrate.

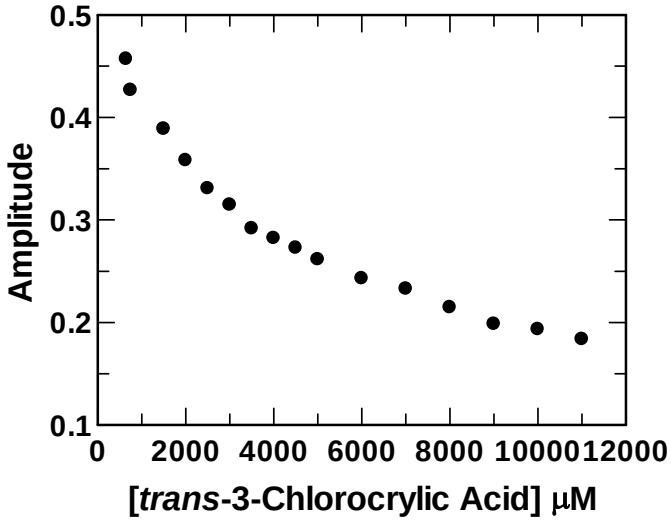

Figure 3.8. Concentration dependence of the amplitude for the slow phase binding of *trans*-3-chloroacrylic acid (25–11,000 μM) to αF39W-CaaD (10 μM) in 20 mM Na_2HPO_4 buffer, pH 9.0, at 22 °C. The data could not be fit. The reported concentrations are those after mixing enzyme and substrate.

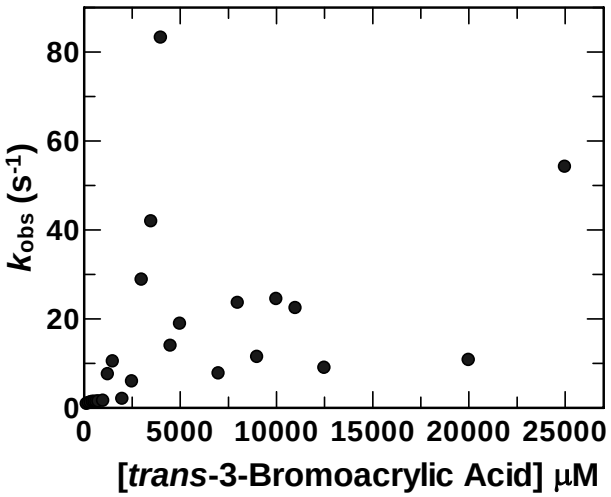

Figure 3.9. Concentration dependence of k_{obs} for binding of *trans*-3-bromoacrylic acid (150–25,000 μM) to αF39W-CaaD (10 μM) in 20 mM Na_2HPO_4 buffer, pH 9.0, at 22 °C. The concentration dependence of the fast phase could not be fit. The reported concentrations are those after mixing enzyme and substrate.

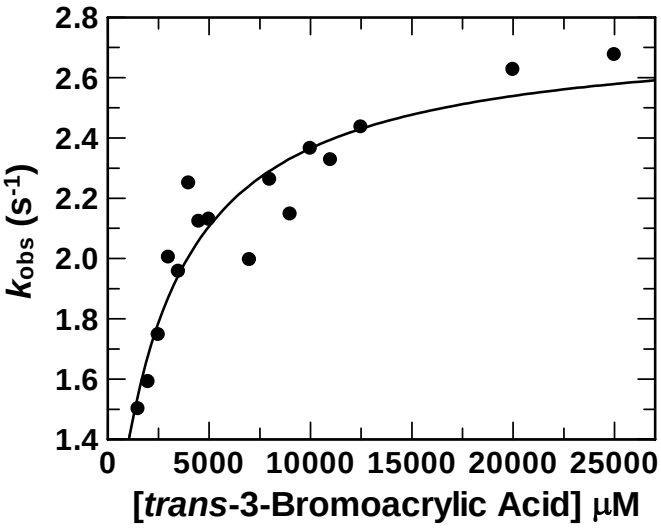

Figure 3.10. Concentration dependence of k_{obs} for binding of *trans*-3-bromoacrylic acid (150–25,000 μM) to αF39W-CaaD (10 μM) in 20 mM Na_2HPO_4 buffer, pH 9.0, at 22 °C. The concentration dependence of the slow phase could be fit to an equation for a hyperbola, but the errors were significant. The reported concentrations are those after mixing enzyme and substrate.

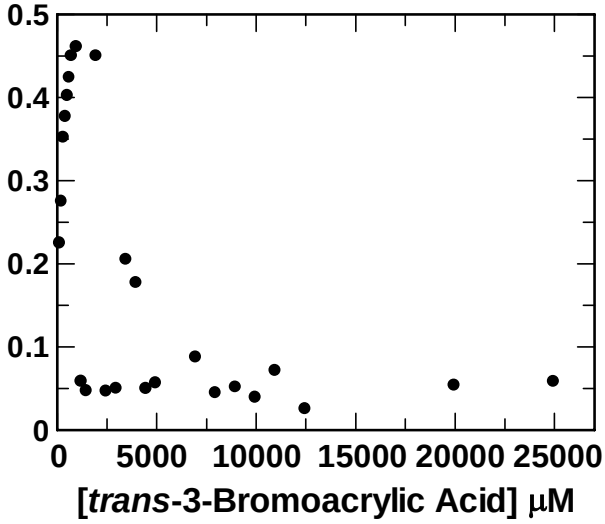

Figure 3.11. Concentration dependence of the amplitude for the fast phase binding of *trans*-3-bromoacrylic acid (150–25,000 μM) to αF39W-CaaD (10 μM) in 20 mM Na_2HPO_4 buffer, pH 9.0, at 22 °C. The concentration dependence of the amplitude for the fast phase could not be fit. The reported concentrations are those after mixing enzyme and substrate.

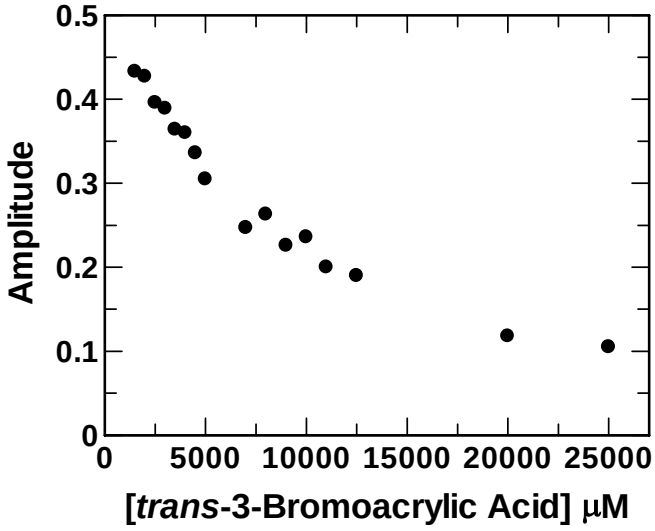

Figure 3.12**.** Concentration dependence of the amplitude for the slow phase binding of *trans*-3-bromoacrylic acid (150–25,000 μM) to αF39W-CaaD (10 μM) in 20 mM Na_2HPO_4 buffer, pH 9.0, at 22 °C. The concentration dependence of the amplitude for the slow phase could not be fit. The reported concentrations are those after mixing enzyme and substrate.

3.4 Discussion

CaaD and *cis*-CaaD carry out hydrolytic dehalogenation reactions on the respective isomers of 3-chloro- and 3-bromoacrylate (1, 2, 9). Although initial studies indicated that the mechanisms of the two enzymes largely paralleled one another with subtle differences (9), subsequent crystallographic (13) and inhibition studies (14) revealed more significant differences. In order to better understand the mechanism of

both enzymes and to determine whether the observed differences had a basis in the microscopic rate constants, a pre-steady state kinetic analysis was initiated.

For *cis*-CaaD, stopped-flow and rapid quench chemical quench experiments provided a five-step minimal kinetic model for the mechanism. A similar strategy is being pursued for CaaD. Thus far, only stopped-flow experiments have been carried out. Unlike *cis*-CaaD, however, CaaD does not have a fluorophore. For this reason, a mutant of CaaD was made where αPhe-39, a residue located in the active site (4), was replaced with a tryptophan residue. The resulting αF39W mutant introduces the only fluorophore in the enzyme. The mutant retains significant dehalogenase activity (~20 % of wild type), and the fluorescence signal was sufficient for kinetic studies.

Stopped-flow experiments were carried out on αF39W-CaaD using two substrates, *trans*-3-chloro- and *trans*-3-bromoacrylic acid. Both of these substrates, when mixed with αF39W-CaaD, produced a decrease in fluorescence signal which could be fit to an equation for a double exponential. The observed rates for both the fast decrease in fluorescence and the slow decrease in fluorescence using *trans*-3-chloroacrylic acid could be fit to a hyperbola and analyzed using non-linear regression. This analysis gave a weak ground state binding constant of 3500 ± 500 μM and a maximum rate of 13.4 ± 0.4 s^{-1}.

The data for the decrease in fluorescence signal observed for αF39W-CaaD and *trans*-3-bromoacrylic acid could also be fit to a double exponential, but the resulting plots versus substrate concentrations could not be fit. It is not clear why the data cannot be fit but it may be related to the size of the bromide coupled with the introduction of the larger tryptophan side chain in the active site.

Scheme 3

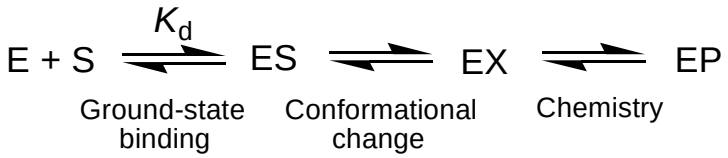

In the absence of additional experiments, the stopped-flow data for *trans*-3-chloroarylic acid was simulated and fit to a two-step binding mechanism followed by chemistry (Scheme 3). A comparison of the K_d value obtained for *cis*-CaaD (~1400 μM) versus CaaD (~3500 μM) shows stronger binding for the *cis*-CaaD substrate. There are (at least) two explanations for this observation. The first one is that substrate binds comparably to both wild type enzymes but the larger side chain of the tryptophan in the αF39W mutant weakens binding. The second explanation is based on the fact that *cis*-CaaD has two additional groups, His-28 and Tyr-103, at the active site (13). The presence of these residues, particularly His-28, may give rise to stronger binding of *cis*-3-chloroacrylate. Stronger binding, may also reflect the importance of substrate activation to the *cis*-CaaD mechanism. The latter explanation is highly speculative but tantalizing. Additional evidence may be provided by the planned pre-steady state kinetic analysis of *cis*-CaaD mutants. Completion of the pre-steady state kinetic analysis of CaaD may uncover how individual rate constants correlate with with observed catalytic properties.

Another goal of this study was to determine the feasibility of pre-steady state kinetic experiments and to identify conditions under which these experiments could be conducted. It is apparent that using the *trans*-3-bromoacrylic acid with αF39W-CaaD in

20 mM Na_2HPO_4 buffer does not produce data that are subject to analysis. It may be possible to circumvent this problem by changing to Tris or $NaHCO_3$ buffers. If these buffers do not produce reliable data, then it will be necessary to develop an ion chromatography method for quantification of chloride ion and use *cis*-3-chloroacrylic acid in all future experiments. These experiments are currently in progress.

3.5 References

1. Poelarends, G.J., Saunier, R., Janssen, D.B. (2001) *trans*-3-Chloroacrylic acid dehalogenase from *Pseudomonas pavonaceae* 170 shares structural and mechanistic similarities with 4-oxalocrotonate tautomerase, *J. Bacteriol. 183*, 4269-4277.

2. Wang, S.C., Person, M.D., Johnson, W.H., Jr., Whitman, C.P. (2003) Reactions of *trans*-3-chloroacrylic acid dehalogenase with acetylene substrates: consequences of and evidence for a hydration reaction, *Biochemistry 42*, 8762-8773.

3. (a) Hartmans, S., Jansen, M.W., van der Werf, M.J., de Bont, J.A.M. (1991) Bacterial metabolism of 3-chloroacrylic acid, *J. Gen. Microb. 137*, 2025-2032. (b) Van Hylckama Vlieg, J.E.T., Janssen, D.B. (1992) Bacterial degradation of 3-chloroacrylic acid and the characterization of *cis*- and *trans*-specific dehalogenases, *Biodegradation 2*, 139-150. (c) Poelarends, G.J., Wilkens, M., Larkin, M.J., van Elsas, J.D., Janssen, D.B. (1998) Degradation of 1,3-dichloropropene by *Pseudomonas cichorii* 170, *Appl. Environ. Microbiol. 64*, 2931-2936.

4. de Jong, R.M., Brugman, W., Poelarends, G.J., Whitman, C.P., Dijkstra, B.W. (2004) The X-ray structure of *trans*-3-chloroacrylic acid dehalogenase reveals a novel hydration mechanism in the tautomerase superfamily, *J. Biol. Chem. 279*, 11546-11552.

5. Azurmendi, H.F., Wang, S.C., Massiah, M.A., Poelarends, G.J., Whitman, C.P., Mildvan, A.S. (2004) The roles of active-site residues in the catalytic mechanism of *trans*-3-chloroacrylic acid dehalogenase: a kinetic, NMR, and mutational analysis, *Biochemistry 43*, 4082-4091.

6. Murzin, A.G. (1996) Structural classification of proteins: new superfamilies, *Curr. Opin. Struct. Biol*. *6*, 386-394.

7. Whitman, C.P. (2002) The 4-oxalocrotonate tautomerase family of enzymes: how nature makes new enzymes using a β-α-β structural motif, *Arch. Biochem. Biophys. 402*, 1-13.

8. Poelarends, G.J., Whitman, C.P. (2004) Evolution of enzymatic activity in the tautomerase superfamily: mechanistic and structural studies of the 1,3-dichloropropene catabolic enzymes, *Bioorg. Chem. 32*, 376-92.

9. Poelarends, G. J., Serrano, H., Person, M. D., Johnson, W. H., Jr., Murzin, A. G., Whitman, C.P. (2004) Cloning, expression, and characterization of a *cis*-3-chloroacrylic acid dehalogenase: insights into the mechanistic, structural, and

evolutionary relationship between isomer-specific 3-chloroacrylic acid dehalogenases, *Biochemistry 43*, 759-772.

10. Sambrook, J., Fritsch, E. F., and Maniatis, T. (1989) *Molecular Cloning: A Laboratory Manual*, 2nd ed, Cold Spring Harbor Laboratory, Cold Spring Harbor, NY.

11. Laemmli, U.K. (1970) Cleavage of structural proteins during the assembly of the head of bacteriophage T4, *Nature 227*, 680-685.

12. Waddell, W. J. (1956) A simple ultraviolet spectrophotometric method for the determination of protein, *J. Lab. Clin. Med. 48*, 311-314.

13. de Jong, R.M., Bazzacco, P., Poelarends, G.J., Johnson, Jr, W.H., Kim, Y.-J., Burks, E.A., Serrano, H., Whitman, C.P., Dijkstra B.W., Crystal structures of wild type and inactivated *cis*-3-chloroacrylic acid dehalogenase: the structural basis for substrate specificity and inactivation by (*R*)-oxirane-2-carboxylate, *J. Biol. Chem. 282*, 2440-2449 (2007).

14. Poelarends, G.J., Serrano, H., Johnson, Jr., W.H., Whitman, C.P. (2004) Stereospecific alkylation of *cis*-chloroacrylic acid dehalogenase by (*R*)-oxirane-2-carboxylate: analysis and mechanistic implications, *Biochemistry 43*, 7187-7196.

15. Johnson, K.A. (1992) Transient state kinetic analysis of enzyme reaction pathways, *The Enzymes,* XX, 1-61.

Chapter 4: Inactivation of Cg10062, a Tautomerase Superfamily Member from *Corynebacterium glutamicum* by (*R*)- and (*S*)-Oxirane-2-carboxylate: Analysis and Implications

4.1 Introduction

Cg10062 is a *cis*-3-chloroacrylic acid dehalogenase (*cis*-CaaD) homologue (~34% sequence similarity) found in *Corynebacterium glutamicum* (*1*). The physiological role and reaction of Cg10062 are unknown and the gene has no clear genomic context. In contrast, *cis*-CaaD catalyzes the conversion of *cis*-3-chloroacrylic acid (**2**, Scheme 1) to malonate semialdehyde (**4**), which is one of the reactions in a catabolic pathway for the nematocide 1,3-dichloropropene (**1**) in coryneform bacterial strain FG41 (*2*,*3*). An enzyme-catalyzed-decarboxylation of **4** completes the overall transformation of **1** to acetaldehyde (**5**). *cis*-CaaD, and its counterpart in *Pseudomonas pavonaceae* 170, *trans*-3-chloroacrylic acid dehalogenase (CaaD), which processes **3** to **4**, are highly specific for their substrates (*4*,*5*). Cg10062 is not isomer-specific and exhibits low level *cis*-CaaD and CaaD activities, with the *cis*-CaaD activity being more pronounced (*6*).

Scheme 1

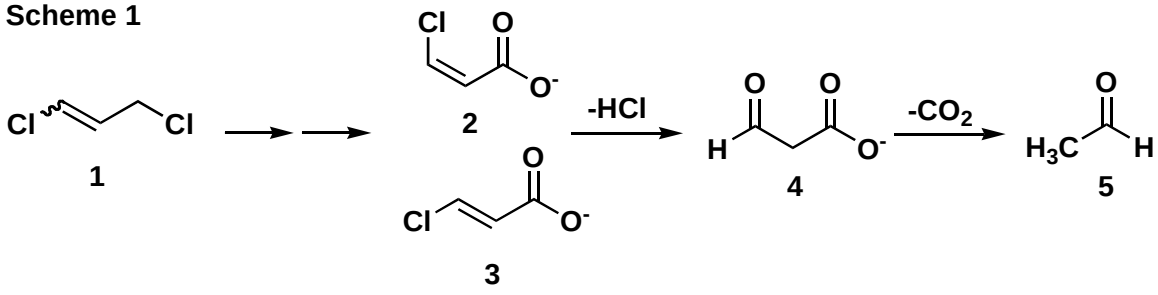

Both Cg10062 and *cis*-CaaD are trimers composed of 149-amino acid monomers, and a sequence comparison shows that six key catalytic residues (Pro-1, His-28, Arg-70, Arg-73, Tyr-103, and Glu-114) in *cis*-CaaD are present in Cg10062 (*1*,*6*,*7*). In the proposed *cis*-CaaD mechanism, Glu-114 and Tyr-103 activate a water molecule for addition to C-3 of **2** (*1*,*7*). His-28, Arg-70, and Arg-73 interact with the C-1 carboxylate group to bind and "activate" the substrate for the conjugate addition of water (*1*,*7*). Pro-1 provides a proton to C-2, which completes the reaction and yields **4**. The sum of these observations suggests that subtle active site differences may account for the diminished dehalogenase activity of Cg10062 and the less stringent substrate specificity.

As part of an effort to delineate these differences, we examined (*R*)- and (*S*)-oxirane-2-carboxylate (**6**) as potential irreversible inhibitors of Cg10062. We have previously reported that *cis*-CaaD is irreversibly inactivated by (*R*)-**6**, due to the covalent modification of Pro-1 (*8*). The (*S*)-enantiomer is not an irreversible inhibitor and neither enantiomer inactivates CaaD. In accord with the relaxed substrate specificity and preference for **2**, we find that Cg10062 is irreversibly inactivated by both enantiomers, with the (*R*)-enantiomer being more potent. Inactivation is due to covalent modification of Pro-1. Pro-1, Arg-70, and Arg-73 are essential for the inactivation of Cg10062, whereas Glu-114 may play a role but not an essential one. These observations parallel those found for *cis*-CaaD but the lack of stereospecificity and the participation of Glu-114 distinguish the inactivation mechanism for Cg10062 from that of *cis*-CaaD. Hence, the inactivation mechanisms will likely be similar, but may result from different orientations in the active site. These results provide the necessary foundation for a

crystallographic analysis of Cg10062 inactivated by (*R*)- and (*S*)-**6** so that these orientations can be determined.

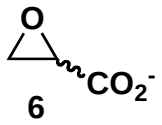

4.2 Materials and Methods

Materials. All reagents, buffers, and solvents were obtained from Sigma Aldrich Chemical Co. (St. Louis, MO), Fisher Scientific Inc. (Pittsburgh, PA), Spectrum Laboratory Products, Inc. (New Brunswick, NJ), or EM Science (Cincinnati, OH), unless noted otherwise. Literature procedures were used for the syntheses of (*R*)- and (*S*)-**6** (*9*) and 2-oxo-3-pentynoate (**7**) (*10*). *cis*-CaaD, malonate semialdehyde decarboxylase (MSAD), Cg10062, and the Cg10062 mutants (P1A, R70A, R73A, and E114Q) (*6*) were purified to homogeneity, as assessed by sodium dodecyl sulfate-polyacrylamide gel electrophoresis (SDS-PAGE), by variations of published procedures (*1*,*6*,*11*). The construction and characterization of the Cg10062 mutants are reported elsewhere (*6*). Pre-packed PD-10 Sephadex G-25 columns were purchased from Biosciences AB (Uppsala, Sweden). Endoproteinase Glu-C (protease V-8) was obtained from F. Hoffmann-La Roche, Ltd. (Basel, Switzerland).

Composition of SOB and SOC Media. The SOB medium was made by mixing tryptone (4 g) and yeast extract (1 g) in 100 mL of deionized water. The mixture was then autoclaved for 45 min and stored in a sealed glass bottle at 22 °C until ready to use.

The SOC medium (10 mL) was made by mixing 4.7 mL of deionized water with SOB medium (5 mL). To this mixture, $MgSO_4$ (0.1 mL of a 1 mg/mL stock solution), NaCl/KCl (0.1 mL of a 1 mg/mL stock solution), and glucose (0.1 mL of a 1 mg/mL stock solution) were added. The solution was mixed at 22 °C and used immediately after being made.

General Methods. Protein was analyzed by SDS-PAGE under denaturing conditions on gels containing 15% polyacrylamide (*12*). The gels were stained with Coomassie brilliant blue. Protein concentrations were determined by the method of Waddell (*13*). Absorbance data were obtained on a Hewlett Packard 8452A Diode Array spectrophotometer. The kinetic data were fitted by nonlinear regression data analysis using the Grafit program (Erithacus Software Ltd., Horley, U.K.) obtained from Sigma Chemical Co**.** Cg10062 activity was determined by following the absorbance increase at 296 nm ($\varepsilon = 7000\ M^{-1}\ cm^{-1}$), which corresponds to formation of acetopyruvate (**8**) by the Cg10062-catalyzed hydration of **7** (*1*,*5*,*6*). Typically, Cg10062 preparations used in these studies have a $K_m = 4.2 \pm 0.3$ mM and a $k_{cat} = 0.16 \pm 0.01\ s^{-1}$ using **7**. *cis*-CaaD activity was measured by following the absorbance decrease at 224 nm ($\varepsilon = 2900\ M^{-1}\ cm^{-1}$), as described elsewhere (*1*). Mass spectral analyses were carried out using the indicated instruments, which are housed in the Analytical Instrumentation Facility Core in the College of Pharmacy at the University of Texas at Austin.

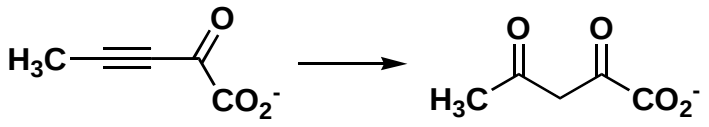

7 8

4.2.1 Transformation, Expression, and Purification for Cg10062 and Mutants

Transformation of Expression Cells for Cg10062. *E. coli* BL21-Gold(DE3) competent cells were thawed and stored on ice. Competent cells (~100 μL) were pipetted into a pre-chilled 15-mL Falcon 2059 tube along with pCC5 (~50 ng) containing the Cg10062 gene (*6*). The reaction mixture was gently incubated on ice for 30 min. During this time, a 900-μL aliquot of SOC medium was preheated in a water bath to 42 °C. The reaction mixture was heat-pulsed for 20 s in a water bath at 42 °C and then incubated on ice for 2 min. Subsequently, the 900-μL aliquot of SOC medium was added to the reaction mixture. The cells were incubated at 37 °C for 1 h in an environmental shaker at 225 rpm. The cells were then concentrated by centrifugation (500 rpm for 5 min), and a 600-μL aliquot of the supernatant was removed. The cells were resuspended in the remaining supernatant. A portion of the resulting transformation reaction mixture (200 μL) was plated, using a sterile spreader, onto an LB/Ap (50 μg/mL) agar plate. The plate was then incubated overnight (~ 16 h) at 37 °C.

Expression and Purification of Cg10062. Wild-type Cg10062 was produced in *E. coli* BL21-Gold(DE3) cells using the T7 expression system. The freshly transformed *E. coli* cells, with the plasmid coding the Cg10062 gene, were collected from a plate and used to inoculate three 2-liter flasks containing 1L of LB/Ap (100 mg/L). After

overnight growth at 30 °C in an environmental shaker at 225 rpm, cells were harvested by centrifugation (15 min at 7,000 rpm) and stored at -20 °C until further use. Typically 1 L of culture yields 6 g of cells.

Cells (18 g) were thawed and suspended in 10 mL of 10 mM Tris-SO_4 buffer, pH 8.0, and placed on ice. Cells were disrupted, while stirring on ice, by sonication at 60 W output (using a W385 sonicator from Heat Systems-Ultrasonics, Inc.) for ten 2-min intervals using 5-s pulses with a cycle time of 50%. After each 2-min interval, cells were allowed to sit for 5 min. DNase (10 μL of a 10 Units/μL solution) and RNase (10 mL of a 500 μg/mL solution) were added to the solution and allowed to stir on ice for 1 h. The lysed cells were then centrifuged at 17,000 rpm for 45 min. The supernatant was retained and centrifuged at 60,000 rpm for 1 h.

Subsequently, the supernatant was filtered through a 0.2 μm-pore diameter filter and applied to a TSKgel DEAE-5PW anion-exchange column (150 × 21.5 mm), which had been previously equilibrated with 10 mM Tris-SO_4 buffer, pH 8.0. The column was washed with 10 mM Tris-SO_4 buffer, pH 8.0, containing 0.5 M Na_2SO_4 for 20 min. The protein was eluted using a linear gradient (0-0.5 M Na_2SO_4) at a flow rate of 5 mL/min over a 90 min period. Fractions were collected at 1.75 min intervals (8.75 mL). Fractions (#8-35) with the highest purity (as determined by SDS-PAGE) were pooled and concentrated to ~20 mL using an Amicon stirred cell equipped with a YM10 (10,000 MW cutoff) ultrafiltration membrane and stored at 4 °C.

Solid $(NH_4)_2SO_4$ was added to the concentrate to make a final concentration of 1.6 M. After stirring for 1 h at 4 °C, the solution was centrifuged at 11,000 rpm for 15

min. The supernatant was then passed through a 0.2 μm-pore diameter filter and applied to a TSKgel Phenyl-5PW column (150 × 21.5 mm) which had previously been equilibrated with 10 mM Tris-SO_4 buffer, pH 8.0, containing 1.6 M $(NH_4)_2SO_4$. The protein was eluted using a decreasing linear gradient [1.6-0 M $(NH_4)_2SO_4$] at a flow rate of 5 mL/min. Fractions were collected at 1.75 min intervals (8.75 mL) during the 90 min program. Fractions (#19-24) with the highest purity (as determined by SDS-PAGE) were pooled and concentrated to ~10 mL by an Amicon stirred cell equipped with a YM10 (10,000 MW cutoff) ultrafiltration membrane, and stored at 4 °C. This purification resulted in ~200 mg of 95% pure protein as assessed by ESI mass spectroscopy and SDS-PAGE. The observed monomer mass for Cg10062 was 17,092 Da (calc. 17,092 Da).

Expression and Purification of P1A-Cg10062. The P1A mutant of the Cg10062 gene was transformed and the gene product expressed in *E. coli* BL21-Gold(DE3) cells as described for wild-type. Typically, 1 L of culture yields 6 g of cells. The cells (~12 g) were lysed and the enzyme purified following the protocol described for the wild-type enzyme. Fractions (#12-35) from the TSKgel DEAE-5PW anion-exchange column with the highest purity (as determined by SDS-PAGE) were pooled and concentrated to ~20 mL using an Amicon stirred cell equipped with an YM10 (10,000 MW cutoff) ultrafiltration membrane. Fractions (#20-22) from the TSKgel Phenyl-5PW column with the highest purity (as determined by SDS-PAGE) were pooled and concentrated to ~1.5 mL using an Amicon stirred cell equipped with an YM10 (10,000 MW cutoff) ultrafiltration membrane and stored at 4 °C. This purification resulted in ~7 mg of 95%

pure protein as assessed by ESI mass spectroscopy and SDS-PAGE. The observed monomer mass for P1A-Cg10062 was 17,067 Da (calc. 17,067 Da).

Expression and Purification of R70A-Cg10062. The R70A mutant of the Cg10062 gene was transformed and the gene product expressed in *E. coli* BL21-Gold(DE3) cells as described for wild-type. Typically, 1 L of culture yields 6 g of cells. The cells (~6 g) were lysed and the enzyme purified following the protocol described for the wild-type enzyme. Fractions (#14-35) from the TSKgel DEAE-5PW anion-exchange column with the highest purity (as determined by SDS-PAGE) were pooled and concentrated to ~18 mL using an Amicon stirred cell equipped with an YM10 (10,000 MW cutoff) ultrafiltration membrane. The fraction (#26) from the TSKgel Phenyl-5PW column with the highest purity (as determined by SDS-PAGE) was concentrated to ~2 mL using an Amicon stirred cell equipped with an YM10 (10,000 MW cutoff) ultrafiltration membrane and stored at 4 °C. This purification resulted in ~35 mg of 95% pure protein as assessed by ESI mass spectroscopy and SDS-PAGE. The observed monomer mass for R70A-Cg10062 was 17,008 Da (calc. 17,008 Da).

Expression and Purification of R73A-Cg10062. The R73A mutant of the Cg10062 gene was transformed and the gene product expressed in *E. coli* BL21-Gold(DE3) cells as described for wild-type. Typically, 1 L of culture yields 6 g of cells. The cells (~6 g) were lysed and the enzyme purified following the protocol described for the wild-type enzyme. Fractions (#14-35) from the TSKgel DEAE-5PW anion-exchange column with the highest purity (as determined by SDS-PAGE) were pooled and concentrated to ~18 mL using an Amicon stirred cell equipped with an YM10 (10,000

MW cutoff) ultrafiltration membrane. The fraction (#24) from the TSKgel Phenyl-5PW column with the highest purity (as determined by SDS-PAGE) was concentrated to ~2 mL using an Amicon stirred cell equipped with an YM10 (10,000 MW cutoff) ultrafiltration membrane and stored at 4 °C. This purification resulted in ~43 mg of 95% pure protein as assessed by ESI mass spectroscopy and SDS-PAGE. The observed monomer mass for R73A-Cg10062 was 17,008 Da (calc. 17,008 Da).

Expression and Purification of E114Q-Cg10062. The E114Q mutant of the Cg10062 gene was transformed and the gene product expressed in *E. coli* BL21-Gold(DE3) cells as described for wild-type. Typically, 1 L of culture yields 6 g of cells. The cells (~6 g) were lysed and the enzyme purified following the protocol described for the wild-type enzyme. Fractions (#14-35) from the TSKgel DEAE-5PW anion-exchange column with the highest purity (as determined by SDS-PAGE) were pooled and concentrated to ~18 mL using an Amicon stirred cell equipped with an YM10 (10,000 MW cutoff) ultrafiltration membrane. The fraction (#25) from the TSKgel Phenyl-5PW column with the highest purity (as determined by SDS-PAGE) was concentrated to ~2 mL using an Amicon stirred cell equipped with an YM10 (10,000 MW cutoff) ultrafiltration membrane and stored at 4 °C. This purification resulted in ~33 mg of 95% pure protein as assessed by ESI mass spectroscopy and SDS-PAGE. The observed monomer mass for E114Q-Cg10062 was 17,092 Da (calc. 17,092 Da).

4.2.2 Inhibition and Protection Experiments of Cg10062

*Irreversible Inhibition of Cg10062 by (R)- and (S)-**6**.* The time-dependent inactivation of Cg10062 by *(R)*- and (*S*)-**6** was characterized using a previously described

protocol (*8*), with the following modifications. Varying concentrations of (*R*)-**6** (0.99-33.0 mM) or (*S*)-**6** (4.8-56.5 mM) were incubated with the enzyme in 20 mM Na_2HPO_4 buffer (pH 9.0) at 22 °C. The initial incubation mixtures (total volume of 110 μL) were made up in 1.5 mL eppendorf micro test tubes and contained 100 μM of Cg10062 (based on monomer concentration). Aliquots (10 μL) from these mixtures were removed at various time intervals, diluted into 1 mL of 20 mM Na_2HPO_4 buffer (pH 9.0), and assayed for residual activity using **7**. Assays were initiated by the addition of **7** (4 μL from a 365 mM stock solution) to give a final concentration of 1.5 mM for **7** in all experiments. Stock solutions of **7** were made up in 100 mM Na_2HPO_4 buffer (pH ~9) and the pH was slowly adjusted to 7.3 by the addition of 2 μL-aliquots of a 1 M NaOH solution. Stocks solutions (100 mM) of (*R*)- or (*S*)-**6** were made up in 100 mM NaH_2PO_4 buffer (pH 7.3). For experiments using the (*R*)-enantiomer, rates were monitored for 120 s and for experiments using the (*S*)-enantiomer, rates were monitored for 200 s. The initial time point (t = 0) corresponded to the rate measured for an aliquot removed before the addition of (*R*)- or (*S*)-**6**. This activity was defined as 100% activity. The addition of inhibitor [(*R*)-**6** = 1-50 μL and (*S*)-**6** = 5-130 μL] diluted the enzyme so that the final enzyme concentration ranged from 67-99 μM for the (*R*)-enantiomer and 44-95 μM for the (*S*)-enantiomer. Hence, for each aliquot removed, the observed rate was divided by the enzyme concentration (in the assay mixture) and the resulting rate was divided by that obtained for the 100% activity. The k_{obs} values were plotted against the initial inhibitor concentrations, and the kinetic parameters (K_I and k_{inact}) were determined as described elsewhere (*14, 15*).

*Protection of Cg10062 from Inactivation by (R)- and (S)-**6**.* The incubation mixtures for the substrate protection studies were made up as described above and elsewhere (*8*), with the following modifications. Accordingly, Cg10062 (100 μM based on monomer concentration) was incubated with varying concentrations of **7** (0-5.25 mM) in 20 mM NaH_2PO_4 buffer (pH 7.3) at 22 °C. After a 30-s interval, a fixed concentration of (*R*)- or (*S*)-**6** (0.4 mM or 4.0 mM, respectively) was added to the mixture. Aliquots (10 μL) were removed at various time intervals, diluted into 1 mL of 20 mM Na_2HPO_4 buffer (pH 9.0) and assayed for residual activity.

*Irreversibility of Inactivation of Cg10062 by (R)- and (S)-**6**.* Three samples were made up containing ~1.5 mg of enzyme (80 μL of a 18.5 mg/mL solution) and a sufficient quantity of 20 mM Na_2HPO_4 buffer (pH 9.0) to give a final volume of 990 μL. Two samples were treated with (*R*)- or (*S*)-**6** [10 μL from a 100 mM stock solution in 100 mM NaH_2PO_4 buffer, pH 7.3] and a third one was treated with 100 mM NaH_2PO_4 buffer, pH 7.3 (10 μL). After a 5-day incubation period at 4 °C, an aliquot (200-μL) was removed from the control and the (*R*)-**6**-modified Cg10062 sample and subjected to Sephadex G-25 chromatography as described (*5*). Subsequently, a solution was made up from each set of fractions such that a final concentration of 2 μM enzyme (~520 μL of a 0.26 mg/mL) was obtained in 3.5 mL of 20 mM Na_2HPO_4 buffer, pH 9.0. A 1-mL aliquot was removed from each solution and assayed for activity using **7**. Activity assays were initiated by the addition of **7** (4 μL from a 365 mM stock solution made up as described above) to give **7** in a final concentration of 1.5 mM. The remaining solution (~ 2.5 mL) was stored at 4 °C and assayed after an additional 3-day incubation period. The

sample containing Cg10062 and (*S*)-**6** was incubated for 10 days at 4 °C, and then processed in a comparable manner.

4.2.3 Irreversible Inactivation of *cis*-CaaD

*Irreversible Inhibition of cis-CaaD by (R)-**6**.* The time-dependent inactivation of *cis*-CaaD by (*R*)-**6** was determined using varying concentrations of inhibitor (0-14 mM) and enzyme (20 μM based on monomer concentration) in 20 mM Na_2HPO_4 buffer (pH 9.0) at 22 °C, as described elsewhere (*8*). The incubation mixtures (total volume of 101-114 μL) were made up in 1.5 mL eppendorf micro test tubes. Aliquots (10 μL) from these mixtures were removed at various time intervals, diluted into 1 mL of 20 mM Na_2HPO_4 buffer (pH 9.0), and assayed for residual activity using **2** in a final concentration of 200 μM. The initial time point (t = 0) corresponded to the aliquot removed immediately after the addition of (*R*)-**6** to the incubation mixture. The *cis*-CaaD activity measured for this aliquot was defined as 100% activity. Activity assays were initiated by the addition of an aliquot of **2** (4 μL) removed from a 50 mM stock solution made up in 100 mM Na_2HPO_4 buffer (pH 9.1). The pH of the stock solution was adjusted ~7.5 by the addition of small quantities of 1 M NaOH.

4.2.4 Mass Spectral Analysis of Cg10062 and Mutants

*Mass Spectral Analysis of Cg10062 and Mutants Incubated with (R)- and (S)-**6**.* The covalently modified Cg10062 samples were prepared for mass spectral analysis by the incubation of the enzyme with (*R*)- or (*S*)-**6** in 20 mM Na_2HPO_4 buffer (pH 9.0) as follows. Each sample contained ~1.5 mg of enzyme (~81 μL of a 18.5 mg/mL solution) and a sufficient quantity of 20 mM Na_2HPO_4 buffer (pH 9.0) to give a final volume of

990 μL. The samples were treated with (*R*)- or (*S*)-**6** [10 μL from a 100 mM stock solution of (*R*)- or (*S*)-**6** in 100 mM NaH_2PO_4 buffer, pH 7.3]. A control sample was made up similarly, but the enzyme was treated with a 10-μL portion of buffer. Subsequently, the mixture containing Cg10062 and (*R*)-**6** was incubated at 4 °C for 24 h and analyzed. The control sample and the sample containing Cg10062 and (*S*)-**6** were incubated at 4 °C for 10 days and aliquots removed and analyzed after 24 h, 48 h, 5 days, and 10 days. The P1A, R70A, R73A, and E114Q mutants of Cg10062 were incubated separately with (*R*)- or (*S*)-**6** in 20 mM Na_2HPO_4 buffer (pH 9.0) as follows. Samples contained ~1.75 mg of enzyme (~100 μL of a 17.5 mg/mL solution) and a sufficient quantity of the 20 mM Na_2HPO_4 buffer to give a final volume of 495 μL. The samples were treated with (*R*)- or (*S*)-**6** [5 μL from a 100 mM stock solution of (*R*)- or (*S*)-**6** in 100 mM NaH_2PO_4 buffer, pH 7.3]. The mixtures were incubated at 4 °C for 10 days and aliquots removed and analyzed after 24 h, 5 days, and 10 days. Samples for electrospray ionization mass spectrometry (ESI-MS) analysis were made up as described (*5*), and analyzed using an LCQ electrospray ion trap mass spectrometer (ThermoFinnigan, San Jose, CA).

4.2.5 Peptide Mapping of Cg10062

*Peptide Mapping of Cg10062 Inactivated by (R)- and (S)-**6**.* Three samples were made up containing ~1 mg of enzyme (39 μL of a 26.5 mg/mL solution) and a sufficient quantity of 20 mM NaH_2PO_4 buffer (pH 7.3) to give a final volume of 500 μL. Two samples were treated with (*R*)- or (*S*)-**6** [5 μL from a 100 mM stock solution in 100 mM

NaH_2PO_4 buffer, pH 7.3] and a third sample was treated with buffer (5 μL). After a 24-h incubation period at 4 °C, the samples were subjected to Sephadex G-25 chromatography as described (*5*), yielding three sets of fractions containing modified Cg10062 [by (*R*)- or (*S*)-**6**] or unmodified Cg10062. A sufficient quantity of protein was removed from the fraction containing the highest concentration of protein (now in 100 mM NH_4HCO_3 buffer, pH 8.0) to give ~27 μg of enzyme, which was diluted into the necessary quantity of 100 mM NH_4HCO_3 buffer to yield a final volume of 45 μL. After the addition of a 5-μL aliquot of 10 M guanidine HCl, the three samples were incubated for 1 h at 37 °C. The protein samples were then incubated for an additional 48 h at 37 °C with sequencing grade protease V-8 (2 μL of a 10 mg/mL stock solution made up in water) (*16*). Subsequently, the V-8-treated samples were made up and analyzed on the delayed extraction Voyager-DE PRO matrix assisted laser desorption/ionization time-of-flight (MALDI-TOF) instrument (PerSeptive Biosystems, Framingham, MA) as described previously (*5*). Selected ions in the samples were also subjected to MALDI-Post-Source Decay (PSD) analysis using the protocol described elsewhere (*5*, *17*).

4.2.6 Mass Spectral Analysis of *cis*-CaaD and MSAD

*Mass Spectral Analysis of cis-CaaD Incubated with (S)-**6** and MSAD Incubated with (R)- and (S)-**6**.* A sample of *cis*-CaaD was made up as described above for Cg10062 and treated with (*S*)-**6** [10 μL from a 100 mM stock solution in 100 mM NaH_2PO_4 buffer, pH 7.3]. Similarly, samples of MSAD were made up and treated with (*R*)- and (*S*)-**6** [10 μL from 100 mM stock solutions in 100 mM NaH_2PO_4 buffer, pH 7.3]. The samples were incubated at 4 °C for 10 days and aliquots removed and analyzed after 24 h, 5 days,

and 10 days as noted in the text. The samples were prepared for mass spectral analysis as described elsewhere (*5*), and subjected to ESI-MS analysis.

4.3 Results

4.3.1 Inactivation and Protection Experiments of Cg10062

*Time-dependent Inactivation of Cg10062 by (R)- and (S)-**6**.* Cg10062 is irreversibly inactivated by both (*R*)- and (*S*)-**6** in a time-dependent first-order process (Figures 1A,B). The k_{obs} values from 18 experiments using (*R*)-**6** and the k_{obs} values from 15 experiments using (*S*)-**6** were plotted versus the initial inhibitor concentrations and fit to a rectangular hyperbola[2]. The values of K_I and k_{inact} obtained from the plot for (*R*)-**6** (Figure 2A) were 14.0 ± 2.1 mM and 0.021 ± 0.001 s^{-1}, respectively. The values obtained from the plot for (*S*)-**6** (Figure 2B) were 71.2 ± 12.7 mM and 0.005 ± 0.001 s^{-1}, respectively. Assuming K_I is an estimate of binding affinity, these values indicate that (*R*)-**6** binds more tightly (~5.1-fold) at the active site than the (*S*)-enantiomer and that at saturating concentrations of inhibitor, the (*R*)-enantiomer is the more potent inactivator (~4.2-fold).

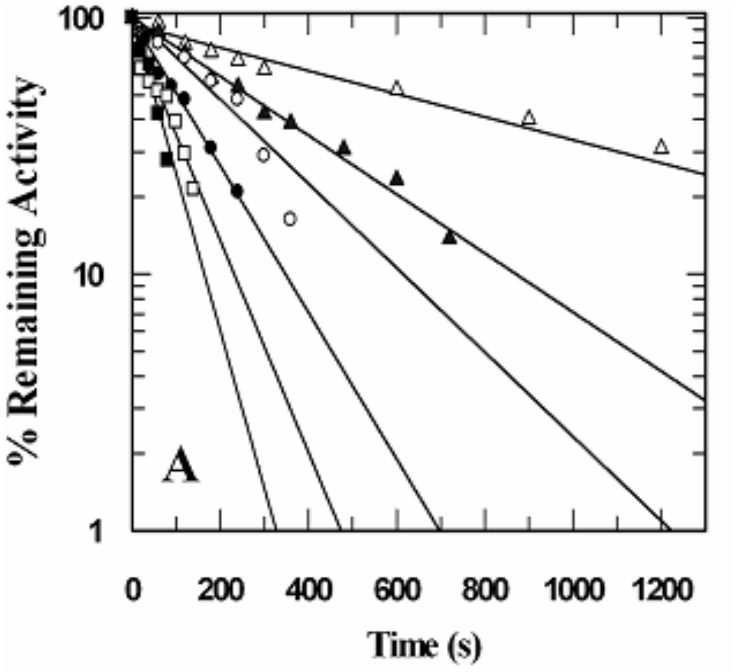
100
10
1
% Remaining Activity
A
0
200
400
600
800
1000
1200
Time (s)

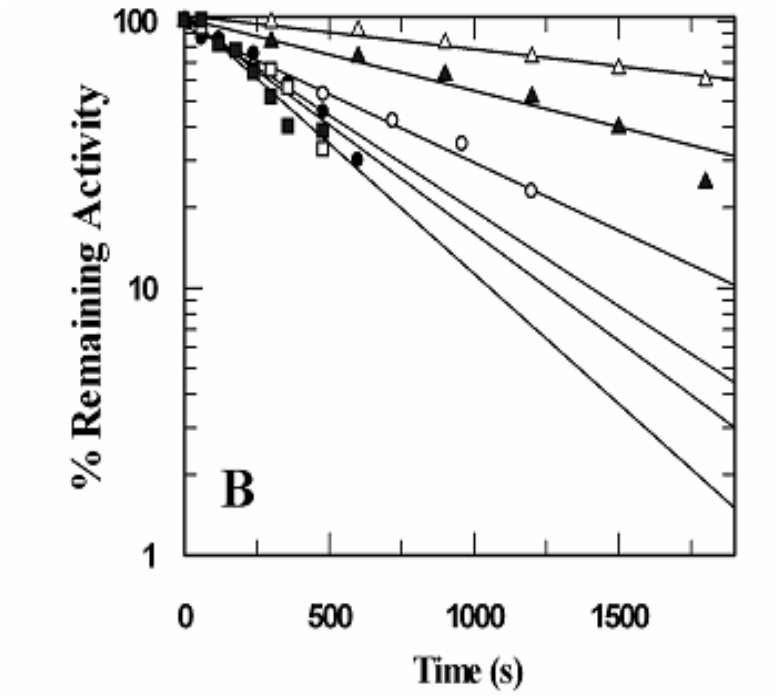
100
10
1
% Remaining Activity
B
0
500
1000
1500
Time (s)

Figure 4.1.

Figure 4.1. Time-dependent inactivation of Cg10062 by (*R*)- and (*S*)-**6**. (A) A logarithmic plot of the percent Cg10062 activity remaining as a function of time using varying amounts of (*R*)-**6** (open triangles, 0.99 mM; filled triangles, 2.9 mM; open circles, 4.8 mM; filled circles, 6.5 mM; open rectangles, 9.1 mM; filled rectangles, 33.0 mM). (B) A logarithmic plot of the percent Cg10062 activity remaining as a function of time using varying amounts of (*S*)-**6** (open triangles, 4.8 mM; filled triangles, 9.1 mM; open circles, 16.7 mM; filled circles, 23.1 mM; open rectangles, 37.5 mM; filled rectangles, 56.5 mM). For purposes of clarity, the rates obtained for six experiments are shown. The data from all of the experiments were used to calculate k_{obsd}.

In order to compare directly the inactivation of Cg10062 with that of *cis*-CaaD, the kinetic parameters for the inactivation of *cis*-CaaD by (*R*)-**6** were determined. Accordingly, the k_{obs} values from 18 experiments using *cis*-CaaD and (*R*)-**6** were fit to a rectangular hyperbola. The values of K_I and k_{inact} obtained from the plot for (*R*)-**6** (Figure 2C) were 10.8 ± 1.6 mM and 0.20 ± 0.02 s^{-1}, respectively[3]. Although (*R*)-**6** binds comparably to both enzymes (as indicated by the similar K_I values), the (*R*)-enantiomer is approximately a 9.5-fold more potent inhibitor of *cis*-CaaD than it is of Cg10062. As noted elsewhere, (*S*)-enantiomer does not inactivate *cis*-CaaD, but functions as a weak competitive inhibitor (*8*).

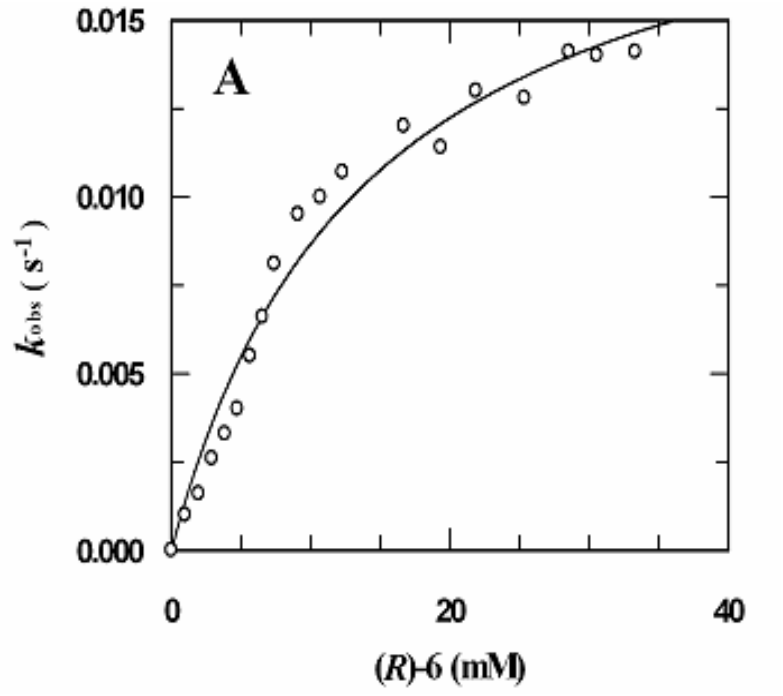
A
0.015
0.010
0.005
0.000
k_{obs} (s^{-1})
0
20
40
(R)-6 (mM)

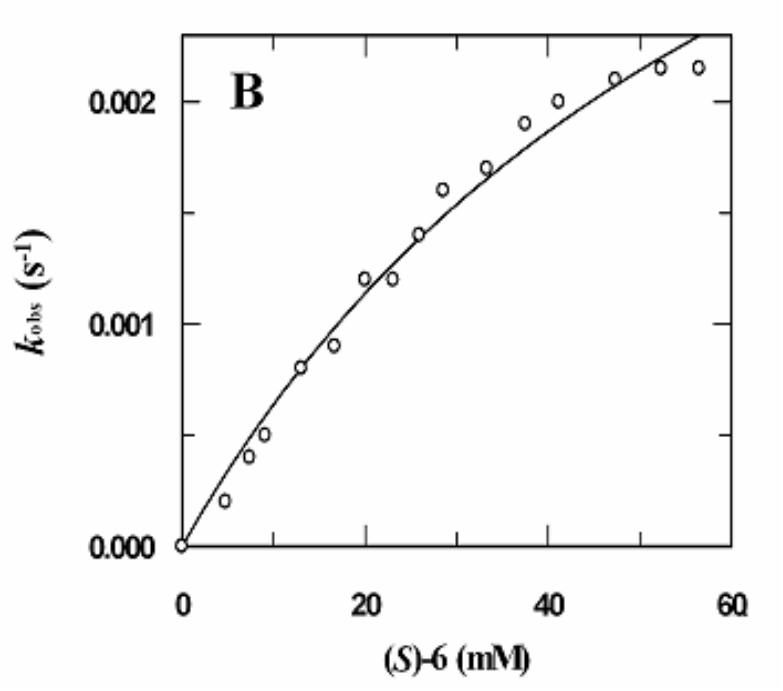
B
0.002
0.001
0.000
k_{obs} (s^{-1})
0
20
40
60
(S)-6 (mM)

Figure 4.2.

Figure 4.2. Plot of k_{obsd} values obtained for the inactivation of Cg10062 by (*R*)- and (*S*)-**6** and *cis*-CaaD by (*R*)-**6** versus the concentrations of inactivator. (A) The k_{obsd} values for 18 experiments using (*R*)-**6** and Cg10062 vs the concentration of (*R*)-**6**. (B) The k_{obsd} values for 15 experiments using (*S*)-**6** and Cg10062 vs the concentration of (*S*)-**6**. (C) The k_{obsd} values for 18 experiments using (*R*)-**6** and *cis*-CaaD vs the concentration of (*R*)-**6**. The data from all of the experiments were used to calculate k_{inact} and K_I, which are reported in the text.

Both plots for the inactivation of Cg10062 show saturation kinetics, indicating that inactivation occurs by the prior formation of a dissociable complex between enzyme and inhibitor at the active site (*18*). Further evidence for binding at the active site comes from substrate protection studies using **7**, which at four different concentrations slows the inactivation of Cg10062 by (*R*)-**6**, and at two different concentrations slows the inactivation of Cg10062 by (*S*)-**6** (Figures 3A,B) (*18*).

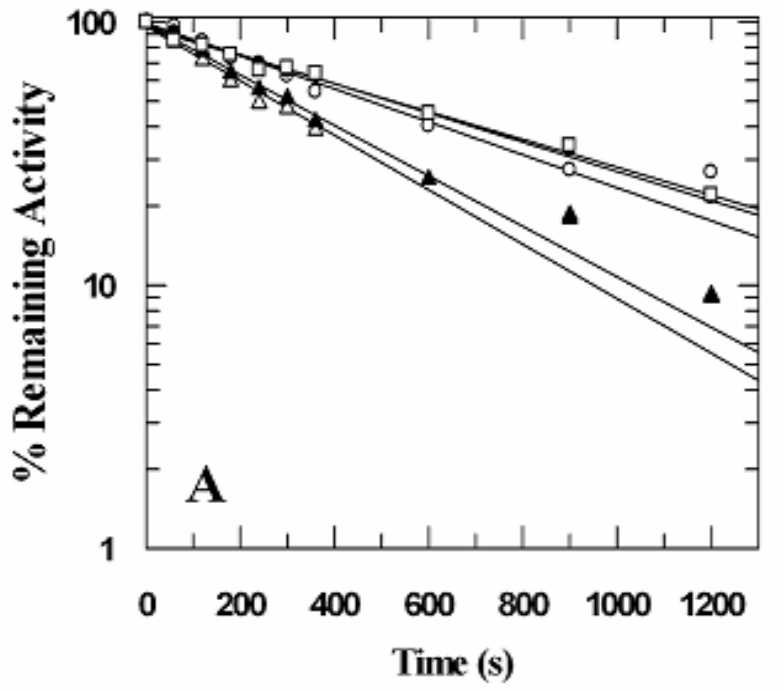
100
10
1
% Remaining Activity
A
0
200
400
600
800
1000
1200
Time (s)

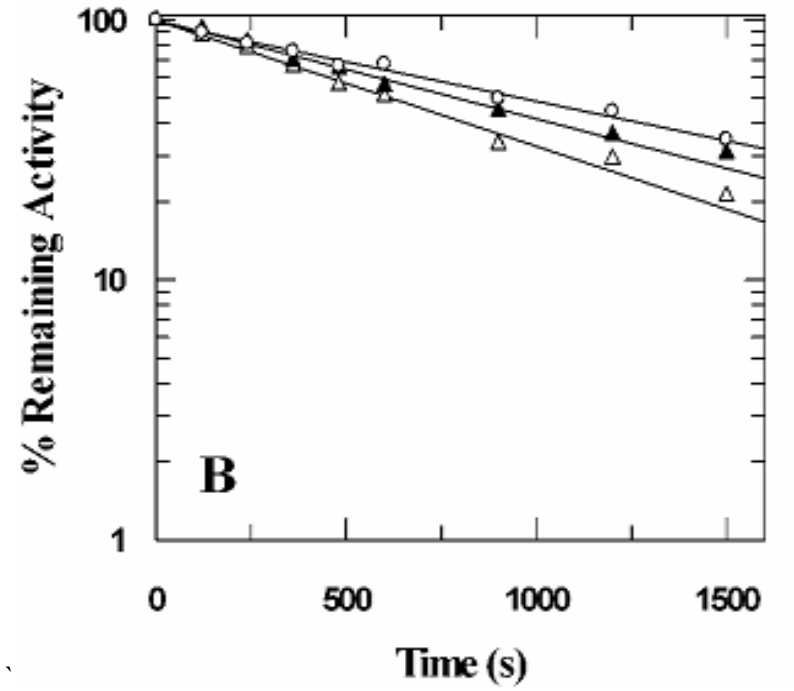
100
10
1
% Remaining Activity
B
0
500
1000
1500
Time (s)

Figure 4.3.

Figure 4.3. Protection of Cg10062 from inactivation by (*R*)- and (*S*)-**6** using substrate **7**. (A) Cg10062 (100 μM) was incubated with four different concentrations of **7** (open triangles, 0 mM; filled triangles, 1.0 mM; open circles, 2.1 mM; filled circles, 3.5 mM; open rectangles, 5.2 mM) for 30 s before the addition of (*R*)-**6** (0.4 mM). (B) The same quantity of Cg10062 was incubated with two different concentrations of **7** (open triangles, 0 mM; filled triangles, 1.7 mM; open circles, 3.5 mM) for 30 s before the addition of (*S*)-**6** (4.0 mM).

The irreversible nature of inactivation was demonstrated by the observation that Cg10062 inactivated by either (*R*)- and (*S*)-**6** did not regain activity after gel filtration on a PD-10 Sephadex G-25 column. After 5 days, Cg10062 incubated with (*R*)-**6** had no residual activity (using **7**) compared to a control. Gel filtration and an additional 3-day incubation period at 4 °C did not result in recovery of activity. Incubation of Cg10062 with (*S*)-**6** completely inactivated the enzyme after a 10-day interval. Once again, gel filtration and an additional 3-day incubation period at 4 °C did not result in recovery of activity.

4.3.2 Mass Spectral Analysis of Cg10062

*Mass Spectral Analysis of Cg10062 Treated with (R)- and (S)-**6**.* Both the (*R*)- and (*S*)-**6**-inactivated Cg10062 were subjected to ESI-MS analysis and the spectra compared to that of wild type. An 11:1 ratio of inhibitor to enzyme concentration (based on monomer molecular mass) was used. For Cg10062 inactivated by the (*R*)-enantiomer, the spectrum acquired after a 24-h incubation period shows a major signal corresponding

to a mass of 17,190 ± 2 Da (data not shown). A similar spectrum is obtained after a 48-h incubation period. The signal corresponds to the mass of Cg10062 (17,092 ± 2 Da) modified by the covalent attachment of a species with a mass of 88 Da. There is no residual signal for unmodified Cg10062 indicating ~100% modification.

For Cg10062 inactivated by the (*S*)-enantiomer, the spectrum acquired after a 24-h incubation period shows signals corresponding to masses of 17,092 ± 2 Da and 17,190 ± 2 Da (data not shown). The signal at 17,092 Da corresponds to that of Cg10062 and the signal at 17,190 Da corresponds to Cg10062 modified by the covalent attachment of the species with a mass of 88 Da. The intensities of the signals suggest 15-30% modification (in two separate runs). The same spectrum is obtained after a 48-h incubation period, where the intensities of the signals now suggest ~45% modification. After 5 days, the intensities of the signals suggest 60-70% modification. After 10 days, the signal at 17,190 Da predominates. The relative intensities of the signals suggest ~90% modification.

For both (*R*)- and (*S*)-**6**-inactivated Cg10062, the increase in mass corresponds to the expected molecular mass of **6** as its ring-opened derivative (*7*,*8*). The mass does not distinguish between the attachment of a 2- or 3-hydroxypropanoate species. However, for both enantiomers, Cg10062 shows only a single site of modification.

4.3.3 Mass Spectral Analysis of *cis*-CaaD and MSAD

*Mass Spectral Analysis of cis-CaaD Treated with (S)-**6** and MSAD Treated with (R)- and (S)-**6**.* In a previous report, covalent modification of *cis*-CaaD by (*S*)-**6** was not detected for a sample analyzed after a 24-h incubation period (*8*). In view of the lengthy

incubation times required for near complete covalent modification of Cg10062 by the (*S*)-enantiomer, *cis*-CaaD was incubated with (*S*)-**6** for 10 days at a ratio of 11 to 1 (inhibitor to enzyme). The spectrum showed only a signal corresponding to the mass of unmodified *cis*-CaaD, confirming that *cis*-CaaD is not covalently modified by (*S*)-**6**. The inactivation of MSAD by (*R*)- and (*S*)-**6** was not previously examined. At ratios of 7 to 1 and 11 to 1 (inhibitor to enzyme), the spectra for MSAD samples incubated with (*R*)- or (*S*)-**6** for a 10-day period show only signals at 14,107 ± 2 Da (data not shown). This mass corresponds to the expected mass of the MSAD monomer (*11*), and indicates that MSAD is not covalently modified by either enantiomer of **6**.

4.3.4 Mass Spectral Analysis of Cg10062 Mutants

*Mass Spectral Analysis of Cg10062 Mutants Treated with (R)- and (S)-**6**.* Four active site mutants of Cg10062 (P1A, R70A, R73A, and E114Q) were incubated in individual reaction mixtures with (*R*)- and (*S*)-**6** for 10 days at 4 °C (*6*). Mass spectral analysis of the reaction mixtures containing the P1A, R70A, and R73A mutants showed that each one produced signals (17,066, 17,007, and 17,006 ± 2 Da, respectively) corresponding to expected molecular masses of the unmodified mutants (*6*). Thus, Pro-1, Arg-70, and Arg-73 are essential for covalent modification of Cg10062 by either (*R*)- or (*S*)-**6**. Mass spectral analysis of the reaction mixture containing the E114Q mutant revealed a more complex situation. Analysis of the mixture containing (*R*)-**6** and the E114Q mutant (7 to 1 ratio) after 24 h, showed two signals corresponding to the masses of the unmodified enzyme (17,092 ± 2 Da) and modified enzyme (17,180 ± 2 Da). The relative intensities suggested 40% covalent modification. Using the same ratio of

inhibitor to enzyme, the wild type Cg10062 was completely modified by (*R*)-**6** after 24 h. After 5 days, mass spectral analysis showed complete covalent modification of the E114Q mutant by (*R*)-**6**. Analysis of the mixture containing (*S*)-**6** and the E114Q mutant (7 to 1 ratio) at 24 hours showed only a mass corresponding to unmodified enzyme. After 5 days, a second signal appeared corresponding to the mass of the modified enzyme. The relative intensities of the signals indicated 20% modification. After 10 days, mass spectral analysis suggested 45% covalent modification of the E114Q mutant by the (*S*)-enantiomer. Using the same ratio of inhibitor to enzyme, the wild type Cg10062 was 60% modified by (*S*)-**6** after 10 days. Thus, in contrast to *cis*-CaaD, where Glu-114 is not required for the inactivation reaction, it plays a role in the alkylation of Cg10062 by (*R*)- and (*S*)-**6**, as replacing it with a glutamine slows the inactivation reaction.

4.3.5 Peptide Mapping of Cg10062

*Identification of Pro-1 as the Site of Modification by (R)- and (S)-**6**.* ESI-MS analysis of incubation mixtures containing Cg10062 and (*R*)- or (*S*)-**6** showed covalent attachment of a species with a mass of 88 Da to the enzyme. The mass is consistent with modification of the enzyme by a 2- or 3-hydroxypropanoate species (*7*,*8*). The modified residue was identified by incubating the three samples (unmodified Cg10062, (*R*)-**6**-modified Cg10062, and (*S*)-**6**-modified Cg10062) with endoproteinase Glu-C (protease V-8) and analyzing the resulting peptide mixtures by MALDI-MS. Although protease V-8 cleaves peptide bonds at the carboxylate side of glutamate and aspartate residues,

(leaving Glu or Asp as the C-terminal residue), glutamates are preferred (in 100 mM ammonium bicarbonate buffer at pH 8.0) (*16*).

Mass spectral analysis identified five major peptide species in all three samples corresponding to peptide bond cleavage at Glu-15, Glu-30, Glu-41, Glu-60, Glu-75, Glu-80, Glu-88, Glu-114, and Glu-126 (Table 1). Additional peptide species were identified in the (*R*)- and (*S*)-**6**-modified Cg10062 samples having masses of 1983.86 Da and 1983.74 Da, respectively. The mass corresponds to the Pro-1 to Glu-15 peptide fragment covalently modified by **6**. The other four peptide fragments (Table 1) had not been modified.

The unmodified (1895.69 Da) and (*R*)- and (*S*)-**6**-modified fragments (1983.86 and 1983.74 Da, respectively) were subjected to MALDI-PSD analysis in order to locate the residue with the covalently attached species (*17*). The PSD spectrum of the unmodified peptide showed N-terminal sequence specific fragment ions b_2 (199) and b_3 (362). The PSD spectrum of the modified peptide showed modified fragment ions b_2 (287), corresponding to a modified Pro-1-Thr-2 fragment, and b_4 (551), corresponding to the modified Pro-1 to Thr-4 fragment. These observations narrowed the site of covalent attachment to Pro-1 or Thr-2. Although the PSD spectra of the unmodified and two modified fragments did not show a b_1 ion, corresponding respectively to Pro-1 or modified Pro-1, a proline immonium ion (70) and a modified proline immonium ion (158) were present in the spectra for the (*R*)- and (*S*)-**6**-modified fragments. Hence, Pro-1 is the site of covalent modification by (*R*)- and (*S*)-**6**.

Table 1. Peptides Identified in the Protease V-8 digestion mixture of unmodified, and (*R*)- and (*S*)-6-modified-Cg10062.

Peptide fragment	Calculated masses[a]	Observed masses[b] Cg10062	Observed masses[b] of (*R*)- and (*S*)-**6**-modified-Cg10062	
^{1}P – ^{15}E	1896.15	1895.69	1983.86	1983.74
^{31}L – ^{41}E	1742.05	1741.75	1741.89	1741.80
^{61}N – ^{75}E	1767.96	1767.67	1767.84	1767.76
^{81}L – ^{88}E	985.19	985.48	985.55	985.52
^{115}Y – ^{126}E	1422.57	1422.47	1422.58	1422.53

[a]The monoisotopic singly charged masses are predicted from analysis of the translated amino acid sequence of the *Cg10062* gene (corresponding to Cg10062) (*6*). [b]The observed masses correspond to the MH^+.

4.4 Discussion

cis-CaaD and CaaD are isomer-specific dehalogenases grouped into different families in the tautomerase superfamily (*1*). Tautomerase superfamily members have a signature β–α–β building block and a catalytic Pro-1 (*19-21*). *cis*-CaaD and CaaD have different quaternary structures (trimer and hetereohexamer, respectively) and somewhat different catalytic mechanisms (*1*,*5*,*7*). Cg10062 is a *cis*-CaaD family member that has CaaD activity, presumably due to a less stringent substrate specificity (*6*). The quaternary structure of Cg10062 is identical to that of *cis*-CaaD and the mechanism is likely to be similar. However, Cg10062 processes both isomers (i.e., **3** and **2**) and is inactivated by both enantiomers of **6**. An understanding of the relaxed specificity of Cg10062 is expected to provide insights into the elements of substrate specificity for *cis*-CaaD and CaaD and suggest how isomeric specificity of these two enzymes diverged.

(*R*)-oxriane-2-carboxylate (**6**) was previously characterized as a stereospecific affinity label of *cis*-CaaD (*8*). Mass spectral and crystallographic analysis established that inactivation resulted from covalent modification of the Pro-1 nitrogen by (*R*)-2-hydroxypropanoate at the C-3 position (*7*,*8*). Pro-1, Arg-70, and Arg-73 were identified as essential active site residues for the inactivation mechanism (*8*). The crystallographic analysis of the inactivated *cis*-CaaD implicated His-28 in the mechanism and suggested roles for Arg-70 and Arg-73 (*7*). On the basis of these observations, it was proposed that Arg-73 and His-28 interact with the carboxylate group and position (*R*)-**6** for covalent modification of Pro-1 (Scheme 2A). The side chain of Arg-70 or an Arg-70-bound water molecule functions as the proton donor for the epoxide ring-opening reaction. This

proposed orientation places the (*R*)-enantiomer in position for the alkylation reaction. If the (*S*)-enantiomer binds similarly, the epoxide ring is flipped such that the Pro-1 nitrogen cannot be alkylated (Scheme 2B).

Scheme 2

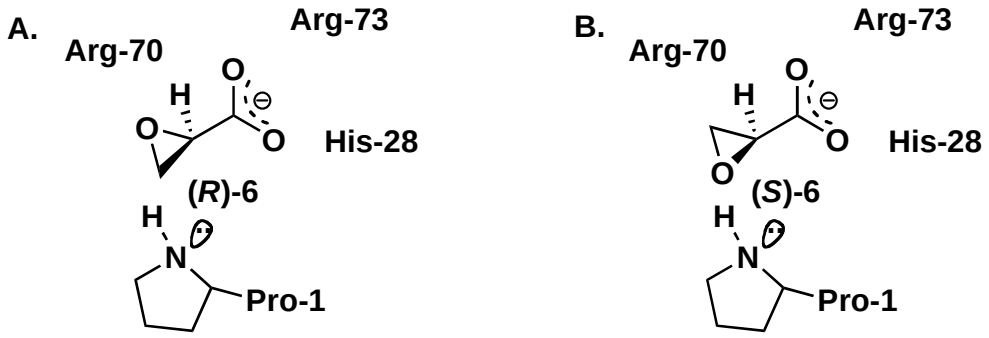

The presence of His-28 in *cis*-CaaD may be a critical factor in the enzyme's vulnerability to alkylation (*7*). CaaD, which is not inactivated by either enantiomer, lacks this residue or an equivalent. Similar to the proposed binding mode for **3**, the carboxylate group of **6** may interact with the two arginines (αArg-8 and αArg-11) in the active site of CaaD, thereby preventing one of the arginines from serving as a necessary proton source to facilitate ring opening. We have also found that MSAD is not inactivated by either enantiomer of **6**. Like CaaD, MSAD has two arginines residues (Arg-73 and Arg-75), but lacks His-28 or an equivalent. The two arginine residues of MSAD are proposed to interact with the substrate, and may likewise interact with the carboxylate group of **6** and prevent one from functioning as a proton source. Evidently, there is not an alternate nearby proton source.

Oxirane-containing compounds have been used extensively as affinity labels of enzymes and the subsequent characterization of the inactivated enzyme has provided considerable mechanistic insight (*22*-*24*). Ring opening, with the concomitant alkylation and inactivation, generally involves acid/base catalysis and proceeds by one of two mechanisms (*25*). In one mechanism, the acid catalyst protonates the oxygen of the oxirane ring (*25*). Ring-opening produces a carbocation, which captures a nearby base catalyst at the more highly substituted carbon (*25*). In a second mechanism, the base catalyst attacks the less sterically hindered carbon of the oxirane in conjugation with polarization of the carbon-oxygen ring by the acid catalyst. The regiochemistry of the ring-opened product generated in the *cis*-CaaD reaction with (*R*)-**6** would suggest that the second mechanism is operative. However, it is unknown whether active site constraints affect the observed outcome (*23*).

The two key findings in this study are that both (*R*)- and (*S*)-**6** inactivate Cg10062 and that Glu-114 is an additional participant in the inactivation mechanism. Otherwise, the inactivation process parallels that observed for *cis*-CaaD, and for the (*R*)-enantiomer, a similar mechanism can be envisioned. Accordingly, the carboxylate group would interact with His-28 and Arg-73, and the side chain of Arg-70 or an Arg-70-bound water molecule would interact with the oxirane oxygen to facilitate ring opening. Pro-1 is positioned to attack at C-3. The lower potency [compared to *cis*-CaaD and (*R*)-**6**] suggests weaker binding and less favorable interactions with the key active site groups, and may reflect some "wobble" in the active site with regard to inhibitor positioning and binding. Glu-114 might further position the epoxide for alkylation or maintain the

position of one of the essential residues such that replacement with a glutamine slows the inactivation process.

There are at least two possible mechanistic explanations (along with variations) for the inactivation of Cg10062 by the (*S*)-enantiomer. If it is assumed that the carboxylate group of (*S*)-**6** interacts with His-28 and Arg-73, one potentially interesting scenario involves a change in the regiochemistry of ring opening such that C-2 is the site of attachment. This scenario could involve another unknown residue functioning as the proton source for the oxirane oxygen. In a second scenario, the epoxide could bind in the active site of Cg10062 in a different orientation where the carboxylate group interacts with Arg-70 and Arg-73. Ring opening could occur at C-2 or C-3 and His-28 could function as a proton source. In both scenarios, the side chain of Glu-114 could favor a productive binding mode (i.e., one that results in alkylation) over a non-productive one.

In the proposed mechanism for Cg10062, Pro-1 functions as a general acid catalyst (*6*), raising the question of how the charged prolyl nitrogen is alkylated. The similarity between the *cis*-CaaD and Cg10062 active sites suggests that the pK_a values for the prolyl nitrogens will be comparable (~9.3) (*1*,*8*). At the pH of the inactivation experiments (pH = 9.0), approximately 33% of the enzyme is in a protonation state where the prolyl nitrogen can function as a nucleophile. Alkylation of the nitrogen perturbs the equilibrium and places an additional amount of enzyme into the nucleophilic and reactive form. In this manner, the enzyme can become entirely alkylated.

The crystallographic analysis of *cis*-CaaD inactivated by (*R*)-**6** uncovered the structural basis for stereospecific inactivation and suggested a mechanism (*7*). In

addition, a comparison of the structure with that of CaaD (inactivated by 3-bromopropiolate) (*26*) identified two potential determinants of the substrate specificities. First, the carboxylate groups of the isomeric substrates may interact at slightly different angles with the two active site arginines (αArg-8, αArg-11) of CaaD or the arginine/histidine cluster (Arg-70, Arg-73, His-28) of *cis*-CaaD such that the substrates are projected into different regions of the enzyme (*7*,*26*). In *cis*-CaaD, the substrate is projected towards the surface (*7*), and in CaaD, the substrate is projected deeper into the enzyme (*26*). In addition, the active site pockets fit the shapes of the respective substrates with Tyr-103 playing a role in blocking the binding of a *trans*-substrate in *cis*-CaaD. Because Cg10062 and *cis*-CaaD share these isomer discriminating residues, our understanding of the factors governing specificity is clearly incomplete. A comparative analysis of the three structures will shed further light on the role of these groups in the individual specificities and how subtle changes relax the specificity. Crystal structures of Cg10062 inactivated by the enantiomers of **6** are currently being pursued.

4.5 Acknowledgements

The mass spectrometry described in this paper was carried out in the Analytical Instrumentation Facility Core housed in the College of Pharmacy at the University of Texas at Austin and supported by Center grant ES 07784. We are grateful to Dr. Elizabeth A. Burks for helpful discussions.

4.6 References

1. Poelarends, G.J., Serrano, H., Person, M.D., Johnson, W.H., Jr., Murzin, A.G., and Whitman, C.P. (2004) Cloning, expression, and characterization of a *cis*-3-chloroacrylic acid dehalogenase: insights into the mechanistic, structural, and evolutionary relationship between isomer-specific 3-chloroacrylic acid dehalogenases. *Biochemistry 43*, 759-772.

2. van Hylckama Vlieg, J.E.T., and Janssen, D.B. (1992) Bacterial degradation of 3-chloroacrylic acid and the characterization of *cis*- and *trans*-specific dehalogenases. *Biodegradation 2*, 139-150.

3. Poelarends, G.J., Wilkens, M., Larkin, M.J., van Elsas, J.D., and Janssen, D.B. (1998) Degradation of 1,3-dichloropropene by *Pseudomonas pavonaceae* 170. *Appl. Environ. Microbiol. 64*, 2931-2936.

4. Poelarends, G.J., Saunier, R., and Janssen, D.B. (2001) *trans*-3-Chloroacrylic acid dehalogenase from *Pseudomonas pavonaceae* 170 shares structural and mechanistic similarities with 4-oxalocrotonate tautomerase. *J. Bacteriol. 183*, 4269-4277.

5. Wang, S.C., Person, M.D., Johnson, W.H., Jr., and Whitman, C.P. (2003) Reactions of *trans*-3-chloroacrylic acid dehalogenase with acetylene substrates: consequences of and evidence for a hydration reaction. *Biochemistry 42*, 8762-8773.

6. Poelarends, G.J., Serrano, H., Person, M.D., Johnson, Jr, W.H., and Whitman, C.P., unpublished observations, 2006.

7. de Jong, R.M., Bazzacco, P., Poelarends, G.J., Johnson, Jr, W.H., Kim, Y.-J., Burks, E.A., Serrano, H., Thunnissen, A.-M.W.H., Whitman, C.P., and Dijkstra B.W. (2006) Crystal structures of native and inactivated *cis*-3-chloroacrylic acid dehalogenase: structural basis for substrate specificity and inactivation by (*R*)-oxirane-2-carboxylate. *J. Biol. Chem.* (submitted).

8. Poelarends, G.J., Serrano, H., Johnson, Jr., W.H., and Whitman, C.P. (2004) Stereospecific alkylation of *cis*-chloroacrylic acid dehalogenase by (*R*)-oxirane-2-carboxylate: analysis and mechanistic implications. *Biochemistry 43*, 7187-7196 (2004).

9. Petit, Y., and Larcheveque, M. (1998) Ethyl glycidate from (*S*)-serine: ethyl (*R*)-(+)-2,3-epoxypropanoate. *Organic Syntheses 75*, 37-44.

10. Johnson Jr., W.H., Czerwinski, R.M., Fitzgerald, M.C., and Whitman, C.P. (1997) Inactivation of 4-oxalocrotonate tautomerase by 2-oxo-3-pentynoate. *Biochemistry 36*, 15724-15732.

11. Poelarends, G. J., Johnson, W.H., Jr., Murzin, A.G., and Whitman, C.P. (2003) Mechanistic characterization of a bacterial malonate semialdehyde decarboxylase: identification of a new activity in the tautomerase superfamily. *J. Biol. Chem. 278*, 48674-48683.

12. Laemmli, U.K. (1970) Cleavage of structural proteins during the assembly of the head of bacteriophage T4. *Nature 227*, 680-685

13. Waddell, W.J. (1956) A simple ultraviolet spectrophotometric method for the determination of protein. *J. Lab. Clin. Med. 48*, 311-314.

14. Stivers, J.T., Abeygunawardana, C., Mildvan, A.S., Hajipour. G., Whitman, C.P., and Chen, L.H. (1996) Catalytic role of the amino-terminal proline in 4-oxalocrotonate tautomerase: affinity labeling and heteronuclear NMR studies. *Biochemistry 35*, 803-813.

15. Wang, S.C., Johnson, W.H., Jr., Czerwinski, R.M., and Whitman, C.P. (2004) Reactions of 4-oxalocrotonate tautomerase and YwhB with 3-halopropiolates: analysis and implications. *Biochemistry 43*, 748-758.

16. Houmard, J., and Drapeau, G.R. (1972) Staphylococcal protease: a proteolytic enzyme specific for glutamoyl bonds. *Proc. Natl. Acad. Sci. U.S.A. 69*, 3506-3509.

17. Person, M.D., Monks, T.J., and Lau, S.S. (2003) An integrated approach to identifying chemically induced posttranslational modifications using comparative MALDI-MS and targeted HPLC-ESI-MS/MS. *Chem. Res. Toxicol*. *16*, 598-608.

18. Meloche, H.P. (1967) Bromopyruvate inactivation of 2-keto-3-deoxy-6-phosphogluconic aldolase. I. Kinetic evidence for active site specificity. *Biochemistry 6*, 2273-2280.

19. Murzin, A.G. (1996) Structural classification of proteins: new superfamilies. *Curr. Opin. Struct. Biol*. *6*, 386-394.

20. Whitman, C.P. (2002) The 4-oxalocrotonate tautomerase family of enzymes: how nature makes new enzymes using a β-α-β structural motif. *Arch. Biochem. Biophys. 402*, 1-13.

21. Poelarends, G.J., and Whitman, C.P. (2004) Evolution of enzymatic activity in the tautomerase superfamily: mechanistic and structural studies of the 1,3-dichloropropene catabolic enzymes. *Bioorg. Chem. 32*, 376-92.

22. Dang, T. and Prestwich G.D. (2000) Site-directed mutagenesis of squalene-hopene cyclase: altered substrate specificity and product distribution. *Chem. Biol. 7*, 643-649.

23. Landro, J.A., Gerlt, J.A., Kozarich, J.W., Koo, C.W., Shah, V.J., Kenyon, G.L., Neidhart, D.J., Fujita, S. and Petsko, G.A. (1994) The role of lysine 166 in the mechanism of mandelate racemase from *Pseudomonas putida*: mechanistic and crystallographic evidence for stereospecific alkylation by (*R*)-α-phenylglycidate. *Biochemistry 33*, 635-643.

24. Ntarima, P., Nerinckx, W., Klarskov, K., Devreese, B., Mahalingeshwara, K.B., Van Beeumen, J., Claeyssens, M., (2000) Epoxyalkyl glycosides of D-xylose and xylo-oligosaccharides are active-site markers of xylanases from glycoside hydrolase family 11, not from family 10. *Biochem. J. 347*, 865-873.

25. Wade, Jr. L.G. (1999) *Organic Chemistry*, 4th ed., pp. 1045-1048, Prentice-Hall, Inc., Upper Saddle River, NJ.

26. de Jong, R. M., Brugman, W., Poelarends, G. J., Whitman, C. P., and Dijkstra, B. W. (2004) The X-ray structure of *trans*-3-chloroacrylic acid dehalogenase reveals a novel hydration mechanism in the tautomerase superfamily. *J. Biol. Chem. 279*, 11546-11552.

4.7 Footnotes

[1]Abbreviations: *cis*-CaaD and CaaD; *cis*- and *trans*-3-chloroacrylic acid dehalogenase, respectively; ESI-MS, electrospray ionization mass spectrometry; MALDI-PSD, matrix assisted laser desorption-ionization post-source decay; MALDI-TOF, matrix assisted laser desorption-ionization time-of-flight; MSAD, malonate semialdehyde decarboxylase; SDS-PAGE, sodium dodecyl sulfate-polyacrylamide gel electrophoresis

[2]A better fit of the data can be obtained using the Hill equation, as found in the Grafit program (data not shown). The resulting fit suggests positive cooperativity and may indicate that the inactivation of one subunit accelerates the rate of inactivation for the two remaining subunits. Positive (or negative) cooperativity has not been detected for Cg10062 or *cis*-CaaD by steady state kinetics.

[3]In a previous report (*8*), the concentrations of **6** were calculated based on a molecular weight of 88 Da, which corresponds to the free acid. Hence, the actual concentrations are lower than the reported concentrations (*8*). The concentrations in this report take into account the fact that **6** is a potassium salt.

Vita

Brooklyn Ames Robertson was born in Roy, Utah in 1977, the son of David Ronald and Nancy Robertson. He graduated from Widefield High School in Colorado Springs, Colorado in 1995, as the valedictorian. He attended Colorado State University, in Fort Collins, Colorado from 1995-1999, and graduated with a Bachelor of Science degree, cum laude, in Chemistry and a minor in Mathematics. In 2000, he began graduate school at The University of Texas at Austin in the Department of Chemistry and Biochemistry. After studying for two years in the Organic Division, Brooklyn transferred to the Biochemistry Division and joined the laboratory of Dr. Christian P. Whitman. He finished his doctoral work and graduated with the degree of Doctor of Philosophy in Biochemistry in August of 2007 from The University of Texas at Austin.

Permanent address: 521 Ft. Thomas Place, Round Rock, TX 78664

This dissertation was typed by the author